A TIME-DEPENDENT MOLECULAR ORBITAL AP-
PROACH TO ION-SOLID SURFACE COLLISIONS

By

ERIC QUINN FENG

To Susan and Michael and to My Mother's Memory

ACKNOWLEDGMENTS

TABLE OF CONTENTS

Abstract of Dissertation Presented to the Graduate School
of the University of Florida in Partial Fulfillment of the
Requirements for the Degree of Doctor of Philosophy

A TIME-DEPENDENT MOLECULAR ORBITAL
APPROACH TO ION-SOLID SURFACE COLLISIONS

By

Eric Quinn Feng

May 1991

Chairman: David A. Micha
Major Department: Physics

A time-dependent molecular orbital method has been developed to study
charge transfer in collisions of ions with metal surfaces at energies between 1 au
and 170 au. A set of localized basis functions, consisting of generalized Wannier
functions for the surface and s- and p- atomic functions for the ion, is used to
separate the system into primary and secondary regions. An effective Hamiltonian
and time-dependent equations for the electron density matrix are obtained in the
primary region, where most charge transfer occurs. The equations for the electron
density matrix are solved with a linearization scheme. The method is suitable to

study atomic orbital polarization for collisions of ions and surfaces. A model calculation for $Na^+ + W(110)$ collisions with a prescribed trajectory is presented. The interaction potentials between the $W(110)$ surface and Na 3s and 3p orbitals are calculated from a Na pseudopotential and a step potential for $W(110)$. Results show that the yield of neutralized atoms oscillates with the collision energy as the result of the near-resonance charge transfer mechanism. The time-dependence of the density matrix provides insight on the dynamics of electron transfer along the atomic trajectory.

CHAPTER 1
INTRODUCTION

1.1 Collisional Charge Transfer at Surfaces

Surfaces and various physical processes occurring near surfaces are receiving increased attention in present scientific research, due mainly to rapidly growing applications in modern analytical techniques. Researchers in fields of surface science, chemical physics, solid state physics, atomic physics, electrical engineering, and even medical science are carrying on extensive, and sometimes overlapping, studies and analyses involving surfaces. One of the most important ways to understand the nature of surfaces is to study various electronic processes occurring in collisions of ions with them. For example, one can learn from scattering about the topology and electronic structures of surfaces, amount of impurities and adsorbates present, surface electron and lattice relaxations, and interactions between surfaces and atoms and molecules. Particular attention has been paid to nonadiabatic processes accompanying charge transfer between scattered particles and surfaces at low collision energies ranging from a few electron volts to a few thousand electron volts, which often involve strong coupling and energy transfer between electronic, translational, vibrational, and rotational degrees of freedom of projectiles and surfaces.

Charge transfer in ion-surface collisions may lead to neutralization or ionization and can be expressed as

$$\Sigma + A^+ \rightarrow \Sigma^+ + A \tag{1.1}$$

and

$$\Sigma + A \rightarrow \Sigma^{\pm} + A^{\mp} \tag{1.2}$$

respectively, where Σ is a surface such as W(110) or Ni(111), and A is an alkali atom such as Li, Na or K. Similar processes occur in beam-foil experiments in which charge exchange takes place when ions or atoms pass through thin foils, instead of being reflected from surfaces.

The two main mechanisms through which charges are exchanged are the near-resonance process and the Auger process [Hagstrum, 78]. In a near-resonance neutralization, an electron in the conduction band of the solid tunnels to an unoccupied level of the ion which lies near or below the Fermi level of the solid. In a near-resonance ionization, an electron from a filled excited state of a neutral atom transits to an empty level in the conduction band or above the Fermi level of the solid. The two energy levels involved in these processes are close, which characterizes the near-resonance processes. The Auger process involves two or more electrons. In two-electron Auger neutralization, one electron jumps from the metal conduction band to the ion ground state below the band and, to conserve energy, the second electron is excited from another level in the band and may leave the surface and be detected by an Auger spectroscopy. For systems

where an ion affinity level is in resonance with the conduction band of the metal, such as in $Na^+ + W(110)$, a near-resonance process is more likely; for systems where an ion ground state is below the conduction band, such as $H^+ + Ni(111)$, the Auger process is usually the dominant charge transfer mechanism. Complicated combinations of the two processes are also possible in certain circumstances.

The rise of interest in these problems has promoted an extensive effort to develop ultra-high vacuum (UHV) and modern spectroscopy techniques to observe and detect various physical properties in much greater detail in the last two decades than before [Hagstrum, 77; Hagstrum, 78]. In these spectroscopy experiments, one measures the intensity of scattering products (atoms, photons or Auger electrons) and their energy and angular momentum distributions which usually depend on the energy and angle of incident beams, the surface properties and, sometimes, on temperature and external fields. The ion scattering spectroscopy (ISS) [Smith, 71; Hulpke, 75; Taglauer and Hailand, 76; Overbosch et al., 80] measures the scattered ion intensity as a function of incident energy and reflected angle, and can be used to determine the topology of surfaces. Oscillation in the intensity of neutralization of ions in the low energy range has been observed for a number of ion-surface combinations, and is ascribed to near-resonance charge transfer [Erickson and Smith, 75; Rusch and Erickson, 77]. In ion neutralization spectroscopy (INS) experiments, one can gain knowledge of the band structure by measuring the kinetic energy of Auger electrons [Hagstrum, 75]. Time of flight (TOF) experiments detect survival probabilities of states of scattered atoms

and their energy distributions [Kasi et al., 88]. So far, most experiments have been done on noble and transition metals, simply because their surfaces are relatively easy to clean and to prepare. However, due to the strong interest in electronics, studies on semiconductor and other material surfaces have been carried out [Richard and Eschenbacher, 84].

In atomic collision studies, people have developed new instruments which have a time resolution of picoseconds to monitor the time evolutions of intermediate atomic states. It has been possible to measure the angular distribution of scattering product orbitals [Hale et al., 84; Hertel et al, 85; Andersen, 87; Campbell and Hertel, 87]. These new techniques provide valuable information about the collision dynamics, and it is expected that they will be soon used in studies of ion-surface collisions.

1.2 A Survey of Theoretical Methods

Advances in spectroscopy techniques in the last two decades have allowed extensive experimental studies of ion-surface collisions. However, the development of the theory lags behind that of experiment in this field, and there are far and away more experimental data than can be understood. This is because the systems we are dealing with are very challenging ones in the sense that they lack translation symmetry. Moreover, they involve dynamical many-electron processes with a strong and time-dependent coupling between the electronic degrees of freedom and nuclear motions. The traditional methods which deal with systems of periodic

lattices or of a few electrons are either not suitable or have to be modified. It seems, however, that theoretical studies are accelerating and are on the verge of reproducing some of the experimental data.

1.2.1 Binary Collision Theory of Charge Transfer

In this theory [Rusch and Erickson, 77; Kasi et al., 89] the scattering of an ion from a surface is described by a single binary collision or a sequence of elastic collisions between the ion and surface atoms. In this theory, the scattering angle θ satisfies the relationship

$$\frac{E_1}{E_0} = \frac{1}{(1+\mu)^2}\left[cos\theta + \left(\mu^2 - sin^2\theta\right)^{1/2}\right]^2 \tag{1.3}$$

where m_1 and m_2 are the masses of the incidental ion and surface atom, $\mu=m_2/m_1$, and E_0 and E_1 are the kinetic energies of the ion before and after the scattering. The yield of the scattered ions for a given scattering angle, $Y(E_0, \theta)$, is

$$Y(E_0,\theta) \propto \sigma(E_0,\theta) \cdot P(E_0,\theta) \tag{1.4}$$

where $\sigma(E_0, \theta)$ is the elastic differential cross section and $P(E_0, \theta)$ is the probability for an ion to remain ionized after the scattering. In classical calculations σ is a monotonically decreasing function of the incident energy and P is given by

$$P \propto exp(-a/v_\perp) \tag{1.5}$$

where a is a constant and $v_\perp$ is the ion velocity perpendicular to the surface. This theory, in which the yield is a smooth function of the incident ion energy, fits the energy dependence of $^4He^+$ scattered from Cu and certain other systems.

However, it cannot explain the oscillatory charge transfer behavior observed in other systems which is believed to be associated with nonadiabatic charge transfer mechanisms.

1.2.2 Many-Electron Treatments

A variety of theoretical methods [Tully, 77; Brako and Newns, 81; Holloway and Gadzuk, 85; Hood et al., 85; Lee and George, 85] have been proposed to account for the many-body processes accompanying charge exchange in ion-surface collisions. The most widely used one is the approach based on the Anderson-Newns Hamiltonian [Anderson, 61] to describe the ion-surface scattering [Blandin et al., 76; Norskov and Lundqvist, 79; Brako and Newns, 81; Lang, 83]. In this approach, neglecting spin and using second quantization notations, the Hamiltonian of the system is written as

$$H = \epsilon_a C_a^+ C_a + \sum_k \epsilon_k C_k^+ C_k + \sum_k \left[V_{ak} C_a^+ C_k + V_{ak}^* C_k^+ C_a \right] \qquad (1.6)$$

where C_a^+, C_a are the creation and destruction operators corresponding to atomic state ψ_a, C_k^+, C_k are the creation and destruction operators corresponding to solid state ψ_k, ϵ_a and ϵ_k are the energies of ψ_a and ψ_k respectively, and $V_{ak} = \langle a|V|k \rangle$, where V is the perturbation due to coupling of the atom to the metal. The last two terms describe the electron hopping between ψ_a and ψ_k. It should be noted that the energy of the atomic level is time dependent through the ion's trajectory $\vec{R}_A(t)$, that is, $\epsilon_a(t) = H_{aa} \left[\vec{R}_A(t) \right]$. A set of equations of motion of electronic

degrees of freedom can be obtained from the Heisenberg equations (with $\hbar = 1$)

$$i\frac{\partial C_a}{\partial t} = -[H, C_a] = \epsilon_a(t)C_a + \sum_k V_{ak}^*(t)C_k \qquad (1.7)$$

$$i\frac{\partial C_k}{\partial t} = -[H, C_k] = \epsilon_k C_k + V_{ak}(t)C_a \qquad (1.8)$$

Eliminating C_k, it yields a differential-integral equation for C_a which can be solved by numerical procedures. The number of electrons on the atom after the scattering is given by

$$n_a(\infty) = \langle\psi_a|C_a^+(\infty)C_a(\infty)|\psi_a\rangle \qquad (1.9)$$

Most studies using the time-dependent Anderson-Newns Hamiltonian have neglected the intra-atomic Coulomb repulsion to simplify the calculations. For most alkali-metal collisions, which produce few negative ions, this approximation seems to be justified. But for scatterings like H-W(110), there is a significant fraction of H⁻ products after scattering, and the intra-atomic Coulomb repulsion plays an important role. Instead of using the above Hamiltonian one should use

$$\begin{aligned}
H = &\sum_\sigma \epsilon_a C_{a\sigma}^+ C_{a\sigma} + \sum_{k\sigma} \epsilon_k C_{k\sigma}^+ C_{k\sigma} \\
&+ \sum_{k\sigma} \left[V_{ak}C_{a\sigma}^+ C_{k\sigma} + V_{ak}^* C_{k\sigma}^+ C_{a\sigma}\right] + U(t)n_{a\uparrow}n_{a\downarrow}
\end{aligned} \qquad (1.10)$$

where σ is a spin index, $n_{a\uparrow} = C_{a\uparrow}^+ C_{a\uparrow}$, $n_{a\downarrow} = C_{a\downarrow}^+ C_{a\downarrow}$, and $U(t)$ is the effective intra-atomic Coulomb repulsion which depends on the distance between the ion and the surface. Using the Hartree-Fock approximation, one obtains a set of

differential-integral equations [Yoshimori et al., 84; Sulston et al., 88] which can be solved numerically. However, the qualitative behavior of the results are found to be not much different. There have been several attempts to go beyond the Hartree-Fock approximation [Sebastian, 83; 85; Kasai and Okiji, 87], by which some preliminary results were obtained.

1.3 Existing Problems

Several problems inherent in the theoretical treatment of ion-surface scattering will be addressed here. We view them as some key points in furthering the theoretical study of ion-surface collisions.

1.3.1 Electronic States and Electronic Couplings

Ion-surface systems are many electron systems which lack translation symmetry. This brings both difficulty and challenge to theoretical studies of the problem. One way to deal with surfaces is to assume that the electronic wave functions in surfaces are the same as those of an infinite periodic system and to treat the colliding ion as a moving defect and the atomic states as localized states. In this way, one can relatively easily calculate surface properties and the scattering yield [Brako and Newns, 81; Lang, 83; Shindo and Kawai, 86]. However, this approximation is not very accurate, and usually can only be used as a starting point. At surfaces, as the results of broken symmetry and the strong perturbation from the colliding ion, the electronic bands are distorted and the electron behavior is different from that of bulks. One of the important features of the metal and

semiconductor electronic structure is the existence of the localized states. While s- and p-electrons are generally described by continuous states, d-electrons are more localized. At surfaces, localized states can also be created by impurities, adsorbates or chemisorbed layers. The presence of localized states greatly affects the local electronic environment; for example, an absorbed layer of alkali on metal surfaces lowers the work function [Gomer, 75; Medvedev et al., 70].

Correctly calculating or estimating the electronic couplings between the ion and surface is obviously important in theoretical calculation. But current theoretical methods do not provide a simple and yet accurate way to estimate the electron hopping matrix elements. People have to rely on semi-empirical calculation. For example, in the time-dependent Anderson-Newns Hamiltonian, V_{ak} measures the coupling between the atomic states and surface states and is related to the lifetime broadening of an atomic state, $\Delta(t)$. Assuming that k and t dependence of V_{ak} are separated,

$$V_{ak}\left[\vec{R}_A(t)\right] = V_k u(t) \tag{1.11}$$

where V_k depends only on k and $u(t)$ only on t, one has

$$\Delta(t) = \Delta(\epsilon)|u(t)|^2 \tag{1.12}$$

where $\Delta(\epsilon)$ is defined by

$$\Delta(\epsilon) = \pi \sum_k |V_k|^2 \delta(\epsilon - \epsilon_k) \tag{1.13}$$

which can be approximately evaluated by methods developed in chemisorption theory. But a common practice is to use parameterization of $\Delta(t)$. For instance,

one can use a simple exponential form which is independent of energy

$$\Delta(t) = \Delta_0 exp(-\gamma Z_A) \qquad (1.14)$$

and determine parameters Δ_0 and γ from experimental data [Brako and Newns, 81; Lang, 83; Hood et al., 85] or from density functional calculation [Lang and Norskov, 83].

Because of the electronic coupling from the surface electrons, the atomic energy ϵ_a is distance dependent. Again, a simple function form is often used (with the electron charge e=1 au),

$$\epsilon_a(z_a) = \epsilon_a(\infty) - \frac{1}{4Z_A} \qquad (1.15)$$

where Z_A is the distance between the ion core and the surface. This is based on the approximation that the change of ϵ_a is due to a classical image charge.

Although the parameterization approach is widely used, it ignores the fact that the electronic coupling is strongly dependent on the rearrangement of charges during collisions, and its validity at short distances is questionable. Ideally, the treatment of the ion-surface systems should contain a self-consistent electronic structure calculation which accounts for localized states. A self-consistent localized orbital method has been developed to deal with transition metal surfaces and chemisorption on metal surfaces [Smith and Gay, 75; Smith et al., 80]. The density functional method [Hohenberg and Kohn, 64] has also been applied to ion-surface interactions [Lang and Williams, 76].

1.3.2 The Treatment of Extended Systems

From the theoretical point of view, it is easier to deal with either a system of a few particles, for example, small molecules, or a system with a periodic structure, such as single crystals. Ion-surface systems, on the other hand, are many-body systems which lack translation symmetry. To combine a full self-consistent calculation of electronic interaction with a dynamic description of ion-surface collisions is a difficult, if not impractical, task.

In developing a better and more physical description of ion-surface systems a very important fact should be noticed, namely that during the collisions, ions interact mainly with local regions of the surface, while the remainder of the solid is relatively unperturbed. This fact provides a hint that it is possible to properly handle electronic motions by concentrating on these local regions. Olson and Garrison [Olson and Garrison, 85] have used a cluster in place of a surface; this enables them to employ the molecular orbital method developed in molecular scattering. Another method to deal with surfaces is the embedding technique [Grimley and Mola, 74; Kirtman and de Melo, 81; Feibelman, 85] used in chemisorption studies, which uses a higher level treatment of electronic interactions within a molecular complex (a small region of the surface plus adsorbates) and a simple description outside of the complex. de Melo et al. [de Melo et al., 87] have developed a self-consistent method using a density matrix and applied it to the Anderson-Newns Hamiltonian for a one dimensional system. McDowell [McDowell, 85] uses an embedding technique to obtain generalized

Langevin type equations for the spin orbitals in a primary zone which couples with the secondary zone through driving terms. These treatments show that, by concentrating on a small number of orbitals, it is possible to achieve self-consistency. Another common feature in these treatments is the use of localized spin orbitals, which allows one to naturally deal with localized phenomena [Feng et al., 91].

1.3.3 Effect of Nuclear Motion

While the electronic motions are treated quantum mechanically, it is reasonable to assume that the nuclear motion evolves according to the classical mechanics for the collision energy in the hyperthermal range. In this classical-quantal approach the nuclear motion, $\vec{R}_A(t)$, can be treated at several levels. In the simple classical treatment, the nuclear trajectory is fully determined by a classical ion-surface potential. In an improved semiclassical treatment, the nuclear potential is coupled with the electronic motion. The classical trajectory is valid only in the high energy range [Tully, 76] as demonstrated in gas-phase collisions. The reason is that at lower energies, trajectories are sensitive to the detail of chemical interactions among the atoms and depend on the electronic states. It has been found that in H-p collisions, the classical trajectory would give rise to a significant error when the collisional energy is lower than 100 ev [Runge et al., 90].

Looking from another angle, the nuclear motion can be treated either by the so-called trajectory approximation or by a multichannel procedure. In the trajectory treatment, the nuclear trajectory is uniquely defined by a single fixed

potential, which can either be a pure classical one or an effective potential which contains the coupling with the electronic degrees of motion. One example is the straight line trajectory resulted from a hard wall potential. Runge et al. [Runge et al., 90] determine the ion trajectory by an effective force which is dependent on the gradient of the electronic density matrix. It has instead been suggested using a trajectory approximation, constructing multidimensional potential energy hypersurfaces describing various atomic configurations and allowing trajectories to hop back and forth between hypersurfaces [Tully, 77; Holloway and Gadzuk, 85; Newns, 85].

A useful procedure in dealing with molecule collisions is the eikonal method developed by Micha [Micha, 83]. In this method the nuclear variables are coupled with the electronic ones and both must be found self-consistently. An application of the eikonal method to ion-surface collision is by Olson and Garrison [Olson and Garrison, 85] who model the surface by a small cluster.

1.3.4 Atomic Orbital Polarization

In atomic scattering, the scattered atoms can be in different electronic states and their distribution of electronic angular momentum can be anisotropic. This causes orbital alignment and orientation [Hippler, 85]. Experimentally, this requires a partial or full determination of the atomic states after the collision in contrast to the conventional study which measures the differential cross section. Orbital polarization has been the subject of much theoretical work [Fano and Macek, 73; Andersen and Nielsen, 87; Nielsen and Andersen, 87], in which the

density matrix [Blum, 81] is extensively used. Although the use of the density matrix in scattering theory is not new, the study of orbital polarization provides a much more severe test of a theory than does the study of cross section, this is because not only the diagonal elements, but also the off-diagonal elements of the density matrix are required to determine the alignment and orientation parameters. Of course, the study of orbital polarization will lead to a deeper insight into the interaction and mechanisms involved in the collisions. Until now, no detailed work on orbital polarization in ion-surface collision had been reported either experimentally or theoretically. It is just a matter of time before the experimental techniques and theory are developed in this field.

1.4 Outline of the Chapters

This dissertation presents a theoretical study of charge transfer in ion-surface collisions based on the time-dependent molecular orbital approach. A partitioning technique is used to divide a ion-surface system into a primary region which contains a few centers on the surface and the scattering ion, and a secondary region containing the remainder of the surface. The charge transfer is calculated by solving the time-dependent Hartree-Fock (TDHF) equation for the electron density matrix in the primary region which couples with the secondary region electronically. This approach permits determination of the atomic states during and after the scattering and calculation of the alignment and orientation parameters. In the following chapters atomic units are used; therefore, electron charge $e=1$, electron mass $m_e=1$ and $\hbar=1$.

In Chapter 2, we present the basic framework of our approach to the ion-surface collisions. TDHF equations are used to describe the time evolution of the molecular orbitals. The formalism is constructed in terms of an electronic density matrix because it can simplify computation and is convenient in the calculation of alignment and orientation parameters. In the later part of the chapter, the TDHF equation is rewritten in the basis of the travelling atomic orbitals (TOA).

In Chapter 3, we define the parameters for average electronic population, electronic multipoles and polarization of atomic orbitals by introducing tensor operators and irreducible operators. The orientation and alignment parameters can be calculated from the density matrix. The orbital polarization parameters for a subsystem are also expressed by the density matrix.

In Chapter 4, we present a local time linearization procedure for solving TDHF equations. The method is based on the assumption that, in a very short time interval, the solution of the TDHF equation is a linear perturbation caused by the motion of the atomic core, added to correct the evolution of the system first calculated as if the nuclei were fixed. Using this procedure, the linearized equations for the perturbations, which contain a time-dependent driving term due to the nuclear motions, are constructed and solved in conjunction with the equations for fixed nuclear positions. The procedure is presented for a general case. In the later part of the Chapter, we apply this procedure to a simple case in which the electron-electron interaction is neglected and obtain analytical solutions for the linearized TDHF equations.

In Chapter 5, a partitioning procedure for ion-surface collisions is presented. The system is divided into a primary region which contains the ion and a few centers on the surface and a secondary region which is the remainder of the surface. The density matrix is approximated in the secondary region by an unperturbed one, which is justified when the collisional energy of the ion is not very low. The effective equations in the primary region are coupled with the secondary region through a driving term. To fit the asymptotic behavior of the system after the partitioning, a correction term is added to the partitioned Hamiltonian. Combining the linearization procedure described in Chapter 4, we obtain the effective equations in the primary region and their formal solutions. Again, we further illustrate this partition method by applying it to a special case when the electron interaction is neglected.

In Chapter 6, we construct a set of localized basis functions to be used in the time-dependent molecular orbital calculation. For the surface part, we introduce a set of generalized Wannier functions (GWFs) which are orthonormal and localized at centers of the surface. A variational procedure is employed to generate these functions. As an example, we calculate the generalized Wannier functions for a three dimensional jellium solid. The basis functions associated with the ion core are assumed to be atomic orbitals and are obtained from a pseudopotential for the ion core. Our basis functions are time-dependent and in the form of linear combinations of Gaussians. The overlap matrix and Hamiltonian matrix are constructed in this basis set.

In Chapter 7, we discuss the computational aspects. At first, we present our algorithm for numerical integration of the time-dependent Hartree-Fock equations as well as the flowchart of the computational program. Then the stability and the convergence of the numerical integration are discussed at length. Effects of some computational parameters are investigated, including step size, initial and final positions of the ion, and tolerances, among others.

In Chapter 8, we present an application of this approach and its results to the neutralization in a normal collision between a Sodium ion and a Tungsten (110) surface. An atom-surface interaction potential is constructed to determine a prescribed trajectory. By using methods described in previous chapters, we obtain the time evolution of the density matrix from which the electronic population and orbital polarization parameters are calculated. We also study the effects of the collision energy on the final yield of the neutral atoms and their polarization after the collision, and compare the results with experimental data. We also briefly discuss the application of the approach to other systems, and to collisions at other scattering angles.

In Chapter 9, we discuss the features of our time-dependent molecular method and its applications to charge transfer in atom-surface collisions in hyperthermal energy range. Analysis and conclusions are related to the physical features and comparison with other theoretical methods in the field. We also discuss the approximations used in the present study. Finally, we offer suggestions for future research.

In Appendix A, we calculate matrix $\mathbf{B}^x$ which is the expansion coefficient matrix of the Wannier functions for free electrons in terms of Gaussians.

In Appendix B, we calculate the total band energy of a jellium slab using the generalized Wannier functions.

In Appendix C, we show how the Fermi energy is calculated for a finite jellium slab.

CHAPTER 2
THE TIME-DEPENDENT HARTREE-FOCK (TDHF) APPROACH

The time-dependent Hartree-Fock approach is suitable for studying the many-body collision dynamics of our problem. Using a one-electron effective field it can describe the evolution of collisional systems and calculate dynamic parameters to compare with experimental data. One of the advantages of the TDHF method is that the self-consistency between the effective field and the orbital coefficients or density matrix is achieved automatically by solving time-dependent differential equations without having to perform the self-consistent iteration procedure required in the time-independent case. TDHF has been extensively applied to collision problems in nuclear physics [Ring and Schuck, 80; Negele, 82; Davies et al., 82], and recently applications in atomic molecular collisions have been reported [Kulander et al., 82; Devi and Garcia, 83; Gazdy and Micha, 86; 87]. Micha and Gazdy [Micha and Gazdy, 87] have proposed a variational procedure which improves the accuracy of transition amplitude calculations using TDHF trial functions. Yoshimori et al. [Yoshimori et al., 84] have discussed using the TDHF method in charge transfer in ion-surface collisions.

In this Chapter, we apply the TDHF method to charge transfer in ion-surface collisions. In Sect. 2.1, by introducing time-dependent molecular orbitals,

19

we derive the TDHF equations for the electron density matrix. The reason we use the density matrix [McWeeny, 60; Cohen and Frishberg, 76] is that it simplifies calculation for a large system. Another advantage is that many interested properties of collisions can be defined and readily calculated from it. One of the key problems in applying the TDHF approach to ion-surface studies is choosing the basis set. With the great number of electrons in the systems, choosing a complete basis set would make any practical calculation out of the question. One has to truncate the complete basis set in a proper way so that the introduced error is minimal. However, we will leave this problem to Chapter 5. In this Chapter, we first describe the ion-surface system. In Sect. 2.2 we derive the basic formalism without specifying the particular form of the basis set except for the condition that each basis function is associated with a certain center of the system. In Sect. 2.3 the TDHF equation is rewritten in the basis of travelling atomic orbitals (TAO).

2.1 The Atom-Surface System

Let's consider a system of a scattering ion and a semi-infinite solid. We will assume the solid has a conduction band of continuous one-electron states and some localized states (This is in contrast to some approaches which are limited to continuous states only). For the colliding atom we assume it has a core and several valence levels. Because the deeper levels of the solid and the core states of the ion are tightly bound and usually do not participate in charge transfer in the energy range we are interested in, they are not considered. For the same

reason, highly excited atomic states and those solid states highly above the Fermi level are not considered either. We also assume that the atomic levels are in the range of or close to the conduction band and that the near-resonance tunnelling of electrons is the dominant charge transfer process. The thermal motion of the nuclei in the solid can be neglected at the collision energies of interest, so that the only moving nucleus is that of the scattering ion. For simplicity, we assume that the collision energy is high enough that the trajectory approximation can be used. In this approximation, the motion of the ion nucleus can be described by a known function $\vec{R}_A(t)$ determined by an effective interaction potential between the ion core and the surface. In Chapter 9 we will discuss the validity of this approximation and the possible improvements which are necessary at low collision energies.

2.2 TDHF Equations of Density Matrix

Let $\Psi(t)$ be the electronic wavefunction which satisfies the time-dependent Shrodinger equation

$$i\frac{\partial}{\partial t}\Psi(t) = H(t)\Psi(t) \tag{2.1}$$

where $H(t)$ is the total Hamiltonian of the system. Using the time-dependent Hartree-Fock approximation, the TDHF wavefucntions have the form of

$$\Psi(t) = N_{el}^{-1/2}det[\psi_i(x_j,t)] \tag{2.2}$$

where N_{el} is the number of electrons and $\psi_i(x, t)$ is the ith spin orbital for electron variables $x = (\vec{r}, \zeta)$. We write $\psi_i(x, t)$ as

$$\psi_i(x, t) = \phi_i^\gamma(\vec{r}, t)\gamma_i(\zeta) \tag{2.3}$$

where $\phi_i^\gamma(\vec{r}, t)$ is the ith time-dependent molecular orbitals for spin γ and $\gamma_i(\zeta)$ is the corresponding spin function. The electron density operator $\hat{\rho}$ is given by

$$\hat{\rho}^\gamma = \sum_{i \in occ} |\phi_i^\gamma\rangle\langle\phi_i^\gamma| \tag{2.4}$$

where the summation is over the occupied orbitals, which is assumed to satisfy the TDHF equation [Dirac, 30]

$$i\hbar\frac{\partial}{\partial t}\hat{\rho}^\gamma = \hat{F}^\gamma\hat{\rho}^\gamma - \hat{\rho}^\gamma\hat{F}^\gamma \tag{2.5}$$

where $\hat{F}$ is the Fock operator which can be written as [Pople and Beveridge, 70]

$$\hat{F}^\gamma(x_1, t) = \hat{H}(\vec{r}_1, t) + \hat{G}^\gamma(x_1, t) \tag{2.6}$$

where

$$\hat{H}(\vec{r}_1, t) = -\frac{1}{2}\nabla_1^2 + V_A(\vec{r}_1, t) + V_M(\vec{r}_1, t) \tag{2.7}$$

is the core Hamiltonian operator with V_A the potential from the atomic core and V_M the potential from atomic cores in the solid; and

$$\hat{G}^\gamma(x_1, t) = \sum_i \int dx_2 \psi_i^*(x_2, t)\frac{1}{r_{12}}[1 - \mathcal{P}_{12}^\gamma]\psi_i(x_2, t) \tag{2.8}$$

is the electron Coulomb potential operator, where $\mathcal{P}_{12}^\gamma$ is the permutation operator exchanging electrons only between spin-orbitals of spin γ. Introducing a set of

time-dependent basis functions $\{\xi_\mu(\vec{r}, t)\}$, $\mu=1, 2, \ldots N_B$, the molecular orbital

is written as a linear combination of the basis functions so that

$$\phi_i^\gamma(\vec{r}, t) = \sum_\mu c_{i\mu}^\gamma(t)\xi_\mu(\vec{r}, t) \qquad\qquad i = 1, 2, \cdots \qquad (2.9)$$

where $c_{i\mu}^\gamma(t)$ is a time-dependent coefficient. The density matrix $\mathbf{P}$ is defined as

$$\hat{\rho}^\gamma = |\xi\rangle \mathbf{P}^\gamma \langle\xi| \qquad\qquad (2.10)$$

where $|\xi\rangle$ and $\langle\xi|$ are row and column matrices of ξ_μ orbitals, respectively. The

matrix element of $\mathbf{P}$ is [Pople and Beveridge, 70; Szabo and Ostlund, 82]

$$P_{\mu\nu}^\gamma(t) = \sum_{i \in occ} c_{i\mu}^{\gamma*}(t)c_{i\nu}^\gamma(t) \qquad\qquad (2.11)$$

The Fock matrix $\mathbf{F}^\gamma$ is defined as

$$\mathbf{F}^\gamma = \langle\xi|\hat{F}|\xi\rangle \qquad\qquad (2.12)$$

Inserting equation (2.6) into the above definition we have

$$\mathbf{F}^\gamma = \mathbf{H} + \mathbf{G}^\gamma\left(\mathbf{P}^\gamma, \mathbf{P}^{\gamma'}\right) \qquad\qquad (2.13)$$

where

$$\mathbf{H} = \mathbf{K} + \mathbf{V}_A + \mathbf{V}_M \qquad\qquad (2.14)$$

is the core Hamiltonian matrix, $\mathbf{G}^\gamma$ the Hartree-Fock electron-electron interaction

matrix, $\mathbf{V}_A$ the atomic potential matrix and $\mathbf{V}_M$ the surface potential matrix. The

matrix elements of $\mathbf{F}^\gamma$ are

$$F_{\mu\nu}^\gamma(t) = H_{\mu\nu}(t) + \sum_{\lambda\sigma}\left\{ P_{\lambda\sigma}^\gamma(t)\langle\mu\nu||\lambda\sigma\rangle + P_{\lambda\sigma}^{\gamma'}(t)\langle\mu\nu|\lambda\sigma\rangle \right\} \qquad (2.15)$$

where γ' is the spin opposite to γ and

$$\langle \mu\nu || \lambda\sigma \rangle = \langle \mu\nu | \lambda\sigma \rangle - \langle \mu\sigma | \lambda\nu \rangle \qquad (2.16)$$

with

$$\langle \mu\nu | \lambda\sigma \rangle = \int d^3 r_1 d^3 r_2 \xi_\mu^*(\vec{r}_1, t) \xi_\nu^*(\vec{r}_2, t) \frac{1}{r_{12}} \xi_\lambda(\vec{r}_1, t) \xi_\sigma(\vec{r}_2, t) \qquad (2.17)$$

To derive the TDHF equation for the density matrix, let's define a matrix

$$\Omega = |\langle \xi | \frac{\partial}{\partial t} \xi \rangle \qquad (2.18)$$

Substitute (2.10) into (2.5), the left hand side is

$$\begin{aligned}
i\frac{\partial}{\partial t}\hat{\rho} &= i\frac{\partial}{\partial t}\{|\xi\rangle \mathbf{P}^\gamma \langle \xi|\} \\
&= i\left\{ \left(\frac{\partial}{\partial t}|\xi\rangle\right) \mathbf{P}^\gamma \langle \xi| + |\xi\rangle \frac{\partial}{\partial t}\mathbf{P}^\gamma \langle \xi| + |\xi\rangle \mathbf{P}^\gamma \frac{\partial}{\partial t}\langle \xi| \right\}
\end{aligned} \qquad (2.19)$$

and the right hand side is

$$\hat{F}^\gamma \hat{\rho}^\gamma - \hat{\rho}^\gamma \hat{F}^\gamma = \hat{F}^\gamma |\xi\rangle \mathbf{P}^\gamma \langle \xi| - |\xi\rangle \mathbf{P}^\gamma \langle \xi| \hat{F}^\gamma \qquad (2.20)$$

Multiply this equation by $\langle \xi|$ from the left and by $|\xi\rangle$ from the right, we have

$$i\Omega \mathbf{P}^\gamma \mathbf{S} + i\mathbf{S}\dot{\mathbf{P}}^\gamma \mathbf{S} + i\mathbf{S}\mathbf{P}^\gamma \Omega^\dagger = \mathbf{F}^\gamma \mathbf{P}^\gamma \mathbf{S} - \mathbf{S}\mathbf{P}^\gamma \mathbf{F}^\gamma \qquad (2.21)$$

where $\mathbf{S} = \langle \xi | \xi \rangle$ is the overlap matrix. Multiply both sides of the above equation by $\mathbf{S}^{-1}$ we obtain the time-dependent Hartree-Fock equation for the density matrix

$$i\dot{\mathbf{P}}^\gamma = \mathbf{S}^{-1}\mathbf{F}^\gamma\mathbf{P}^\gamma - \mathbf{P}^\gamma\mathbf{F}^\gamma\mathbf{S}^{-1} - i\mathbf{S}^{-1}\Omega\mathbf{P}^\gamma - i\mathbf{P}^\gamma\Omega^\dagger\mathbf{S}^{-1} \qquad (2.22)$$

The last two terms on the right hand side of Eq. (2.22) arise from the time-dependence of the basis functions.

2.3 TDMOs as Linear Combinations of Travelling Atomic Orbitals

When the molecular orbitals are expanded in a basis set of atomic functions, it sometimes introduces artificial couplings at large distance which originates in the dependence of the atomic orbitals on the position of the moving nuclei [Bates and McCarroll, 1958]. To avoid this one can choose the atomic basis functions in the form of travelling atomic orbitals (TAO). We choose ξ_μ to be a travelling atomic orbital (TAO) associated with the mth center at $\vec{R}_m(t)$,

$$\xi_\mu(\vec{r}, t) = \chi_\mu\left[\vec{r} - \vec{R}_m(t)\right] T_m(\vec{r}, t) \tag{2.23}$$

where $\vec{r}$ is the position vector with respect to the origin of the reference frame, χ_μ is the atomic orbital centered at $\vec{R}_m(t)$ and the translation factor $T_m(\vec{r}, t)$ is defined by

$$T_m(\vec{r}, t) = exp\left[im_e\left(\vec{v}_m \cdot \vec{r} - \int_{t_{in}}^{t} \frac{|\vec{v}_m|^2}{2} dt'\right)\right] \tag{2.24}$$

where m_e is the electron mass and $\vec{v}_m = d\vec{R}_m/dt$ is the local velocity of the mth center in a space-fixed system. Thus,

$$\frac{\partial}{\partial t}|\xi_\nu\rangle = \left(\frac{\partial}{\partial t}\right)_{\vec{R}_n}|\xi_\nu\rangle + \vec{v}_n \cdot \vec{\nabla}_n|\xi_\nu\rangle \tag{2.25}$$

and

$$\begin{aligned}\Omega_{\mu\nu} &= \langle\xi_\mu|\frac{\partial}{\partial t}\xi_\nu\rangle \\ &= \langle\xi_\mu|\left(\frac{\partial}{\partial t}\right)_{\vec{R}_n}\xi_\nu\rangle + \langle\xi_\mu|\left(\vec{v}_n \cdot \vec{\nabla}\right)\xi_\nu\rangle\end{aligned} \tag{2.26}$$

Using (2.22) we find

$$\Omega_{\mu\nu} = -im_e\frac{|\vec{v}_n|^2}{2}S_{\mu\nu} + \langle\chi_\mu|T_m^*T_n\left(\vec{v}_n \cdot \vec{\nabla}_n\right)|\chi_\nu\rangle \tag{2.27}$$

where

$$\langle \chi_\mu | T_m^* T_n \left(\vec{v}_n \cdot \vec{\nabla}_n \right) | \chi_\nu \rangle$$
$$= \int d^3 r \chi_\mu^*(\vec{r}) T_m^*(\vec{r}) T_n(\vec{r}) \left[\left(\vec{v}_n \cdot \vec{\nabla}_n \right) \chi_\nu(\vec{r}) \right] \tag{2.28}$$

Noticing that $\vec{\nabla} | \chi_\nu \rangle = -\vec{\nabla}_n | \chi_\nu \rangle$, the kinetic energy matrix in this basis is

$$\langle \xi_\mu | K | \xi_\nu \rangle = -\langle \xi_\mu | -\frac{1}{2} \nabla^2 | \xi_\nu \rangle$$
$$= \frac{m_e |\vec{v}_n|^2}{2} S_{\mu\nu} + i \langle \chi_\mu | T_m^* T_n \left(\vec{v}_n \cdot \vec{\nabla}_n \right) | \chi_\nu \rangle + \langle \chi_\mu | \tilde{K} | \chi_\nu \rangle \tag{2.29}$$
$$= i\Omega_{\mu\nu} + \tilde{K}_{\mu\nu}$$

where Eq. (2.26) has been used and

$$\tilde{K}_{\mu\nu} = \langle \chi_\mu | \tilde{K} | \chi_\nu \rangle = \int d^3 r \, T_m^*(\vec{r}, t) T_n(\vec{r}, t) \, \chi_\mu(\vec{r}, t) \hat{K} \chi_\nu(\vec{r}, t) \tag{2.30}$$

Substituting Eq. (2.30) into Eq. (2.22) it becomes

$$i\dot{\mathbf{P}}^\gamma = \mathbf{S}^{-1} \tilde{\mathbf{F}}^\gamma \mathbf{P}^\gamma - \mathbf{P}^\gamma \tilde{\mathbf{F}}^{\gamma\dagger} \mathbf{S}^{-1} \tag{2.31}$$

with a modified Fock-like matrix

$$\tilde{\mathbf{F}}^\gamma = \tilde{\mathbf{H}} + \mathbf{G}^\gamma \tag{2.32}$$

where

$$\tilde{\mathbf{H}} = \tilde{\mathbf{K}} + \mathbf{V}_A + \mathbf{V}_M \tag{2.33}$$

Equation (2.31) is our basic equation. It appears in a simpler form in the TAO basis, but the price paid is that the matrix $\tilde{\mathbf{F}}^\gamma$ is no longer Hermitian.

This equation can be solved numerically if the nuclear trajectory is known, which may or may not include the effect of the coupling between the electron

and nuclear degrees of freedom. In the eikonal treatment, this equation should be solved with the equations of motion for nuclei simultaneously. Runge et al. [Runge et al., 90] have applied this method to charge transfer in the collision between a hydrogen atom and a proton.

So far, we have put no restrictions on the choice of basis functions except that the functions are localized at certain centers of the system. In Chapter 6 we will discuss in detail the choice of basis functions, which is a key part to our approach for handling extended systems.

CHAPTER 3
AVERAGE ELECTRONIC POPULATIONS, ELECTRIC MULTIPOLES AND ORBITAL POLARIZATION

One of the parameters which characterizes scattering phenomena is the cross section, which has the dimension of area and, roughly speaking, measures the size of electron clouds. The total cross section and the differential cross section for state to state transitions can be measured in experiments and provide fundamental information about excitation mechanisms. Thus extensive efforts have been made to develop theories and methods to calculate the cross section. On the other hand, during collisions with targets, absorption of energy will excite atoms to various states which can be anisotropic. Electron clouds not only change their sizes but also change their shapes and rotations, which is termed orbital polarization. The shape change and rotation of the electron cloud are characterized by alignment and orientation. Recent advances in experimental techniques have made it possible to completely determine the states of scattered atoms. For example, in the H^+-H experiment [Hippler et al., 86], H experiences a 2s to 2p excitation and the distribution of electrons on $m=1$ and $m=-1$ states varies with the collision energy. The orbital polarization reflects some of the specific and subtle aspects of the collision processes which can not be fully unveiled in the cross section study. Obviously, knowledge of orbital polarization properties can offer a deeper insight

into the collision mechanism and a more detailed understanding of the dynamics of collisions. Such a study will also provide a sensitive test to the scattering theories and models.

The density matrix method has been proved to be a powerful tool in investigations of orbital polarization in scatterings [Fano and Macek, 73; Andersen, 87; Hippler et al., 86]. Using the language of the density matrix, the diagonal elements are related to the cross section, and the off-diagonal elements contain the information about the shape and rotation of the electron cloud. Usually, the density matrix is constructed to calculate the orbital polarization parameters for the electron cloud associated with the scattered atom. In this way one assumes that the electron cloud contains only the electrons in the orbitals of the scattered atoms and that the contribution from the target electrons is excluded. Such an approach is suitable for most experimental situations where the scattered atoms are detected far away from the target but before or in the course of decaying from their excited states. However, at short or medium distances, the atomic orbitals are mixed with the surface orbitals and the electron cloud associated with the atom contains also the contribution from the surface electrons. The above approach does not seem satisfactory from our theoretical point of view, since we are interested in following the time evolution of the electron cloud which requires to describe the orbital polarization of the atom at all distances. The definitions of the orbital polarization parameters should be consistent with that for an isolated atom as the distance between the atom and the surface becomes infinitely large.

In this Chapter, we use the electronic density matrix to define parameters characterizing the orbital polarization. Unlike other studies [Fano and Macek, 73; Nielsen and Andersen, 87], we start with the electronic density matrix of the full system, i.e., the atom plus the surface, and then define the orbital parameters for a subsystem which either is the scattered atom alone or is a molecular complex containing the atom and a part of the surface. Because the mixing between the atomic orbitals and the surface orbitals are taken into account, the electron cloud associated with the scattered atom contains also the contribution from the surface electrons. This permits us to examine the evolution of the electron cloud and gives a dynamic picture of the orbital polarization at all the distances during the collision. As the distance between the atom and the surface becomes very large, the contribution from the surface electrons becomes insignificant and our polarization parameters for the atom orbitals are asymptotically equal to those defined in other approaches.

In Section 3.1, we describe two coordinate systems: the collision frame and the natural frame. The collision frame seems suitable to describe the scattering; the natural frame is more convenient to picture orbital polarization. In Section 3.2, using coordinate tensor operators, we define electric multipoles which provide a picture of the spacial distribution of the electron cloud. In Section 3.3, the alignment and orientation parameters are defined by use of the irreducible tensor operators and expressed them in terms of the density matrix. In Section 3.4, the polarization parameters are defined for a subsystem which contains either the

scattered atom alone or the atom plus a small part of the surface. This is useful for comparison with experimental data from spectroscopies. The connection between the orbital polarization parameters for a subsystem and that for an isolated atom is discussed.

3.1 Coordinate Frames

Since symmetry plays an essential role in the study of scatterings and orbital polarization, it is the first thing one should look at when choosing a coordinate frame. Let's consider the symmetry of the p-orbitals. The three eigenfunctions of the angular momentum operator for $J=1$, $|p_{+1}\rangle$, $|p_0\rangle$ and $|p_{-1}\rangle$ correspond to the magnetic quantum number $m=1$, 0 and -1 respectively. We can also use three real p-orbital functions $|p_x\rangle$, $|p_y\rangle$ and $|p_z\rangle$ which are symmetric along x-, y- and z-axes respectively. The orbital $|p_z\rangle = |p_0\rangle$ has a negative reflection symmetry with respect to the X-Y plan and others have positive reflection symmetry.

The collision plane is determined by the incoming velocity vector $\vec{v}_{in}$ and outgoing velocity vector $\vec{v}_{out}$ of the projectile. For an atom-surface collision, the collision plane is perpendicular to the solid surface. The collision frame (X_c, Y_c, Z_c) is defined such that the X_c-Z_c plane coincides with the collision plane with the Z_c axis perpendicular to the surface and that the X_c axis parallel to the surface, and the X_c-Y_c plane coincides with the solid surface with the Y_c axis perpendicular to the collision plane, see Fig. 1. Because many collision systems have certain type of symmetry about the Z_c axis or with respect to the collision plane, this frame is convenient for collision problems [Andersen, 86].
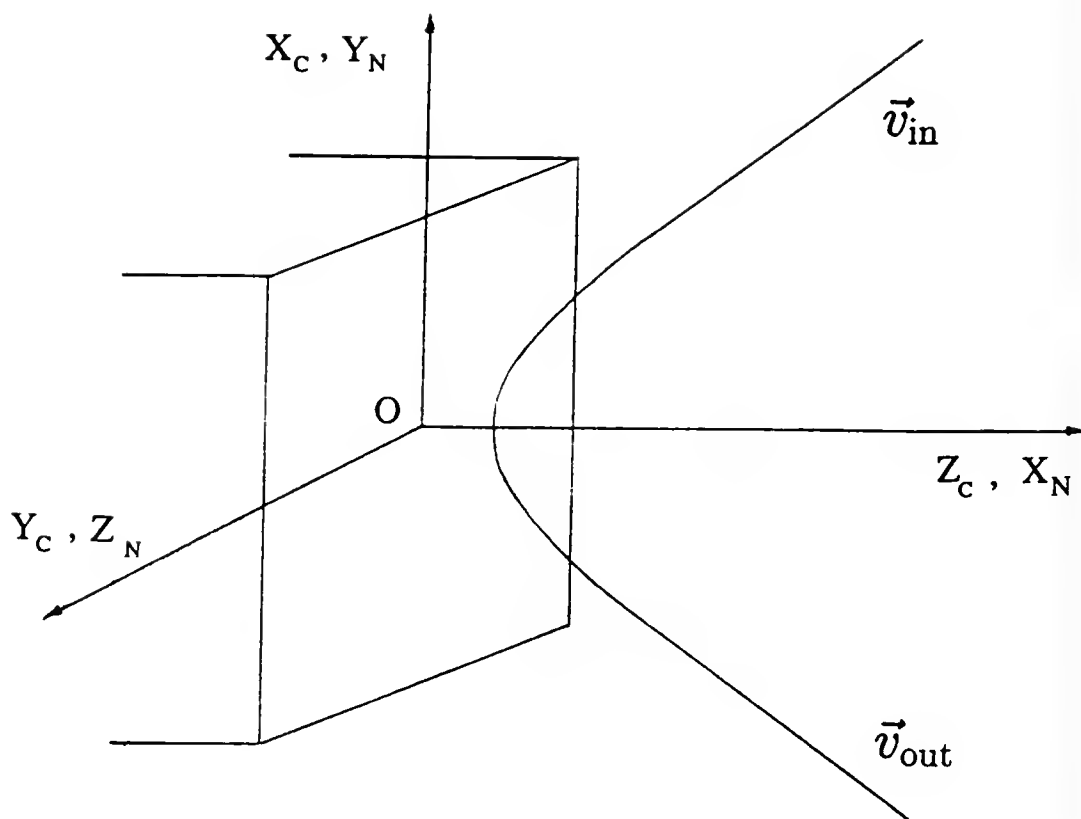
Figure 1.1. The coordinate frames used for the description of orbital polarization of the electron cloud. The collision frame (X_c, Y_c, Z_c) and the natural frame (X_n, Y_n, Z_n) are shown. The incoming velocity vector $\vec{v}_{in}$ and the outgoing velocity vector $\vec{v}_{out}$ are in the collision plane which is perpendicular to the solid surface and coincides with the X_c-Z_c plane of the collision frame and the X_n-Y_n plane of the natural frame.

In the natural frame (X_n, Y_n, Z_n), as shown in Fig. 1.1, the X_n-Y_n plane is in the collision plane with the X_n axis perpendicular to the solid surface, the Y_n-Z_n plane coincides with the solid surface with the Z_n axis perpendicular to the collision plane. This frame seems to be "natural" to the analysis of the angular momentum transfer and orbital polarization, since the expectation value of the z-component of angular momentum is related to the orientation and alignment [Andersen, 86].

3.2 Electric Multipoles

One way to describe the shape of the electron cloud is to consider its electric multipoles. For this purpose we introduce a set of tensor operators in the Cartesian coordinates,

$$
\begin{aligned}
I^{(0)} &= 1 \\
I_i^{(1)} &= r_i \\
I_{ij}^{(2)} &= r^2 \delta_{ij} - 3r_i r_j \\
&\ \ \vdots
\end{aligned}
\tag{3.1}
$$

where i, j=x, y, z, and the super indices in the parentheses indicate the ranks of the tensor operators. The electric multipoles are defined as

$$
\mathbf{P}^{(k)} = \langle \mathbf{I}^{(k)} \rangle
\tag{3.2}
$$

where $\mathbf{I}^{(k)}$ represents the tensor operator defined in Equation (3.1), and the symbol $< >$ indicates the ensemble average which can be expressed in terms of the density

operator $\hat{\rho}$ and the electronic density matrix $\mathbf{P}^\gamma$ in a basis set $\{\xi_\mu\}$

$$\langle \mathbf{I}^{(k)} \rangle = \frac{\text{Tr}\left(\hat{\rho}\mathbf{I}^{(k)}\right)}{\text{Tr}(\hat{\rho})} = \frac{\sum_\gamma \sum_{\mu\nu} P^\gamma_{\mu\nu} \left(\mathbf{I}^{(k)}\right)_{\nu\mu}}{\sum_\gamma \sum_{\mu\nu} P^\gamma_{\mu\nu} S_{\nu\mu}} \tag{3.3}$$

where the trace is over both orbital indices μ, ν and spin index γ, and $S_{\mu\nu}$ is the overlap matrix element in this basis. The denominator

$$\text{Tr}(\hat{\rho}) = \sum_\gamma \sum_{\mu\nu} \mathrm{P}^\gamma_{\mu\nu} S_{\nu\mu} = \sum_\gamma n^\gamma = n \tag{3.4}$$

is the total electronic population, and

$$n^\gamma = \sum_{\mu\nu} \mathrm{P}^\gamma_{\mu\nu} S_{\nu\mu} \tag{3.5}$$

is the average electronic population for spin γ.

The electric multipoles contain the information about the spacial distribution of the electron cloud. For $k=0$, $P^{(0)} = 1$. For $k > 0$,

$$P_i^{(1)} = \frac{\text{Tr}(\hat{\rho}\mathrm{r_i})}{\text{Tr}(\hat{\rho})} = \frac{1}{n} \sum_\gamma \sum_{\mu\nu} \mathrm{P}^\gamma_{\mu\nu} (\mathrm{r_i})_{\nu\mu} \tag{3.6}$$

is the component of the dipole moment $\vec{\mathrm{P}}$ (since the electron mass is 1 au) and

$$P_{ij}^{(2)} = \frac{\text{Tr}\left[\hat{\rho}\left(\mathrm{r}^2\delta_{ij} - 3\mathrm{r_i}\mathrm{r_j}\right)\right]}{\text{Tr}[\hat{\rho}]} = \frac{1}{n} \sum_\gamma \sum_{\mu\nu} P^\gamma_{\mu\nu} \left(\mathrm{r}^2\delta_{ij} - 3\mathrm{r_i}\mathrm{r_j}\right)_{\nu\mu} \tag{3.7}$$

is the component of the quadrupole tensor $\overset{\leftrightarrow}{\mathrm{I}}$ of the electron cloud.

The electric multipoles can be defined either in the collision frame or in the natural frame. It is also useful to define them in a body-fixed "atomic frame" centered at the scattered atom, in which the axes are along the major axes of the electron cloud and the quadrupole matrix appears diagonal.

3.3 Alignment and Orientation Parameters

Another way to analyze the orbital polarization is to examine the anisotropy of the distribution of the orbital angular momentum of the electron cloud. For the orbitals of certain total angular momentum J, if the distributions of the orbitals for all $|JM\rangle$ states are the same the cloud is isotropic; if the orbital distributions on these states are different, the cloud is said to be oriented; if the orbital distribution for $|JM\rangle$ and $|J-M\rangle$ are equal but differ for different magnetic number M the cloud is said to be aligned. To precisely describe these polarization properties, we define the orientation and alignment parameters through rotational moments [Fano and Macek, 73; Blum, 81].

Introduce a set of spherical irreducible tensor operators

$$J_0^{(0)} = 1$$

$$J_{\pm 1}^{(1)} = \mp \frac{1}{\sqrt{2}} J_{\pm}$$

$$J_0^{(1)} = J_z$$

$$J_{\pm 2}^{(2)} = \frac{1}{2} J_{\pm}^2 \tag{3.8}$$

$$J_{\pm 1}^{(2)} = \mp \frac{1}{2} J_{\pm}(2J_z \pm 1)$$

$$J_0^{(2)} = \frac{1}{\sqrt{6}} (3J_z^2 - J^2)$$

$$\vdots$$

where J is the angular momentum operator and J_z is its z-component, J_+ and J_- are the raising and lowing operators. The irreducible tensor operator $J_q^{(k)}$ satisfies

the following relations [Zare, 88]

$$\left[J_z, J_q^{(k)} \right] = q J_q^{(k)} \tag{3.9}$$

$$\left[J_\pm, J_q^{(k)} \right] = [k(k+1) - q(q+1)]^{\frac{1}{2}} J_{q\pm 1}^{(k)} \tag{3.10}$$

$$J_{\pm k}^{(k)} = \left[J_{\pm 1}^{(1)} \right]^k \tag{3.11}$$

We define the orientation vector $O_q^{(1)}$ and the alignment tensor $A_q^{(2)}$ as

$$O_q^{(1)}(J) = \frac{1}{\sqrt{J(J+1)}} Re \langle J_q^{(1)} \rangle \tag{3.12}$$

$$A_q^{(2)}(J) = \frac{\sqrt{6}}{\sqrt{J(J+1)}} Re \langle J_q^{(2)} \rangle \tag{3.13}$$

where $<>$ indicates the ensemble average for a given J. Using the density operator
and density matrix, the average of the irreducible operator can be written as

$$\langle J_q^{(k)} \rangle = \frac{\text{Tr}\left(\hat{\rho} J_q^{(k)} \right)}{\text{Tr}(\hat{\rho})} = \frac{1}{n} \sum_\gamma \sum_{\mu\nu} P_{\mu\nu}^\gamma \left(J_q^{(k)} \right)_{\nu\mu} \tag{3.14}$$

The vector $O_q^{(1)}(J)$ describes a preferred direction of angular momentum. The
tensor $A_q^{(2)}(J)$ describes the preferred spatial distribution of angular momentum
corresponding to each $|M|$. $O_0^{(1)}(J)$ is also called the orientation parameter. In the
natural frame, it is the measure of the average component of angular momentum
perpendicular to the collision plane, $J_\perp$.

The meaning of these parameters is more transparent and the calculation is easier in the natural frame. But some collision problems are more conveniently dealt with in the collision frame. One can first construct the electron density matrix in the collision frame and then calculate orientation and alignment parameters in the natural frame after a frame rotation.

The density matrix contains all the information on the electron states and can be used to define other parameter to describe the orbital polarization. For example, we can define the alignment angle $\alpha(J)$ which measures the angle between the major axis of the J component of the electron cloud and the X_n axis. Choosing the basis set such that $\mu = JM$, we define, for $J=1$ [Nielsen and Andersen, 87]

$$\alpha(1) = \frac{1}{2}\left[\pi + arg\left(P_{11,1\bar{1}}\right)\right] \tag{3.15}$$

and for $J=2$

$$\alpha(2) = \frac{1}{2}\left[\pi + arg\left(P_{22,20} + P_{20,2\bar{2}}\right)\right] \tag{3.16}$$

where $\bar{M} = -M$. We can also define, for $J>2$, the octupolar angle shift $\eta(J)$. For instance, for $J=2$

$$\eta(2) = \frac{1}{4}arg\left(P_{22,2\bar{2}}\right) - \alpha(2) \tag{3.17}$$

The parameters $L_{\perp}$, $\alpha(J)$ and $\eta(J)$ have practical meanings and can be compared with experimental date to test the theoretical model and methods used in obtaining the density matrix [Panev et. al., 87; Andersen et. al., 86].

3.4 Multipoles and Alignment and Orientation Parameters in a Subsystem

The parameters defined above describe the orbital polarization of the whole system. Sometimes we are more interested in the orbital polarization of a subsystem. For example, in atom-surface collision experiments, spectroscopies detect scattered atoms at the distances where the influence of the surface is negligible and only the polarization of the atomic orbitals is of interest. Even in the theoretical description of the collision states at short distance, only a small part of the surface should be taken into account, since the atom usually interacts mainly with a small region of the surface. Let's divide a system into a primary region and a secondary region which are labeled by p and s respectively. In the case of atom-surface collisions, the primary region can be chosen to contain the scattered atom and a small part of the surface and the interaction between the atomic states and those in the secondary region is assumed to be small. In the natural frame the ensemble average of $J_q^{(k)}$ for the whole system can be written as

$$
\begin{aligned}
\langle J_q^{(k)} \rangle \sim \mathrm{Tr}\left(\rho J_q^{(k)}\right) &= \sum_\gamma \sum_\mu \sum_\nu P_{\mu\nu}^\gamma \left(J_q^{(k)}\right)_{\nu\mu} \\
&= \sum_\gamma \{ \sum_{\mu\in p} \sum_{\nu\in p} P_{\mu\nu}^\gamma \left(J_q^{(k)}\right)_{\nu\mu} + \sum_{\mu\in p} \sum_{\nu\in s} P_{\mu\nu}^\gamma \left(J_q^{(k)}\right)_{\nu\mu} \\
&\quad + \sum_{\mu\in s} \sum_{\nu\in p} P_{\mu\nu}^\gamma \left(J_q^{(k)}\right)_{\nu\mu} + \sum_{\mu\in s} \sum_{\nu\in s} P_{\mu\nu}^\gamma \left(J_q^{(k)}\right)_{\nu\mu} \}
\end{aligned}
\tag{3.18}
$$

The last term comes from the secondary region and is not of interest. The second and third terms contains the mixing between the primary region and the secondary region.

Because we are interested in the orbital polarization of the scattered atom we define a set of irreducible operators

$$L_0^{(0)} = 1$$

$$L_{\pm 1}^{(1)} = \mp \frac{1}{\sqrt{2}} L_{\pm}$$

$$L_0^{(1)} = L_z$$

$$L_{\pm 2}^{(2)} = \frac{1}{2} L_{\pm}^2 \qquad\qquad (3.19)$$

$$L_{\pm 1}^{(2)} = \mp \frac{1}{2} L_{\pm}(2L_z \pm 1)$$

$$L_0^{(2)} = \frac{1}{\sqrt{6}}(3L_z^2 - L^2)$$

$$\vdots$$

where L is the orbital angular momentum of the scattered atom, L_z its z-component, and L_+ and L_- the raising and lowing operators. The average of $L_q^{(k)}$ is

$$\langle L_q^{(k)} \rangle = \frac{\mathrm{Tr}_A\left(\hat{\rho} L_q^{(k)}\right)}{\mathrm{Tr}_A(\hat{\rho})} = \frac{1}{n_A} \sum_\gamma \sum_{\mu \in A} \sum_{\nu \in p} P_{\mu\nu}^\gamma \left(L_q^{(k)}\right)_{\nu\mu} \qquad (3.20)$$

where trace is over the subspace of atomic states, and

$$n_A = \mathrm{Tr}_A(\hat{\rho}) = \sum_\gamma \sum_{\mu \in A} \sum_{\nu \in p} P_{\mu\nu}^\gamma S_{\nu\mu} \qquad (3.21)$$

is the average electron population on the atom. The contribution to the electron cloud associated with the secondary region is not included since the mixing between the second region orbitals and the atomic states is small. In this way we can define the orientation and alignment parameters for the scattered atom as

$$O_q^{(1)}(L)_A = \frac{1}{\sqrt{L(L+1)}} Re\langle L_q^{(1)} \rangle \qquad (3.22)$$

$$A_q^{(2)}(L)_A = \frac{\sqrt{6}}{\sqrt{L(L+1)}} Re\langle L_q^{(2)}\rangle \qquad (3.23)$$

The alignment angle and octupolar angle shift can also be defined in the similar way. At small distance, the surface electrons contribute to the atomic orbital polarization. At large distance, mixing between the atomic orbitals and the surface orbitals becomes small and the summation of ν vanishes unless for $\nu \in A$, the polarization parameters are equal to those defined for an isolated atom.

CHAPTER 4
LINEARIZATION OF TDHF EQUATIONS

The TDHF equation developed in Chapter 2 can be solved straightforwardly only for simple systems requiring small basis sets. If the system is complicated, the TDHF equations can instead be solved by some linearization procedures. However, one has to be very careful when developing a linearization method for cases where the density matrix oscillates rapidly with time, such as in collisions accompanied by a charge transfer through a near-resonance process, since the solutions of the linearized TDHF may converge slowly or not converge at all.

In this chapter, we describe a local time linearization procedure for solving the TDHF equations for the near-resonance charge transfer process. It tackles the rapid variation of the density matrix by defining a time-dependent reference density matrix $P^{0\gamma}(t)$. In section 4.1, we develop the local time linearization procedure for a general case and obtain a linearized equation for $P^{0\gamma}(t)$, which is a solution for $P(t)$ when the ion position is fixed in space, and a linearized equation for matrix $Q^{\gamma}(t)$, which is the first order change of the density matrix due to the time-dependent perturbation caused by the nuclear motion. The formal solutions for $P^{0\gamma}(t)$ and $Q^{\gamma}(t)$ are obtained with use of an exponential transformation. In section 4.2, we apply this procedure to a system in which the electron-electron

Coulomb interaction is ignored. For this special case, the coefficient matrices in the equations of $\mathbf{P}^{0\gamma}(t)$ and $\mathbf{Q}^{\gamma}(t)$ are time independent and the analytical solutions can be obtained.

4.1 The Linearization Procedure

In a collision which involves charge transfer through a near-resonance process, electrons jump back and forth among several close energy levels and this leads to a rapid oscillation of the density matrix. In the contrast, the change of the density matrix under the time-dependent perturbation caused by the motion of the nuclei is relatively slow. We separate the two time scales in what follows.

For a small time interval $t_0 \leq t \leq t_1$, we define a matrix $\mathbf{P}^{0\gamma}(t)$ to satisfy the equation

$$i\dot{\mathbf{P}}^{0\gamma}(t) = \mathbf{S}_0^{-1}\tilde{\mathbf{F}}_0^{\gamma}\mathbf{P}^{0\gamma}(t) - \mathbf{P}^{0\gamma}(t)\tilde{\mathbf{F}}_0^{\gamma\dagger}\mathbf{S}_0^{-1} \qquad (4.1)$$

and the initial condition $\mathbf{P}^{0\gamma}(t_o) = \mathbf{P}^{\gamma}(t_o)$, with $\tilde{\mathbf{F}}_0^{\gamma} = \tilde{\mathbf{F}}^{\gamma}(t_o)$ and $\mathbf{S}_0 = \mathbf{S}(t_o)$. Hence $\mathbf{P}^{0\gamma}(t)$ can be interpreted as a solution of the TDHF equation when the ion nuclei are fixed at $\vec{R}_A(t_0)$. The evolution $\mathbf{P}^{0\gamma}(t)$ oscillates with time reflecting the charge transfer among the energy levels with frequencies proportional to the inverses of the energy differences of energy levels. On the other hand, if the time interval is small, the change of the density matrix due to the nuclear motion is small. To get a linearized equation for the this change, we define

$$\mathbf{Q}^{\gamma}(t) = \mathbf{P}^{\gamma}(t) - \mathbf{P}^{0\gamma}(t) \qquad (4.2)$$

$$\Delta \mathbf{S}^{-1}(t) = \mathbf{S}^{-1}(t) - \mathbf{S}_0^{-1} \tag{4.3}$$

and

$$\Delta \tilde{\mathbf{F}}^\gamma(t) = \tilde{\mathbf{F}}^\gamma(t) - \tilde{\mathbf{F}}_0^\gamma \tag{4.4}$$

From (2.32) we have

$$\Delta \tilde{\mathbf{F}}(t) = \Delta \tilde{\mathbf{H}} + \Delta_e \mathbf{G}^\gamma(t) + \Delta_n \mathbf{G}^\gamma(t) \tag{4.5}$$

The matrices $\Delta_e \mathbf{G}$ and $\Delta_n \mathbf{G}$ are related to the electron-electron interaction and are given by

$$\Delta_e G_{\mu\nu}^\gamma(t) = \sum_{\kappa\lambda} Q_{\kappa\lambda}^\gamma(t)(\mu\nu||\kappa\lambda)_{t_0} + Q_{\kappa\lambda}^{\gamma'}(t)(\mu\nu|\kappa\lambda)_{t_0} \tag{4.6}$$

and

$$\Delta_n G_{\mu\nu}^\gamma(t) = \sum_{\kappa\lambda} P_{\kappa\lambda}^{0\gamma}(t)\Delta(\mu\nu||\kappa\lambda)_t + P_{\kappa\lambda}^{0\gamma'}(t)\Delta(\mu\nu|\kappa\lambda)_t \tag{4.7}$$

where $(\mu\nu|\kappa\lambda)_t$ and $(\mu\nu||\kappa\lambda)_t$ are the Coulomb and Coulomb symmetrized 2–electron integrals respectively when the scattering atomic core is at $\vec{R}_A(t)$. Inserting Eqs. (4.1)—(4.5) into Eq. (2.31), we obtain to first order in $\mathbf{Q}^\gamma(t)$,

$$\begin{aligned}
i\dot{\mathbf{Q}}^\gamma(t) &= \mathbf{S}_0^{-1}\tilde{\mathbf{F}}_0^\gamma \mathbf{Q}^\gamma(t) - \mathbf{Q}^\gamma(t)\tilde{\mathbf{F}}_0^{\gamma\dagger}\mathbf{S}_0^{-1} \\
&\quad + \mathbf{S}_0^{-1}\Delta\tilde{\mathbf{H}}(t)\mathbf{P}^{0\gamma}(t) - \mathbf{P}^{0\gamma}(t)\Delta\tilde{\mathbf{H}}(t)^\dagger\mathbf{S}_0^{-1} \\
&\quad + \mathbf{P}^{0\gamma}(t)\tilde{\mathbf{F}}_0^{\gamma\dagger}\Delta\mathbf{S}^{-1}(t) - \Delta\mathbf{S}^{-1}(t)\tilde{\mathbf{F}}_0^\gamma\mathbf{P}^{0\gamma}(t) \\
&\quad + \mathbf{S}_0^{-1}\Delta_e\mathbf{G}^\gamma(t)\mathbf{P}^{0\gamma}(t) - \mathbf{P}^{0\gamma}(t)\Delta_e\mathbf{G}^\gamma(t)^\dagger\mathbf{S}_0^{-1} \\
&\quad + \mathbf{S}_0^{-1}\Delta_n\mathbf{G}^\gamma(t)\mathbf{P}^{0\gamma}(t) - \mathbf{P}^{0\gamma}(t)\Delta_n\mathbf{G}^\gamma(t)^\dagger\mathbf{S}_0^{-1}
\end{aligned} \tag{4.8}$$

To introduce a shorthand notation, we use a double index notation to replace the single index notation in the following. Let upper case Roman letters refer to double indices, then, $K = (\mu\nu)$ and $L = (\kappa\lambda)$. With this notation, matrices $\mathbf{P}^{0\gamma}$, $\mathbf{Q}^{\gamma}$, $\Delta_e\mathbf{G}^{\gamma}$ and $\Delta_n\mathbf{G}^{\gamma}$ become column matrices $\mathcal{P}^{0\gamma}$, $\mathcal{Q}^{\gamma}$, $\Delta_e\mathcal{G}$ and $\Delta_n\mathcal{G}$. Defining two square double index matrices $\mathcal{X}(t)$ and $\mathcal{Y}(t)$ such that

$$\mathcal{X}_{KL}(t) = X_{\mu\nu,\kappa\lambda}(t) = (\mu\nu||\kappa\lambda)_t \tag{4.9}$$

$$\mathcal{Y}_{KL}(t) = Y_{\mu\nu,\kappa\lambda}(t) = (\mu\nu|\kappa\lambda)_t \tag{4.10}$$

we can rewrite Eqs. (4.6) and (4.7) as

$$\Delta_e\mathcal{G}_K^{\gamma}(t) = \sum_L [\mathcal{X}_{0KL}\mathcal{Q}_L^{\gamma}(t) + \mathcal{Y}_{0KL}\mathcal{Q}_L^{\gamma'}(t)] \tag{4.11}$$

$$\Delta_n\mathcal{G}_K^{\gamma}(t) = \sum_L [\Delta\mathcal{X}_{KL}\mathcal{P}_L^{0\gamma}(t) + \Delta\mathcal{Y}_{KL}\mathcal{P}_L^{0\gamma'}(t)] \tag{4.12}$$

or in the matrix form,

$$\Delta_e\mathcal{G}^{\gamma} = \mathcal{X}_0\mathcal{Q}^{\gamma} + \mathcal{Y}_0\mathcal{Q}^{\gamma'} \tag{4.13}$$

$$\Delta_n\mathcal{G}^{\gamma} = \Delta\mathcal{X}\,\mathcal{P}^{0\gamma} + \Delta\mathcal{Y}\,\mathcal{P}^{0\gamma'} \tag{4.14}$$

where $\mathcal{X}_0 = \mathcal{X}(t_o)$, $\mathcal{Y}_0 = \mathcal{Y}(t_o)$ and

$$\Delta\mathcal{X} = \mathcal{X}(t) - \mathcal{X}_0 \tag{4.15}$$

$$\Delta \mathcal{Y} = \mathcal{Y}(t) - \mathcal{Y}_0 \tag{4.16}$$

Taking advantage of using the double index notation, the linearized TDHF equations (4.1) and (4.8) can be written in a neat form

$$i\dot{\mathcal{P}}^{0\gamma} = \mathcal{A}^{\gamma\gamma}\mathcal{P}^{0\gamma} + \mathcal{A}^{\gamma\gamma'}\mathcal{P}^{0\gamma'} - \mathcal{P}^{0\gamma}\mathcal{A}^{\gamma\gamma\dagger} - \mathcal{P}^{0\gamma'}\mathcal{A}^{\gamma'\gamma\dagger} \tag{4.17}$$

and

$$i\dot{\mathcal{Q}}^{\gamma} = \mathcal{A}^{\gamma\gamma}\mathcal{Q}^{\gamma} + \mathcal{A}^{\gamma\gamma'}\mathcal{Q}^{\gamma'} - \mathcal{Q}^{\gamma}\mathcal{A}^{\gamma\gamma\dagger} - \mathcal{Q}^{\gamma'}\mathcal{A}^{\gamma'\gamma\dagger} + \mathcal{D}^{\gamma} \tag{4.18}$$

where $\mathcal{A}^{\gamma\gamma}$ and $\mathcal{A}^{\gamma\gamma'}$ are square matrices in double index notation or four index matrices in single index notation,

$$\mathcal{A}^{\gamma\gamma}_{KL} = A^{\gamma\gamma}_{\mu\nu,\kappa\lambda} = \sum_{\zeta\eta} S^{-1}_{0\mu\zeta} \left(\tilde{F}^{\gamma}_{0\zeta\eta} \delta_{\kappa\eta} \delta_{\lambda\nu} + X_{0\zeta\eta,\kappa\lambda} P^{0\gamma}_{\eta\nu} \right) \tag{4.19}$$

$$\mathcal{A}^{\gamma\gamma'}_{KL} = A^{\gamma\gamma'}_{\mu\nu,\kappa\lambda} = \sum_{\zeta\eta} S^{-1}_{0\mu\zeta} Y_{0\zeta\eta,\kappa\lambda} P^{0\gamma}_{\eta\nu} \tag{4.20}$$

and the column matrix $\mathcal{D}^{\gamma}$ is a driving term with elements

$$\mathcal{D}^{\gamma}_{K} = [\mathbf{S}_0^{-1}\left(\Delta\tilde{\mathbf{H}} + \Delta_n\mathbf{G}\right)\mathbf{P}^{0\gamma} - \mathbf{P}^{0\gamma}\left(\Delta\tilde{\mathbf{H}}^\dagger + \Delta_n\mathbf{G}^\dagger\right)\mathbf{S}_0^{-1}$$
$$+ \Delta\mathbf{S}^{-1}\tilde{\mathbf{F}}^{\gamma}_0\mathbf{P}^{0\gamma} - \mathbf{P}^{0\gamma}\tilde{\mathbf{F}}^{\dagger}_0\Delta\mathbf{S}^{-1}]_{\mu\nu} \tag{4.21}$$

If we collect $\mathcal{P}^{0\gamma}$ and $\mathcal{P}^{0\gamma'}$ into a column matrix $\mathcal{P}^0$, $\mathcal{Q}^{\gamma}$ and $\mathcal{Q}^{\gamma'}$ into a column matrix $\mathcal{Q}$, $\mathcal{D}^{\gamma}$ and $\mathcal{D}^{\gamma'}$ into a column matrix $\mathcal{D}$ and let

$$\mathcal{A} = \begin{pmatrix} \mathcal{A}^{\gamma\gamma} & \mathcal{A}^{\gamma\gamma'} \\ \mathcal{A}^{\gamma'\gamma} & \mathcal{A}^{\gamma'\gamma'} \end{pmatrix} \tag{4.22}$$

then Eqs. (4.17) and (4.18) become

$$i\dot{\mathcal{P}}^0 = \mathcal{A}\mathcal{P}^0 - \mathcal{P}^0\mathcal{A}^\dagger \tag{4.23}$$

and

$$i\dot{\mathcal{Q}} = \mathcal{A}\mathcal{Q} - \mathcal{Q}\mathcal{A}^\dagger + \mathcal{D} \tag{4.24}$$

These are the linearized TDHF equations for the density matrix in $t_0 \leq t \leq t_1$. It should be noted that the matrix $\mathcal{A}$ is generally time-dependent.

To solve the above equations, we let

$$\mathcal{U}(t,t_o) = T\left[exp\left\{-i\left[\int_{t_o}^{t} \mathcal{A}(t')dt'\right]\right\}\right] \tag{4.25}$$

$$\mathcal{U}(t,t_o)^\dagger = T\left[exp\left\{i\left[\int_{t_o}^{t} \mathcal{A}(t')^\dagger dt'\right]\right\}\right] \tag{4.26}$$

where $T\left[exp\{\int \cdots\}\right]$ denotes a time-ordered exponential expansion. We consider transformations

$$\mathcal{P}^0(t) = \mathcal{U}(t,t_o)\mathcal{P}^0_D(t)\mathcal{U}(t,t_o)^\dagger \tag{4.27}$$

and

$$\mathcal{Q}(t) = \mathcal{U}(t,t_o)\mathcal{Q}_D(t)\mathcal{U}(t,t_o)^\dagger \tag{4.28}$$

Replacing Eq. (4.27) into the left hand side of Eq. (4.23) and Eq. (4.28) into the left hand side of Eq. (4.24) we have

$$i\dot{\mathcal{P}}^0(t) = \mathcal{A}\mathcal{P}^0 - \mathcal{P}^0\mathcal{A}^\dagger + i\mathcal{U}(t,t_o)\dot{\mathcal{P}}^0_D(t)\mathcal{U}(t,t_o)^\dagger \tag{4.29}$$

and

$$i\dot{\mathcal{Q}}(t) = \mathcal{A}\mathcal{Q} - \mathcal{Q}\mathcal{A}^\dagger + i\mathcal{U}(t, t_0)\dot{\mathcal{Q}}_{\mathcal{D}}(t)\mathcal{U}(t, t_0)^\dagger \tag{4.30}$$

Comparing them with the right hand side of Eqs. (4.23) and (4.24), we obtain

$$i\dot{\mathcal{P}}_{\mathcal{D}}^0(t) = 0 \tag{4.31}$$

and

$$i\dot{\mathcal{Q}}_{\mathcal{D}}(t) = i\mathcal{U}(t, t_0)^{-1}\mathcal{D}(t)\left[\mathcal{U}(t, t_0)^\dagger\right]^{-1} \tag{4.32}$$

Their solutions are

$$\mathcal{P}_{\mathcal{D}}^0(t) = \mathcal{P}_{\mathcal{D}}^0(t_0) = \mathcal{P}^0(t_0) \tag{4.33}$$

and

$$\mathcal{Q}_{\mathcal{D}}(t) = \mathcal{Q}_{\mathcal{D}}(t_0) - i\int_{t_0}^{t} \mathcal{U}(t', t_0)^{-1}\mathcal{D}(t')[\mathcal{U}(t', t_0)^\dagger]^{-1}dt' \tag{4.34}$$

Using Eqs. (4.27) and (4.29) and noticing that $\mathcal{Q}(t_0) = 0$, we obtain the formal solutions for $\mathcal{P}^0(t)$ and $\mathcal{Q}(t)$

$$\mathcal{P}^0(t) = \mathcal{U}(t, t_0)^{-1}\mathcal{P}^0(t_0)\left[\mathcal{U}(t, t_0)^\dagger\right]^{-1} \tag{4.35}$$

and

$$\mathcal{Q}(t) = -i\mathcal{U}(t, t_0)\int_{t_0}^{t} \mathcal{U}(t', t_0)^{-1}\mathcal{D}(t')\left[\mathcal{U}(t', t_0)^\dagger\right]^{-1}dt'\mathcal{U}(t, t_0)^\dagger$$

$$= -i\int_{t_0}^{t} \mathcal{U}(t, t')\mathcal{D}(t')\mathcal{U}(t, t')^\dagger dt' \tag{4.36}$$

4.2 The Case without Electron-Electron Interaction

In this section, we will show the use of our linearization procedure by applying it to a special case where the electron-electron is ignored. In this case $\mathbf{G} = \mathbf{0}$ and $\tilde{\mathbf{F}} = \tilde{\mathbf{H}}$. Since the different spins are then uncorrelated, we return to the notation involving κ, λ, μ and ν, and drop the spin index γ to write Eqs. (4.23) and (4.24) as

$$i\dot{\mathbf{P}}^0(t) = \mathbf{W}\mathbf{P}^0(t) - \mathbf{P}^0(t)\mathbf{W}^\dagger \tag{4.37}$$

and

$$i\dot{\mathbf{Q}}(t) = \mathbf{W}\mathbf{Q}(t) - \mathbf{Q}(t)\mathbf{W}^\dagger + \mathbf{D}'(t) \tag{4.38}$$

where

$$\mathbf{W} = \mathbf{S}_0^{-1}\tilde{\mathbf{H}}_0 \tag{4.39}$$

$$\tilde{\mathbf{H}}_0 = \tilde{\mathbf{H}}(t_0) \tag{4.40}$$

$$\mathbf{D}'(t) = \mathbf{S}_0^{-1}\Delta\tilde{\mathbf{H}}(t)\mathbf{P}^0(t) - \mathbf{P}^0(t)\Delta\tilde{\mathbf{H}}^\dagger(t)\mathbf{S}_0^{-1}$$
$$+\mathbf{P}^0(t)\tilde{\mathbf{H}}_0^\dagger\Delta\mathbf{S}^{-1}(t) - \Delta\mathbf{S}^{-1}(t)\tilde{\mathbf{H}}_0\mathbf{P}^0(t) \tag{4.41}$$

Unlike in the general situation, the coefficient matrices $\mathbf{W}$ and $\mathbf{W}^\dagger$ are time-independent.

To solve this equation let us consider transformations

$$\mathbf{P}^0(t) = exp[-i\mathbf{W}(t - t_o)]\mathbf{P}_\mathbf{D}^0(t)exp\left[i\mathbf{W}^\dagger(t - t_o)\right] \tag{4.42}$$

and

$$\mathbf{Q}(t) = exp[-i\mathbf{W}(t - t_0)]\mathbf{Q_D}(t)exp\Big[i\mathbf{W}^\dagger(t - t_0)\Big] \qquad (4.43)$$

Inserting them into Eqs. (4.37) and (4.38) respectively, we get equations for $\mathbf{P_D}^0$ and $\mathbf{Q_D}$

$$i\dot{\mathbf{P}}_{\mathbf{D}}^0(t) = 0 \qquad (4.44)$$

and

$$i\dot{\mathbf{Q}}_{\mathbf{D}}(t) = exp[i\mathbf{W}(t - t_0)]\mathbf{D}(t)exp\Big[-i\mathbf{W}^\dagger(t - t_0)\Big] \qquad (4.45)$$

The latter has a solution of

$$\mathbf{Q_D}(t) = -i\int_{t_0}^{t} exp[i\mathbf{W}(t' - t_0)]\mathbf{D}'\Big(t'\Big)exp\Big[-i\mathbf{W}^\dagger(t' - t_0)\Big]dt' \qquad (4.46)$$

since $\mathbf{Q_D}(t_0) = 0$. From the above equations we can write the formal solutions for $\mathbf{P}^0$ and $\mathbf{Q}$

$$\mathbf{P}^0(t) = exp[-i\mathbf{W}(t - t_0)]\mathbf{P}^0(t_0)exp\Big[i\mathbf{W}^\dagger(t - t_0)\Big] \qquad (4.47)$$

and

$$\mathbf{Q}(t) = -i\int_{t_0}^{t} exp\Big[-i\mathbf{W}\Big(t - t'\Big)\Big]\mathbf{D}'\Big(t'\Big)exp\Big[i\mathbf{W}^\dagger\Big(t - t'\Big)\Big]dt' \qquad (4.48)$$

We assume that the matrix $\mathbf{W}$ can be diagonalized by a linear transformation, that is, there exists a matrix $\mathbf{L}$ such that,

$$\mathbf{W} = \mathbf{L}\mathbf{w}\mathbf{L}^{-1} \qquad (4.49)$$

where **w** is a diagonal matrix. Then

$$Q_{\mu\nu}(t) = -i \sum_{kl} L_{\mu k} \left[\sum_{\lambda\rho} \left(\mathbf{L}^{-1}\right)_{k\lambda} \Gamma_{k\lambda\rho l}(t,t_0) \left(\mathbf{L}^{-1}\right)^{\dagger}_{\rho l} \right] L^{\dagger}_{l\nu} \qquad (4.50)$$

where

$$\Gamma_{k\lambda\rho l}(t,t_0) = \int_{t_0}^{t} exp\big[-i(w_k - w_l^*)(t-t')\big] D_{\lambda\rho}(t')dt' \qquad (4.51)$$

The formalism developed in this section can be directly applied to systems with a few electrons. We have used it to calculated charge transfer in H+H⁺ collisions [Runge et al., 90]. However, it must be modified when applied to extended systems. In Chapter 6 we describe a partitioning procedure which simplifies the treatment of the scattering of atoms by surfaces.

CHAPTER 5
PARTITION OF EXTENDED SYSTEMS

For an ion-surface system which involve a great number of electrons, the TDHF equations obtained in Ch. 2 usually require a huge basis set. Some technique for truncating the system as well as the basis set must be developed to solve the equations.

Partitioning techniques have been used to treat various kinds of extended systems [Lowdin, 70; Ying 77; Williams et al, 82; Kirtman and de Melo 81; de Melo et al., 87; McDowell, 82, 85]. The main idea is to divide the system into two regions and to employ some relatively accurate treatments to deal with electronic interactions in a primary region, which is of main interest, while using certain approximations in a secondary region. The difference among a variety of methods is in the treatments of the secondary region and of the interaction between the two regions. For some systems the interaction between the two regions is small and the secondary region can be treated as a small perturbation. For other systems the secondary regions are often approximated by some simpler systems, for example, in studying Kondo effect [Kondo, 69; Heeger, 69; Anderson, 61], an approximation is to treat the conduction electrons surrounding isolated magnetic ions as a free electron sea.

For ion-surface systems, it has been found that, during collisions, electron rearrangement occurs mainly within local regions of surfaces [Grimley et al., 83; McDowell, 85]. Based on this observation we design a partitioning technique to truncate the ion-surface system into two parts and treat electronic interactions and electronic state evolution in these parts differently. This partitioning technique is suitable to deal with time-dependent processes in extended systems with a strong local coupling. It requires a set of localized basis functions, but does not depends on the concrete form of the functions. All the formal derivations in this chapter are done with localized basis functions which can be of any form.

In Section 5.1 we describe our partitioning method and derive the effective linearized TDHF equation for the density matrix in the primary region, which includes a driving term containing the coupling with the secondary region. In Section 5.2, we introduce an approximation to the secondary region and the couplings between the two regions, which enables us to solve the effective TDHF equations in the primary region. We apply this method to a simple case, where the electron-electron interaction is ignored, and obtain analytical solutions for the density matrix in the primary region.

5.1 Partition Procedure

We divide an ion-surface system into two regions: (i) the primary region that consists of the scattering ion and a small impact area of the surface, where the perturbation by the ion is strongly felt during the collision; (ii) the secondary region which consists of the remainder of the surface, where the influence of the

ion is assumed to be felt indirectly through the coupling between the electrons in the two parts of the surface. Considering a set of localized basis functions for the solid and the ion, and letting p be the index of the primary region and s the index of the secondary region, the matrix $\mathbf{P}^0$ is written as

$$\mathbf{P}^0 = \begin{pmatrix} \mathbf{P}^0_{pp} & \mathbf{P}^0_{ps} \\ \mathbf{P}^0_{sp} & \mathbf{P}^0_{ss} \end{pmatrix} \tag{5.1}$$

and other matrices are partitioned in a similar way. In the case where the electron-electron interaction is ignored, Eqs. (4.37) and (4.38) are then split into eight equations for $\mathbf{P}^0_{pp}(t)$, $\mathbf{P}^0_{ps}(t)$, $\mathbf{P}^0_{sp}(t)$, $\mathbf{P}^0_{ss}(t)$, $\mathbf{Q}_{pp}(t)$, $\mathbf{Q}_{ps}(t)$, $\mathbf{Q}_{sp}(t)$ and $\mathbf{Q}_{ss}(t)$

$$i\dot{\mathbf{P}}^0_{pp}(t) = \mathbf{W}_{pp}\mathbf{P}^0_{pp}(t) - \mathbf{P}^0_{pp}(t)\mathbf{W}^\dagger_{pp}$$
$$+ \mathbf{W}_{ps}\mathbf{P}^0_{sp}(t) - \mathbf{P}^0_{ps}(t)\mathbf{W}^\dagger_{sp} \tag{5.2}$$

$$i\dot{\mathbf{P}}^0_{ps}(t) = \mathbf{W}_{pp}\mathbf{P}^0_{ps}(t) - \mathbf{P}^0_{pp}(t)\mathbf{W}^\dagger_{ps}$$
$$+ \mathbf{W}_{ps}\mathbf{P}^0_{ss}(t) - \mathbf{P}^0_{ps}(t)\mathbf{W}^\dagger_{ss} \tag{5.3}$$

$$i\dot{\mathbf{P}}^0_{sp}(t) = \mathbf{W}_{sp}\mathbf{P}^0_{pp}(t) - \mathbf{P}^0_{sp}(t)\mathbf{W}^\dagger_{pp}$$
$$+ \mathbf{W}_{ss}\mathbf{P}^0_{sp}(t) - \mathbf{P}^0_{ss}(t)\mathbf{W}^\dagger_{sp} \tag{5.4}$$

$$i\dot{\mathbf{P}}^0_{ss}(t) = \mathbf{W}_{sp}\mathbf{P}^0_{ps}(t) - \mathbf{P}^0_{sp}(t)\mathbf{W}^\dagger_{ps}$$
$$+ \mathbf{W}_{ss}\mathbf{P}^0_{ss}(t) - \mathbf{P}^0_{ss}(t)\mathbf{W}^\dagger_{ss} \tag{5.5}$$

$$i\dot{\mathbf{Q}}_{pp}(t) = \mathbf{W}_{pp}\mathbf{Q}_{pp}(t) - \mathbf{Q}_{pp}(t)\mathbf{W}^\dagger_{pp}$$
$$+ \mathbf{W}_{ps}\mathbf{Q}_{sp}(t) - \mathbf{Q}_{ps}(t)\mathbf{W}^\dagger_{sp} + \mathbf{D}'_{pp}(t) \tag{5.6}$$

$$i\dot{\mathbf{Q}}_{ps}(t) = \mathbf{W}_{pp}\mathbf{Q}_{ps}(t) - \mathbf{Q}_{pp}(t)\mathbf{W}^\dagger_{ps}$$
$$+ \mathbf{W}_{ps}\mathbf{Q}_{ss}(t) - \mathbf{Q}_{ps}(t)\mathbf{W}^\dagger_{ss} + \mathbf{D}'_{ps}(t) \tag{5.7}$$

$$i\dot{\mathbf{Q}}_{\mathrm{sp}}(t) = \mathbf{W}_{\mathrm{sp}}\mathbf{Q}_{\mathrm{pp}}(t) - \mathbf{Q}_{\mathrm{sp}}(t)\mathbf{W}_{\mathrm{pp}}^{\dagger}$$
$$+ \mathbf{W}_{\mathrm{ss}}\mathbf{Q}_{\mathrm{sp}}(t) - \mathbf{Q}_{\mathrm{ss}}(t)\mathbf{W}_{\mathrm{sp}}^{\dagger} + \mathbf{D}_{\mathrm{sp}}'(t) \tag{5.8}$$

$$i\dot{\mathbf{Q}}_{\mathrm{ss}}(t) = \mathbf{W}_{\mathrm{sp}}\mathbf{Q}_{\mathrm{ps}}(t) - \mathbf{Q}_{\mathrm{sp}}(t)\mathbf{W}_{\mathrm{ps}}^{\dagger}$$
$$+ \mathbf{W}_{\mathrm{ss}}\mathbf{Q}_{\mathrm{ss}}(t) - \mathbf{Q}_{\mathrm{ss}}(t)\mathbf{W}_{\mathrm{ss}}^{\dagger} + \mathbf{D}_{\mathrm{ss}}'(t) \tag{5.9}$$

where $\mathbf{D}_{\mathrm{pp}}'(t)$, $\mathbf{D}_{\mathrm{ps}}'(t)$, $\mathbf{D}_{\mathrm{sp}}'(t)$ and $\mathbf{D}_{\mathrm{ss}}'(t)$ are the submatrices of $\mathbf{D}'(t)$ defined in Eq. (4.21). For example, the matrix $\mathbf{D}_{\mathrm{pp}}'(t)$ is given by

$$\mathbf{D}_{\mathrm{pp}}'(t) = \left(\mathbf{S}_0^{-1}\right)_{\mathrm{pp}}\Delta\tilde{\mathbf{H}}_{\mathrm{pp}}(t)\mathbf{P}_{\mathrm{pp}}^0(t) - \mathbf{P}_{\mathrm{pp}}^0(t)\Delta\tilde{\mathbf{H}}_{\mathrm{pp}}^{\dagger}(t)\left(\mathbf{S}_0^{-1}\right)_{\mathrm{pp}}$$
$$+ \left(\mathbf{S}_0^{-1}\right)_{\mathrm{pp}}\Delta\tilde{\mathbf{H}}_{\mathrm{ps}}(t)\mathbf{P}_{\mathrm{sp}}^0(t) - \mathbf{P}_{\mathrm{ps}}^0(t)\Delta\tilde{\mathbf{H}}_{\mathrm{sp}}^{\dagger}(t)\left(\mathbf{S}_0^{-1}\right)_{\mathrm{pp}}$$
$$+ \left(\mathbf{S}_0^{-1}\right)_{\mathrm{ps}}\Delta\tilde{\mathbf{H}}_{\mathrm{sp}}(t)\mathbf{P}_{\mathrm{pp}}^0(t) - \mathbf{P}_{\mathrm{pp}}^0(t)\Delta\tilde{\mathbf{H}}_{\mathrm{ps}}^{\dagger}(t)\left(\mathbf{S}_0^{-1}\right)_{\mathrm{sp}}$$
$$+ \left(\mathbf{S}_0^{-1}\right)_{\mathrm{ps}}\Delta\tilde{\mathbf{H}}_{\mathrm{ss}}(t)\mathbf{P}_{\mathrm{sp}}^0(t) - \mathbf{P}_{\mathrm{ps}}^0(t)\Delta\tilde{\mathbf{H}}_{\mathrm{ss}}^{\dagger}(t)\left(\mathbf{S}_0^{-1}\right)_{\mathrm{sp}}$$
$$+ \mathbf{P}_{\mathrm{pp}}^0(t)\tilde{\mathbf{H}}_{0\mathrm{pp}}^{\dagger}\left(\Delta\mathbf{S}^{-1}\right)_{\mathrm{pp}}(t) - \left(\Delta\mathbf{S}^{-1}\right)_{\mathrm{pp}}(t)\tilde{\mathbf{H}}_{0\mathrm{pp}}\mathbf{P}_{\mathrm{pp}}^0(t)$$
$$+ \mathbf{P}_{\mathrm{pp}}^0(t)\tilde{\mathbf{H}}_{0\mathrm{ps}}^{\dagger}\left(\Delta\mathbf{S}^{-1}\right)_{\mathrm{sp}}(t) - \left(\Delta\mathbf{S}^{-1}\right)_{\mathrm{ps}}(t)\tilde{\mathbf{H}}_{0\mathrm{sp}}\mathbf{P}_{\mathrm{pp}}^0(t)$$
$$+ \mathbf{P}_{\mathrm{ps}}^0(t)\tilde{\mathbf{H}}_{0\mathrm{sp}}^{\dagger}\left(\Delta\mathbf{S}^{-1}\right)_{\mathrm{pp}}(t) - \left(\Delta\mathbf{S}^{-1}\right)_{\mathrm{pp}}(t)\tilde{\mathbf{H}}_{0\mathrm{ps}}\mathbf{P}_{\mathrm{sp}}^0(t)$$
$$+ \mathbf{P}_{\mathrm{ps}}^0(t)\tilde{\mathbf{H}}_{0\mathrm{ss}}^{\dagger}\left(\Delta\mathbf{S}^{-1}\right)_{\mathrm{sp}}(t) - \left(\Delta\mathbf{S}^{-1}\right)_{\mathrm{ps}}(t)\tilde{\mathbf{H}}_{0\mathrm{ss}}\mathbf{P}_{\mathrm{sp}}^0(t) \tag{5.10}$$

The primary region where charge transfer, energy transfer and other collision phenomena take place is our main interest. But, solving the effective equations in the primary region, Eqs. (5.2) and (5.6), is not any easier than solving the original linearized TDHF equations, since they contain the density matrix elements in the secondary region and have to be solved simultaneously with the equations for density matrix elements involved the secondary region. Obviously, some

approximation has to be made in the secondary region to make this partition procedure practical.

5.2 The Approximation in the Secondary Region

When considering the secondary region, we notice that during the collision, the charge exchange is mainly restricted to the primary region. To understand it, let us consider the interaction and the evolution of the electronic states in the two parts of the surfaces, i.e., a small impact area on the surface which is close to the scattering ion during the collision and the remainder of the surface. During the collision, the impact area experiences a strong and time-dependent perturbation from the ion and the evolution of the electronic states in the area is significantly altered from that of the unperturbed surface. As the result, charge in the impact area may move to or from the ion. In the remainder of the surface, the direct interaction with the ion is much weaker, the electrons in this area feel the effect of the ion indirectly through their coupling with electrons in the impact area. Because the time scale of charge rearrangement in the solid, τ_{rearr}, is much longer than the duration of the collision at the surface, τ_{col}, at the collision energies of present interest, the electrons in the remainder of the surface do not have time to adjust to the charge rearrangement in the impact area, and the electronic states follow approximately the evolution pattern of an unperturbed system. Thus, it is reasonable to assume that the secondary region is basically unperturbed by the ion during the collision. In this approximation, the submatrices of $\mathbf{Q}$ associated with the secondary region, $\mathbf{Q}_{\text{ps}}(t)$, $\mathbf{Q}_{\text{sp}}(t)$ and $\mathbf{Q}_{\text{ss}}(t)$, are found to be negligible

compared to $\mathbf{Q}_{pp}$, and the submatrices $\mathbf{P}_{ps}^0(t)$, $\mathbf{P}_{sp}^0(t)$ and $\mathbf{P}_{ss}^0(t)$ can be replaced by those of the uncoupled system, $\bar{\mathbf{P}}_{ps}(t)$, $\bar{\mathbf{P}}_{sp}(t)$ and $\bar{\mathbf{P}}_{ss}(t)$. Other submatrices are treated in the similar way.

For an unperturbed surface, the coefficient of the molecular orbital has the form of

$$\bar{c}_{i\mu}(t) = \bar{c}_{i\mu}(t_{in})exp[-i\varepsilon_i(t - t_{in})] \tag{5.11}$$

where ε_i is the energy of the ith orbital. From Eq. (2.11)

$$\begin{aligned}\bar{P}_{\mu\nu}(t) &= \sum_{i=occ} \bar{c}_{i\mu}^*(t)\bar{c}_{i\nu}(t) = \sum_{i=occ} \bar{c}_{i\mu}^*(t_{in})\bar{c}_{i\nu}(t_{in}) \\ &= \bar{P}_{\mu\nu}(t_{in})\end{aligned} \tag{5.12}$$

As the result of these approximations, we need to solve only the effective equations in the primary region

$$i\dot{\mathbf{P}}_{pp}^0(t) = \mathbf{W}_{pp}\mathbf{P}_{pp}^0(t) - \mathbf{P}_{pp}^0(t)\mathbf{W}_{pp}^\dagger \tag{5.13}$$

and

$$i\dot{\mathbf{Q}}_{pp}(t) = \mathbf{W}_{pp}\mathbf{Q}_{pp}(t) - \mathbf{Q}_{pp}(t)\mathbf{W}_{pp}^\dagger + \bar{\mathbf{D}}_{pp}'(t) \tag{5.14}$$

The equation for $\mathbf{Q}_{pp}(t)$ is coupled with the secondary region through terms within $\bar{\mathbf{D}}_{pp}'(t)$ which is

$$\begin{aligned}\bar{\mathbf{D}}_{pp}'(t) &= \left(\mathbf{S}_0^{-1}\right)_{pp}\Delta\tilde{\mathbf{H}}_{pp}(t)\mathbf{P}_{pp}^0(t) - \mathbf{P}_{pp}^0(t)\Delta\tilde{\mathbf{H}}_{pp}^\dagger(t)\left(\mathbf{S}_0^{-1}\right)_{pp} \\ &\quad + \mathbf{P}_{pp}^0(t)\tilde{\mathbf{H}}_{0pp}^\dagger\left(\Delta\mathbf{S}^{-1}\right)_{pp}(t) - \left(\Delta\mathbf{S}^{-1}\right)_{pp}(t)\tilde{\mathbf{H}}_{0pp}\mathbf{P}_{pp}^0(t) \\ &\quad + \mathbf{P}_{ps}^0(t_{in})\tilde{\mathbf{H}}_{0sp}^\dagger\left(\Delta\mathbf{S}^{-1}\right)_{pp}(t) - \left(\Delta\mathbf{S}^{-1}\right)_{pp}(t)\tilde{\mathbf{H}}_{0ps}\mathbf{P}_{sp}^0(t_{in})\end{aligned} \tag{5.15}$$

Given the matrix elements S_0^{-1} and $\tilde{H}_0$, the driving term $\bar{D}_{pp}'(t)$ can be calculated and the density matrix in the primary region can be obtained either analytically or numerically by using Eqs. (4.50) and (4.51).

It should be pointed out that the validity of our approximation in the secondary region depends on two factors, the ratio of τ_{col}/τ_{rearr} and the size of the primary region. For metal surfaces and colliding atoms with their kinetic energy above 1eV, τ_{col}/τ_{rearr} is small and our partitioning procedure should apply. As for the size of the primary region, the larger the primary region, the more accurate the result. But increasing its size will significantly enlarge the basis set in the primary region and increase the computing time. In Ch. 9 we will discuss the effect of the primary region size in more detail.

CHAPTER 6
ELECTRONIC BASIS FUNCTIONS AND MATRIX ELEMENTS

The use of the localized basis functions in the present study appears necessary for our partition procedure introduced in Chapter 4, however, the real reason underlying it is the local nature of the phenomena associated with surfaces. For example, localized surface states, surface adsorptions, chemisorption and atom-surface collisions have their effects basically confined to small regions. Experimental results have also provided evidence that charge densities and local densities of states, while remarkably different from those of bulks on the top layers of surfaces, quickly recover to the bulk values on deeper layers. For example, the electron energy distribution results obtained from the ion neutralization spectroscopy, which probes only the top layer of atoms, show a qualitative difference from those of the bulk [Hagstrum and Becker, 73], but the results from the ultraviolet photoemission spectroscopy, which probes about four atom layers, are essentially dominated by the bulk density of states [Eastman and Grobman, 72].

Localized basis functions have been used in calculating electronic structure of bulk materials; the examples are Wannier functions and atomic-like basis functions used in the tight-binding method. The local nature of the surface phenomena suggests that some of the electronic behaviors of surfaces could

be more advantageously and conveniently described in terms of localized basis functions which return to the form of the bulk functions on deeper layers.

Recently, some works have reported using atomic orbitals to calculate surface electronic properties. Smith and his colleagues use a set of atomic–like basis functions to calculate surface band structure for transition metals [Smith and Gay, 75; Smith et al., 80; Alinghaus, et al., 80]. Their basis functions are constructed by fitting them to the solutions found by solving the Kohn-Sham equations [Kohn and Sham, 65]. Kohn and Onffory introduce the concept of the generalized Wannier functions which can be used in the theoretical study and calculation of electronic structures for extended systems lacking translational symmetry [Kohn and Onffroy, 73]. These functions are localized on the lattice sites and, as they result form a unitary transformation of the eigenfunctions of the system, are orthonormal and complete. Gay and Smith [Gay and Smith, 74] proposed a variation method for determining the generalized Wannier functions without having to first calculate the eigenfunctions of systems.

This chapter is devoted to constructing localized functions as our basis function set for atom-surface systems, which consists of a set of localized functions for the surface and a set of atomic functions for the atom, and to calculating the relevant matrix elements in this basis. Although the localized basis functions used by Smith and his colleagues are successful in giving good results for transition metals, their calculation and application are complicated. As a test of our time-dependent molecular orbital method and the partition procedure, we feel that a set

of simple localized functions would be adequate and hence choose the generalized Wannier functions as a part of our basis set.

In Section 6.1, the definition of the generalized Wannier functions is introduced and a variation procedure for determination of these functions is described. In Section 6.2, we apply the variation procedure to a jellium surface to obtain the generalized Wannier functions. For convenience in the calculation of the matrix elements, the generalized Wannier functions are written as linear combinations of Gaussians. In Section 6.3, the atomic functions for the atom are constructed by using a pseudopotential for the Sodium atom core. In Section 6.4, we calculate the matrix elements of the overlap and Hamiltonian. Some of the details of the calculation are given in Appendices A and B.

6.1 Generalized Wannier Functions

6.1.1 Definition of Generalized Wannier Functions (GWFs)

We first consider an infinite periodic system with a Hamiltonian $\hat{H}^0$. Its eigenfunction $\phi^0_{i\vec{k}}(\vec{r})$ is a Bloch function labeled by the wave vector $\vec{k}$ and band index i and satisfies the Schrodinger equation

$$\hat{H}^0 \phi^0_{i\vec{k}}(\vec{r}) = \epsilon_{i\vec{k}} \phi^0_{i\vec{k}}(\vec{r}) \tag{6.1}$$

where $\epsilon^0_{i\vec{k}}$ is the eigenvalue associated with i and $\vec{k}$. The functions $\phi^0_{i\vec{k}}(\vec{r})$ are then collected in a row matrix

$$\Phi^0_i = \left(\phi^0_{i\vec{k}_1}, \phi^0_{i\vec{k}_2}, \cdots \right) \tag{6.2}$$

and the above Schrodinger equation has a matrix form

$$\hat{H}^0 \mathbf{\Phi}_i^0 = \mathbf{\Phi}_i^0 \mathbf{E}_i^0 \tag{6.3}$$

where $\mathbf{E}_i^0$ is a diagonal matrix with diagonal elements $\epsilon_{i\vec{k}}^0$.

For each energy band of a periodic lattice, Wannier functions are defined by [Wannier, 37]

$$w_{i\vec{n}}^0(\vec{r}) = \frac{1}{\sqrt{N}} \sum_{\vec{k} \in BZ} e^{-i\vec{k} \cdot \vec{R}_{\vec{n}}} \phi_{i\vec{k}}^0(\vec{r}) \tag{6.4}$$

where N is the number of the lattice points, $\vec{R}_{\vec{n}}$ is the lattice vector labeled by a vector index $\vec{n}$, the summation is over the Brillouin zone. The Wannier function $w_{i\vec{n}}^0(\vec{r})$ is localized about the lattice point $\vec{R}_{\vec{n}}$. In matrix form, the above transformation can be written as

$$\mathbf{w}_i^0 = \mathbf{\Phi}_i^0 \, \mathbf{U}^{0\dagger} \tag{6.5}$$

where

$$\mathbf{w}_i^0 = \left(w_{i\vec{n}_1}^0, w_{i\vec{n}_2}^0, \cdots \right) \tag{6.6}$$

and

$$U_{\vec{n}\vec{k}}^0 = \frac{1}{\sqrt{N}} exp\left(i\vec{k} \cdot \vec{R}_{\vec{n}} \right) \tag{6.7}$$

Since matrix $\mathbf{U}^0$ is unitary, the Wannier functions are orthonormal and are an alternative set of basis functions in electronic structure calculation [See, for example, Slater and Koster, 54].

For a semi–infinite solid with its surface parallel to the x-y plane, its Hamiltonian $\hat{H}$ and eigenfunction $\phi_{i\vec{k}}(\vec{r})$, which is characterized by the band index i and the wave vector $\vec{k}$, satisfy the Schrodinger equation

$$\hat{H}\phi_{i\vec{k}}(\vec{r}) = \epsilon_{i\vec{k}}\phi_{i\vec{k}}(\vec{r}) \tag{6.8}$$

where $\epsilon_{i\vec{k}}$ is the eigenvalue. Collecting the functions $\phi_{i\vec{k}}(\vec{r})$ in a row matrix

$$\Phi_i = \left(\phi_{i\vec{k}_1}, \phi_{i\vec{k}_2}, \cdots\right) \tag{6.9}$$

the above Schrodinger equation can be written in matrix form

$$\hat{H}\Phi_i = \Phi_i \mathbf{E}_i \tag{6.10}$$

where $\mathbf{E}_i$ is a diagonal matrix with diagonal elements $\epsilon_{i\vec{k}}$. In the following, we drop the band index i with an understanding that all the functions and matrices involved are referred to a particular band.

As a results of breaking translation symmetry in the direction perpendicular to the surface, the eigenfunctions $\phi_{\vec{k}}(\vec{r})$ are no longer of Bloch–type and the functions defined in Eq. (6.4) are no longer meaningful. Kohn and Onffroy point out that it is possible to construct a set of orthonormal functions for systems with defects, called generalized Wannier functions [Kohn and Onffroy, 73]. Following their idea, we define the generalized Wannier functions of an electronic band as a unitary transformation of the eigenfunctions of the system, that is,

$$\mathbf{w} = \Phi\, \mathbf{U}^\dagger \tag{6.11}$$

where

$$\mathbf{w} = (w_{\vec{n}_1}, w_{\vec{n}_2}, \cdot \cdot \cdot) \tag{6.12}$$

is the row matrix of generalized Wannier functions and $\mathbf{U}$ is a unitary matrix to be determined. Obviously, $\mathbf{w}$ is orthonormal, i.e.,

$$\langle \mathbf{w} | \mathbf{w} \rangle = \mathbf{I} \tag{6.13}$$

It has been proved that Generalized Wannier functions are localized about the lattice sites $\vec{R}_{\vec{n}}$ and are exponentially decaying away from their center [Kohn and Onffroy, 73]. The well-behaved localization property of the generalized Wannier functions combined with their orthonormality make them particular useful to investigate the electronic structures or localized phenomena for non-periodic systems.

6.1.2 Generalized Wannier Functions as Linear Combinations of Gaussians

For the purpose of practical applications we write the generalized Wannier functions as linear combinations of Gaussian functions centered at different sites. For a certain energy band only Gaussian functions with proper symmetry should be used to construct the generalized Wannier function. Thus,

$$w_{\alpha\vec{n}}(\vec{r}) = \sum_{\vec{m}} B_{\vec{n}\vec{m}} \cdot g_{\alpha\vec{m}}(\beta_{\alpha\vec{m}}, \vec{r}) \tag{6.14}$$

where $B_{\vec{n}\vec{m}}$ is a coefficient, $\alpha=(nlm)$ is a compound index, and

$$g_{\alpha\vec{m}}(\beta_{\alpha\vec{m}}, \vec{r}) = b_\alpha Y_{lm}(\theta, \varphi) r^l e^{-\beta_{\alpha\vec{m}}(\vec{r}-\vec{R}_{\vec{n}})^2} \tag{6.15}$$

is the α type Gaussian primitive function centered at $\vec{R}_{\vec{m}}$, where $Y_{lm}(\theta, \varphi)$ is the spherical harmonic functions and b_α a normalization factor. Letting

$$\mathbf{g} = (g_{\alpha \vec{m}_1}, \; g_{\alpha \vec{m}_2}, \; \cdot \; \cdot \; \cdot \;) \tag{6.16}$$

(here we have dropped index α in $\mathbf{g}$ since α is the same for all the Gaussians for a given band), Eq. (6.14) can be written in a matrix form

$$\mathbf{w} = \mathbf{B}\mathbf{g} \tag{6.17}$$

where

$$(\mathbf{B})_{\vec{n}\vec{m}} = B_{\vec{n}\vec{m}} \tag{6.18}$$

Substituting Eq. (6.17) into the normalization relation Eq. (6.13) yields

$$\mathbf{B}^\dagger \mathbf{G} \mathbf{B} = \mathbf{I} \tag{6.19}$$

where

$$\mathbf{G} = \langle \mathbf{g} | \mathbf{g} \rangle \tag{6.20}$$

is the overlap matrix of Gaussians, we find that a possible choice for $\mathbf{B}$ is

$$\mathbf{B} = \mathbf{G}^{-\frac{1}{2}} \tag{6.21}$$

where the matrix $\mathbf{G}^{-\frac{1}{2}}$ satisfies

$$\mathbf{G}^{-\frac{1}{2}} \mathbf{G} \mathbf{G}^{-\frac{1}{2}} = \mathbf{I} \tag{6.22}$$

6.1.3 Determination of Generalized Wannier Functions

The generalized Wannier functions can be constructed from the eigenfunctions $\phi_{\vec{k}}(\vec{r})$ according to their definition (6.11). However, one of the important features of the generalized Wannier functions is that they can be directly determined from the system Hamiltonian without having to know the original eigenfunctions [Kohn and Onffroy, 73; Gay and Smith, 74], which allows freedom to construct them as desired. In this study we use a variational procedure [Gay and Smith, 74] to find the generalized Wannier functions $\mathbf{w}$.

Since

$$\mathbf{E} = \langle \Phi | \hat{H} | \Phi \rangle \tag{6.23}$$

the total energy of a band

$$
\begin{aligned}
E_B = Tr(\mathbf{E}) &= Tr\left(\langle \Phi | \hat{H} | \Phi \rangle \right) \\
&= Tr\left(\langle \mathbf{w} | \hat{H} | \mathbf{w} \rangle \right) = E_B[\mathbf{w}]
\end{aligned}
\tag{6.24}
$$

is a functional of the $\mathbf{w}$'s, and we have used in the second line the orthonormality Eq. (6.13). The variational principle proposed by Kohn and Onffory [Kohn and Onffroy, 73] says that the total energy of a band attains its minimum if a correct set of $\mathbf{w}$'s is used. Thus the generalized Wannier functions can be determined by minimizing $E_B[\mathbf{w}]$, that is,

$$\min_{\{\mathbf{w}\}} \{ E_B[\mathbf{w}] \} = \mathcal{E} \tag{6.25}$$

while being subject to the constraint Eq. (6.13).

Once **w** is known we can insert Eq. (6.11) into the eigenequation of the system to have

$$\hat{H}\mathbf{w}\mathbf{U} = \mathbf{w}\mathbf{U}\mathbf{E} \tag{6.26}$$

or, using Eq. (6.13),

$$\langle \mathbf{w}|\hat{H}|\mathbf{w}\rangle \mathbf{U} = \mathbf{U}\mathbf{E} \tag{6.27}$$

This equation can be used to find the matrix **U** as well as the eigenfunction $\phi_{\vec{k}}(\vec{r})$.

By writing the generalized Wannier functions as linear combinations of Gaussians, the functional $E_B[\mathbf{w}]$ becomes a function of $\beta_{\vec{m}}$'s, $\Omega(\beta_1, \beta_2, \cdots)$, and the problem of searching for a set of **w** becomes one of finding a set of optimized $\beta_{\vec{m}}$'s, i.e.,

$$\min_{\beta_1,\beta_2,\cdots} [\Omega(\beta_1, \beta_2, \cdots)] \rightarrow \beta_1, \beta_2, \cdots \tag{6.28}$$

One may recall that the above procedure for writing the generalized Wannier functions as linear combinations of Gaussians is similar to those used in molecular orbital calculation. However the difference is that the Gaussian function or the exponent $\beta_{\vec{m}}$ depend on the site position $\vec{R}_{\vec{m}}$. For a surface, due to the periodicity in x and y directions, all the generalized Wannier functions on the same layer are the same and the exponent $\beta_{\vec{m}}$ changes only with layers. From now on we will denote $\beta_{\vec{m}}$ by β_{m_z}, where m_z is the z component of the vector index $\vec{m}$, to indicate that it is the exponent for the m_zth layer.

Before proceeding to find β_{m_z}'s we notice an asymptotic behavior of the generalized Wannier functions; they approach the Wannier functions of a periodic system in an exponential manner, as proved by Kohn and Onffory [Kohn and Onffroy, 73]. This indicates that only a small number of the generalized Wannier functions need to be determined for near-periodic lattices which loose translation symmetry only in local areas or in certain directions, such as imperfect crystals and surfaces. For a perfect bulk, the Wannier functions $w_{\vec{m}}^0(\vec{r})$'s on all the sites $\vec{R}_{\vec{m}}$ are the same and have the same exponent parameter β^0. For a semi-infinite lattice with its surface at $m_z=1$, the generalized Wannier function $w_{\vec{m}}(\vec{r})$ approaches $w_{\vec{m}}^0(\vec{r})$'s and β_{m_z} approaches β^0 when $\vec{R}_{\vec{m}}$ is deep inside the surface. There exists a cutoff M such that when $m_z \geq M$ it is found approximately that

$$\beta_{m_z} = \beta^0 \qquad (6.29)$$

The variation procedure (6.28) now becomes

$$\min_{\beta_1,\beta_2,\cdots} [\Omega(\beta_1,\beta_2,\cdots)] = \min_{\beta_1,\beta_2,\cdots\beta_M} [\Omega(\beta_1,\beta_2,\cdots,\beta_M)] \rightarrow \beta_1,\beta_2,\cdots,\beta_M \quad (6.30)$$

Thus only M variational parameters, β_1, β_2, $\cdots$, β_M, must be determined. The choice of the number M depends on the system and the accuracy requirement of calculations.

6.2 Generalized Wannier Functions for a Jellium Surface

The method developed in the previous section can be applied to construct generalized Wannier functions for any system for which the effective one electron

Hamiltonian is known, although the calculation of the three dimensional matrix $G^{-\frac{1}{2}}$ is a little time-consuming [Gay and smith, 74]. In this section we apply the method to a simple model, a jellium slab with a step potential. A jellium is a system with the atom core lattice replaced by an uniform positive charge background and, as a result, it completely ignores the effect of the atomic lattice. Because of its simplicity in the electronic structure calculation, jellium is often used in condensed matter physics as a testing model for theory or methods. We also assume that there is only one band and use 1s type Gaussians to construct generalized Wannier functions. We fit the band parameters such as Fermi level, and the energy of the bottom of the band to those of W(110).

For a finite jellium slab with a thickness D in z-direction and a step potential

$$V(\vec{r}) = \left\{ \begin{array}{ll} 0 & z \geq 0 \\ -V_0 & -D \leq z < 0 \\ 0 & z < -D \end{array} \right\} \tag{6.31}$$

the Hamiltonian is

$$H(\vec{r}) = -\frac{1}{2}\nabla^2 + V(\vec{r})$$
$$= H^x(x) + H^y(y) + H^z(z) \tag{6.32}$$

where $H^x(x)$ and $H^y(y)$ equal to the kinetic energies in x and y directions and

$$H^z(z) = -\frac{1}{2}\frac{\partial^2}{\partial^2 z} + V^z(z) \tag{6.33}$$

with

$$V^z(z) = V(\vec{r}) \tag{6.34}$$

Labeling x, y and z components by superscripts x, y and z, the eigenfunction $\phi_{\vec{k}}(\vec{r})$, which is assumed to satisfy cyclic boundary conditions in x- and y-directions, and

eigenvalue $E_{\vec{k}}$ have the forms of

$$\phi_{\vec{k}}(\vec{r}) = \phi_{k_x}^x(x)\phi_{k_y}^y(y)\phi_{k_z}^z(z) \tag{6.35}$$

and

$$E_{\vec{k}} = E_{k_x} + E_{k_y} + E_{k_z} \tag{6.36}$$

respectively. In Appendix C we describe the evaluation of the Fermi energy.

We now consider an artificial cubic mesh in the slab, which contains $N_s=N_xN_yN_z$ sites with a distance d between sites, where N_x, N_y and N_z are the numbers of sites in x-, y- and z-directions, respectively. The generalized Wannier functions for the slab are associated with sites and are written as

$$w_{\vec{n}}(\vec{r}) = w_{n_x}^x(x)w_{n_y}^y(y)w_{n_z}^z(z) \tag{6.37}$$

Recalling Eq. (6.11), the matrix $\mathbf{U}$ can then be written as a product of x, y and z component matrices

$$\mathbf{U} = \mathbf{U^x U^y U^z} \tag{6.38}$$

with $\mathbf{U_x}$, $\mathbf{U_y}$ and $\mathbf{U_z}$ lead to the transformations

$$w_{n_x}^x(x) = \sum_{k_x}\left(U^{x\dagger}\right)_{k_x n_x}\phi_{k_x}^{0x}(x) \tag{6.39}$$

$$w_{n_y}^y(y) = \sum_{k_y}\left(U^{y\dagger}\right)_{k_y n_y}\phi_{k_y}^{0y}(y) \tag{6.40}$$

$$w_{n_z}^z(z) = \sum_{k_z}\left(U^{z\dagger}\right)_{k_z n_z}\phi_{k_z}^z(z) \tag{6.41}$$

respectively. For this system, therefore, a three dimensional calculation is simplified to a one dimensional one.

For this system, the x- and y-components of the eigenfunctions are

$$\phi_{k_x} = \frac{1}{\sqrt{(N_x - 1)d}} exp(ik_x x)$$
$$\phi_{k_y} = \frac{1}{\sqrt{(N_y - 1)d}} exp(ik_y x)$$

(6.42)

the generalized Wannier functions in the x- and y-directions are just the Wannier function for periodic lattice

$$w^x_{n_x}(x) = \frac{1}{(N_x - 1)\sqrt{d}} \cdot \frac{\sin\left[\frac{\pi(x - n_x d)}{d}\right]}{sin\left[\frac{\pi(x - n_x d)}{(N_x - 1)d}\right]}$$

(6.43)

$$w^y_{n_y}(y) = \frac{1}{(N_x - 1)\sqrt{d}} \cdot \frac{\sin\left[\frac{\pi(y - n_y d)}{d}\right]}{sin\left[\frac{\pi(y - n_y d)}{(N_x - 1)d}\right]}$$

(6.44)

and the component transformation matrices U^x and U^y are

$$U^x_{n_x k_x} = \frac{1}{\sqrt{N_x - 1}} exp(ik_x n_x d)$$

(6.45)

$$U^y_{n_y k_y} = \frac{1}{\sqrt{N_y - 1}} exp(ik_y n_y d)$$

(6.46)

In the z direction, the generalized Wannier function for n_zth layer, $w^z_{n_z}(z)$, is written as linear combination of Gaussians

$$w^z_{n_z}(z) = \sum_{m_z} B^z_{n_z m_z} g^z_{m_z}(\beta_{m_z}, z)$$

(6.47)

where the normalized one dimensional Gaussian function in the z direction $g_{m_z}^z(\beta_{m_z}, z)$ is centered at Z_{m_z} on m_zth layer with an exponent β_{m_z}, and $\mathbf{B}^z = (\mathbf{G}^z)^{-\frac{1}{2}}$ with $\mathbf{G}^z = \langle \mathbf{g}^z | \mathbf{g}^z \rangle$ the overlap matrix of Gaussians in the z direction. As discussed in the previous section, only the exponent parameters on the first M layers are assumed to be different; that is, $\beta_1 = \beta_{N_z}$, $\beta_2 = \beta_{N_z-1}, \cdots, \beta_{M-1} = \beta_{N_z-M+2}$, but $\beta_M = \beta_{M-1} = \cdots = \beta_{N_z-M+1}$.

In the x and y directions, the Wannier functions on the m_zth layer are written as linear combinations of one dimensional Gaussians with an exponent β_{m_z}. For example, the Wannier function in the x direction is

$$w_{n_x}^{x,m_z}(x) = \sum_{m_x} B_{n_x m_x}^x(\beta_{m_z}) g_{m_x}^x(\beta_{m_z}, x) \tag{6.48}$$

where the superscript m_z for the function is used to indicate the layer the function is on. The coefficient matrix element $B_{n_x m_x}^x(\beta_{m_z})$ is obtained by the least square principle [Shavitt, 63] by fitting Eq. (6.48) with Eq. (6.43). The details of the calculation are given in Appendix A.

From Eq. (6.24) the total energy is

$$\begin{aligned} E_B &= \sum_{\vec{n}} \langle w_{\vec{n}} | \mathbf{H} | w_{\vec{n}} \rangle \\ &= \sum_{\vec{n}} \sum_{\vec{m}} \sum_{\vec{m}'} B_{\vec{m}\vec{n}}^{\dagger} B_{\vec{n}\vec{m}'} \langle g_{\vec{m}}(\beta_{m_z}) | \mathbf{H} | g_{\vec{m}'}(\beta_{m_z'}) \rangle \quad . \tag{6.49} \\ &= \Omega(\beta_1, \beta_2, \cdots, \beta_M) \end{aligned}$$

with the details of the calculation given in Appendix B. Minimizing Ω respect to the β's gives a set of optimized β's.

To determine the matrix $\mathbf{U}^z$, we substitute Eq. (6.41) into the eigenequation of $\phi_{k_z}^z(z)$

$$\mathrm{H}^z \phi_{k_z}^z(z) = E_{k_z} \phi_{k_z}^z(z) \tag{6.50}$$

to have

$$\sum_{m_z} U_{k_z m_z} \mathrm{H}^z w_{m_z}^z(z) = E_{k_z} \sum_{m_z} U_{k_z m_z} w_{m_z}^z(z) \tag{6.51}$$

Multiplying it by $w_{n_z}^z(z)^*$ and integrating over z give the equation for transformation matrix $\mathbf{U}^z$

$$\sum_{m_z} U_{k_z m_z} \langle w_{n_z}^z | \mathrm{H}^z | w_{m_z}^z \rangle = E_{k_z} U_{k_z n_z} \tag{6.52}$$

6.2.1 Results

We have calculated the generalized Wannier functions for a finite jellium slab modeling W(110), with the depth of the potential well $V_0 = 0.846$ au. The distance between sites, d, is not equal to the lattice constant of W, and is chosen to be $d = 2.61$ au so that the average number of electrons in the volume associated with a site is one. The optimum exponents of the Gaussians, β_{m_z}, which are determined by minimizing the total energy Eq. (6.49), are listed in Table 6.1. It has been found that the optimum exponent decreases for the first couple of layers but changes very little after the third layer. This shows that the effect of the surface on the generalized Wannier functions is basically limited to the several top layers. Gay and Smith also find that the exponents are different from that

Table 6.1 The optimum Gaussian exponents for the first three layers.

Layer	First	Second	Third
β_{m_z}	0.53	0.52	0.30

of the bulk only on the top two or three layers even though they use different potentials [Gay and Smith, 75].

The generalized Wannier functions for the first four layers are plotted in Figs. 6.1, 6.2, 6.3 and 6.4, assuming β_{m_z}=0.30 for $m_z > 3$. These figures show that the generalized Wannier functions are well localized about their centers with long decaying tails. For the first two layers, the effect of the surface is significant, the generalized Wannier functions are asymmetric and their tails oscillate little. On moving to the deeper layers, the generalized Wannier functions are more and more characteristic of an infinite bulk. For the fourth layer the tail of the generalized Wannier function towards the center of the slab is very similar to that of the bulk Wannier function. Although the surface is a severe perturbation, our results show that the generalized Wannier functions rapidly become the bulk Wannier functions when moving away from the surface, which is in agreement with the theoretical prediction for the generalized Wannier functions [Kohn and Onffroy, 73].

To exam the validity of using generalized Wannier functions as basis functions, we compare the eigenvalues and wavefunctions calculated from these functions with the exact ones. Table 6.2 lists both exact and calculated eigenvalues, Figs. 6.5, 6.6 and 6.7 depict both exact and calculated wavefunctions for E_{k_z}=−0.8444,

−0.6906 and −0.3990 for states j_z=1, 10, 17 respectively. The agreements are good for all the energies, and especially for lower energies. Since the point-by-point comparison of wavefuntions is probably the most stringent test of the accuracy, the good agreement in our calculation will assure the accuracy in the calculation of observables such as charge density.

In the x and y directions, the Wannier functions $w_{n_x}^x(x)$ and $w_{n_y}^y(y)$ on the m_zth layer are approximated by linear combinations of Gaussians with the m_zth layer exponent β_{m_z}. The accuracy of the approximation depends on the number of Gaussians used. It is found that for the larger β_{m_z} (close to the surface in our case) more Gaussians are needed to achieve the same accuracy. Figs. 6.8, 6.9 and 6.10 show the exact and calculated Wannier functions for the first three layers when 21 Gaussians are used.

The calculation and application of generalized Wannier functions for a jellium slab reveal some nice features of these functions. Firstly, they are well localized about their centers with their tails characterizing the translation symmetry of the systems. The functions rapidly recover to the bulk Wannier functions away from defects or surfaces, thus only a few generalized Wannier functions need to be determined. Secondly, the generalized Wannier functions can reproduce the wavefunctions and eigenvalues to a satisfactory accuracy. These attractive features make generalized Wannier function suitable for electronic structure calculations for surfaces or other systems with a broken translation symmetry, and makes them useful in studies of local phenomena.
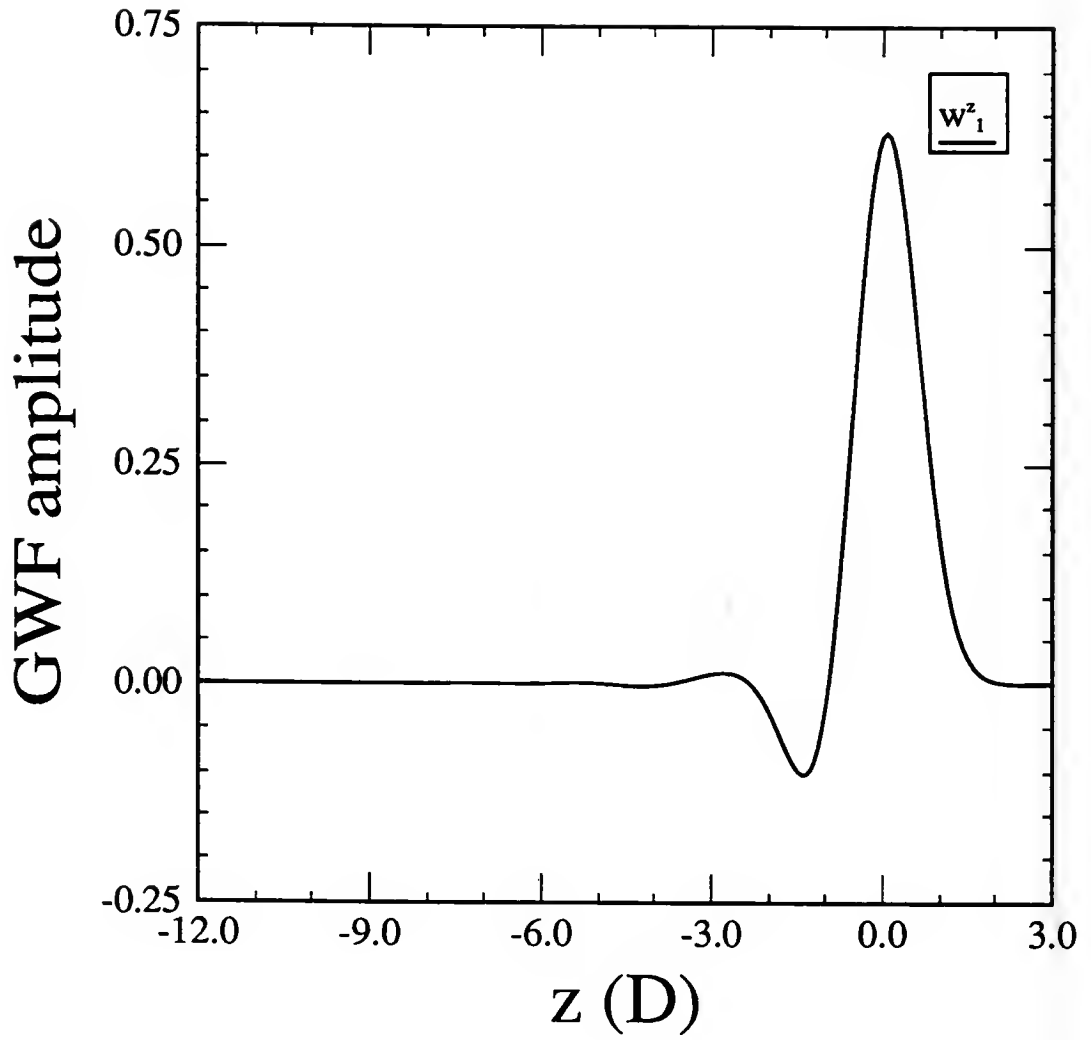
Figure 6.1 Generalized Wannier function $w_{n_z}^z(z)$ on the first layer of a jellium slab with a square well potential and a potential depth V_0=0.846. The surfaces of the slab are located at z=0 and z=–21d, where d=2.61 au is the distance between layers.
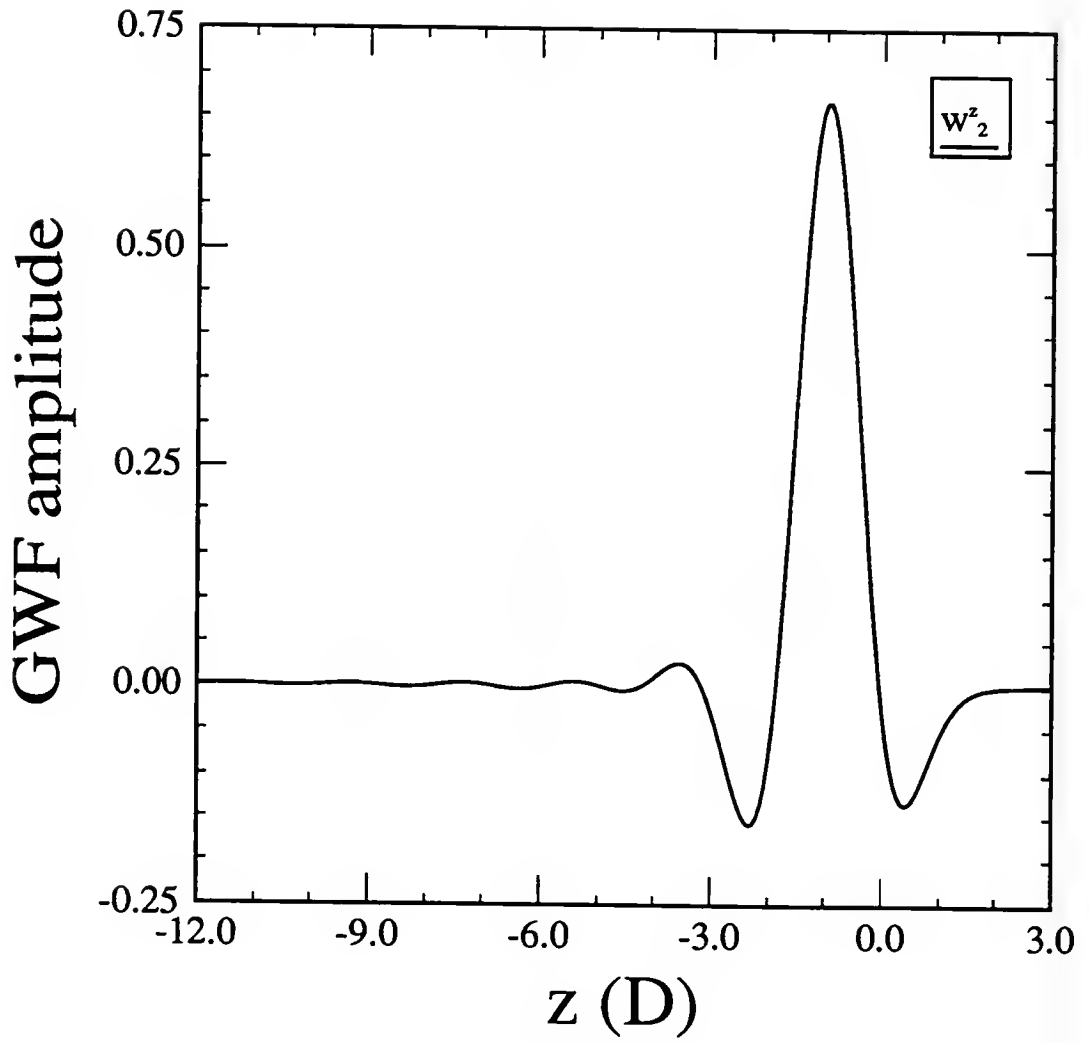
Figure 6.2 Generalized Wannier function $w_{n_z}^z(z)$ on the second layer of a jellium slab with a square well potential.
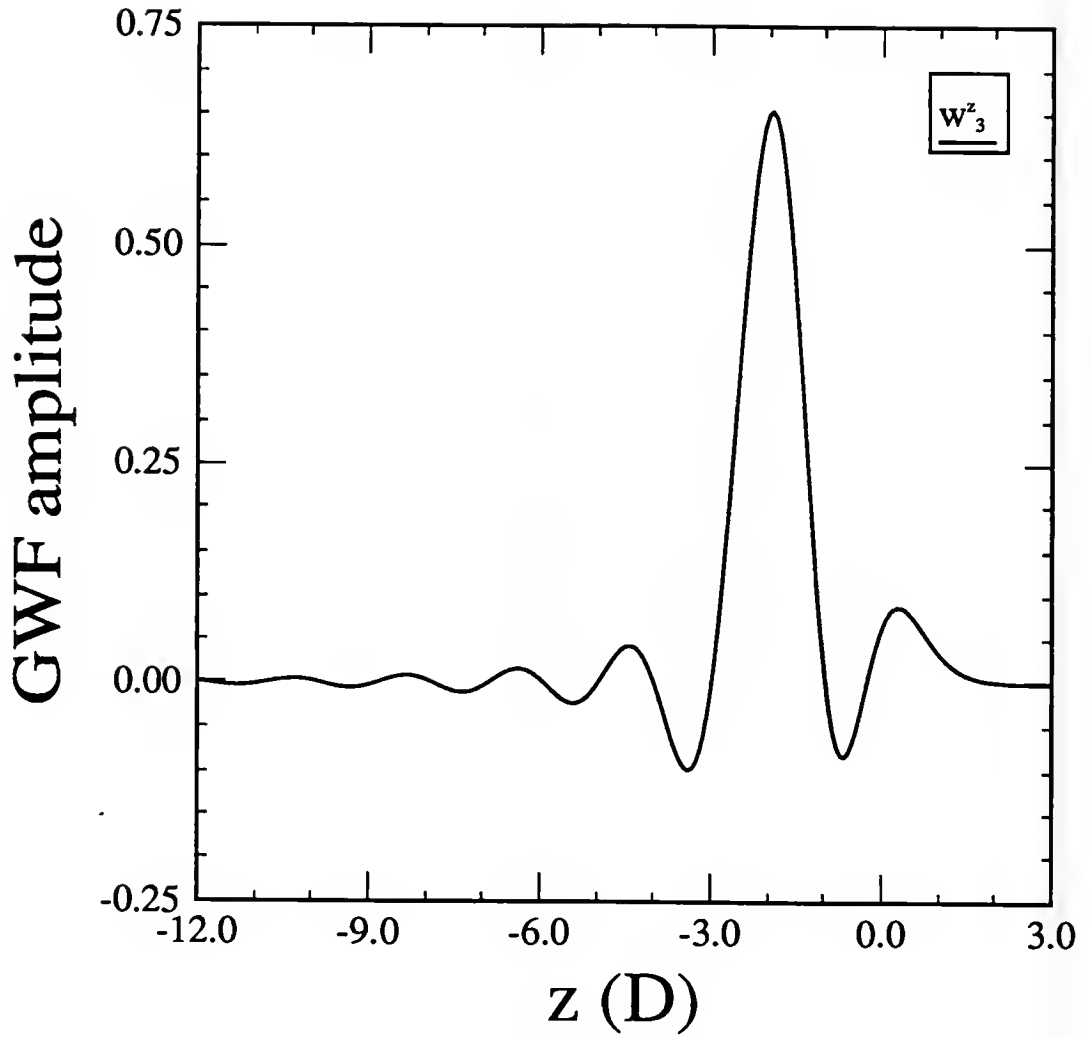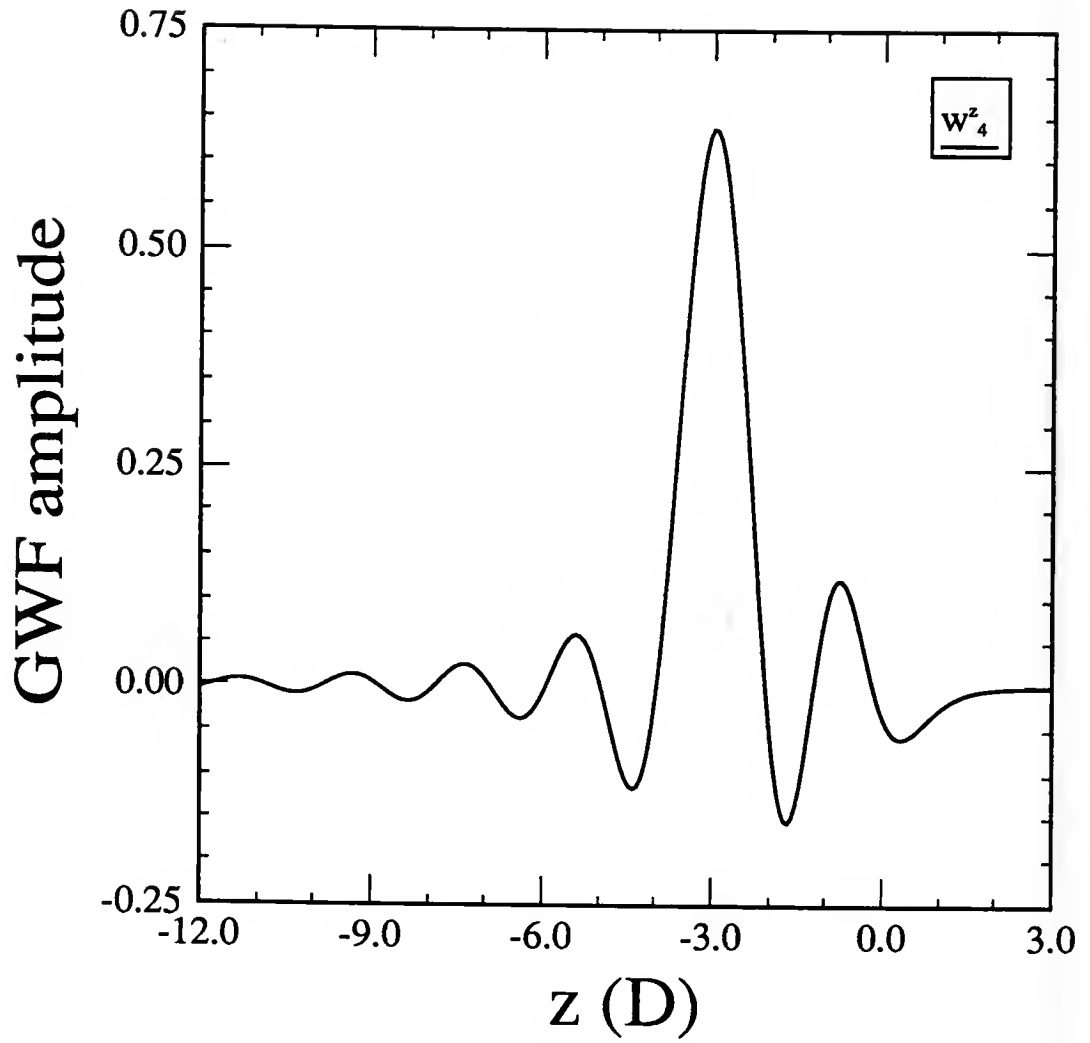
Figure 6.3 Generalized Wannier function $w^z_{n_s}(z)$ on the third layer of a jellium slab with a square well potential.

Figure 6.4 Generalized Wannier function $w_{n_z}^z(z)$ on the fourth layer of a jellium slab with a square well potential.

Table 6.2 Exact eigenvalues and approximate eigenvalues calculated by using generalized Wannier functions for a slab with a square well potential given by Eq. (6.31).

Exact eigenvalue	Approximate eigenvalue
-0.8444	-0.8444
-0.8398	-0.8397
-0.8320	-0.8320
-0.8211	-0.8209
-0.8071	-0.8068
-0.7900	-0.7895
-0.7698	-0.7690
-0.7465	-0.7453
-0.7201	-0.7185
-0.6906	-0.6883
-0.6580	-0.6549
-0.6224	-0.6181
-0.5837	-0.5778
-0.5420	-0.5340
-0.4973	-0.4864
-0.4496	-0.4349
-0.3990	-0.3792
-0.3454	-0.3185
-0.2890	-0.2517
-0.2299	-0.1769
-0.1682	-0.1299
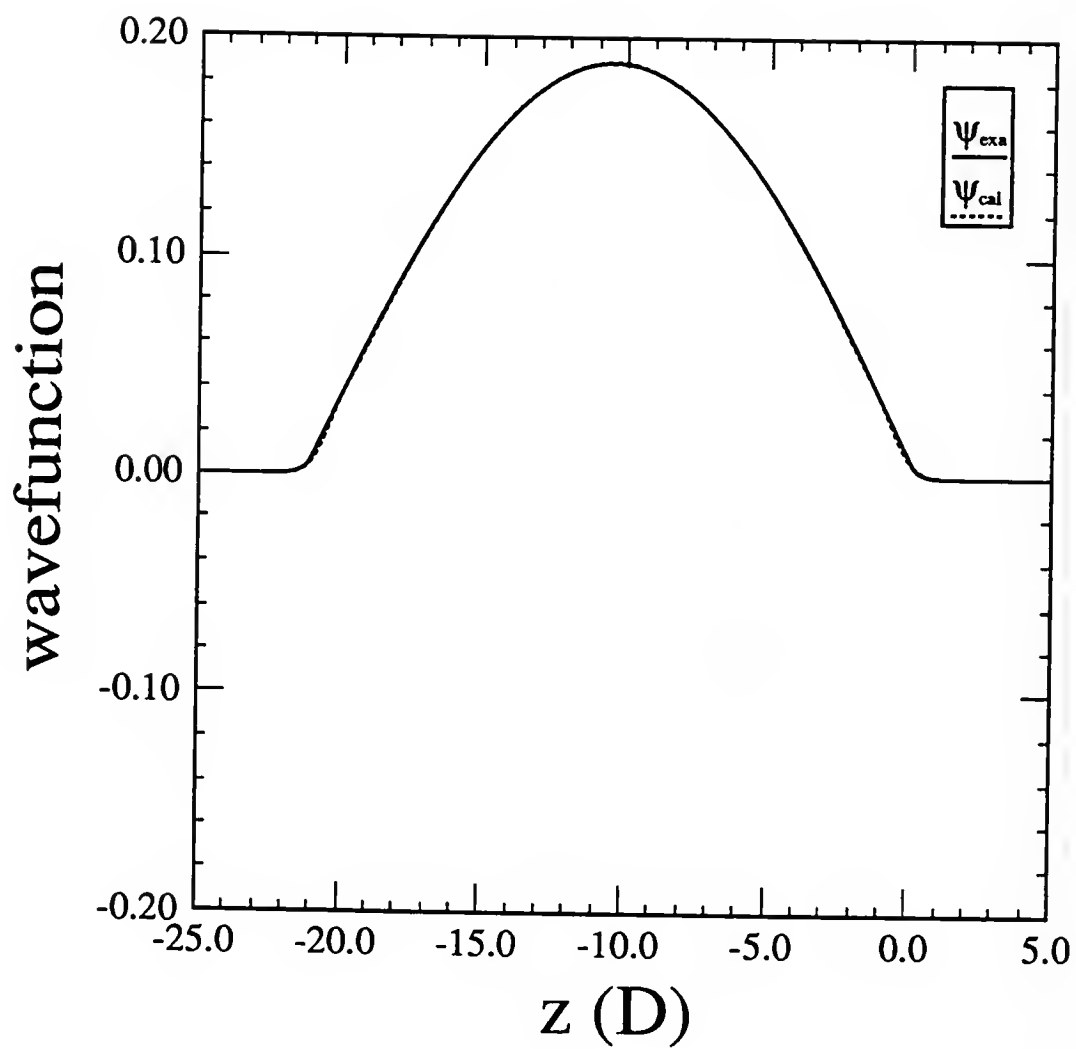
Figure 6.5 Exact and approximate wavefunctions associated with the exact eigenvalue –0.8444 au for an one-dimensional square well.
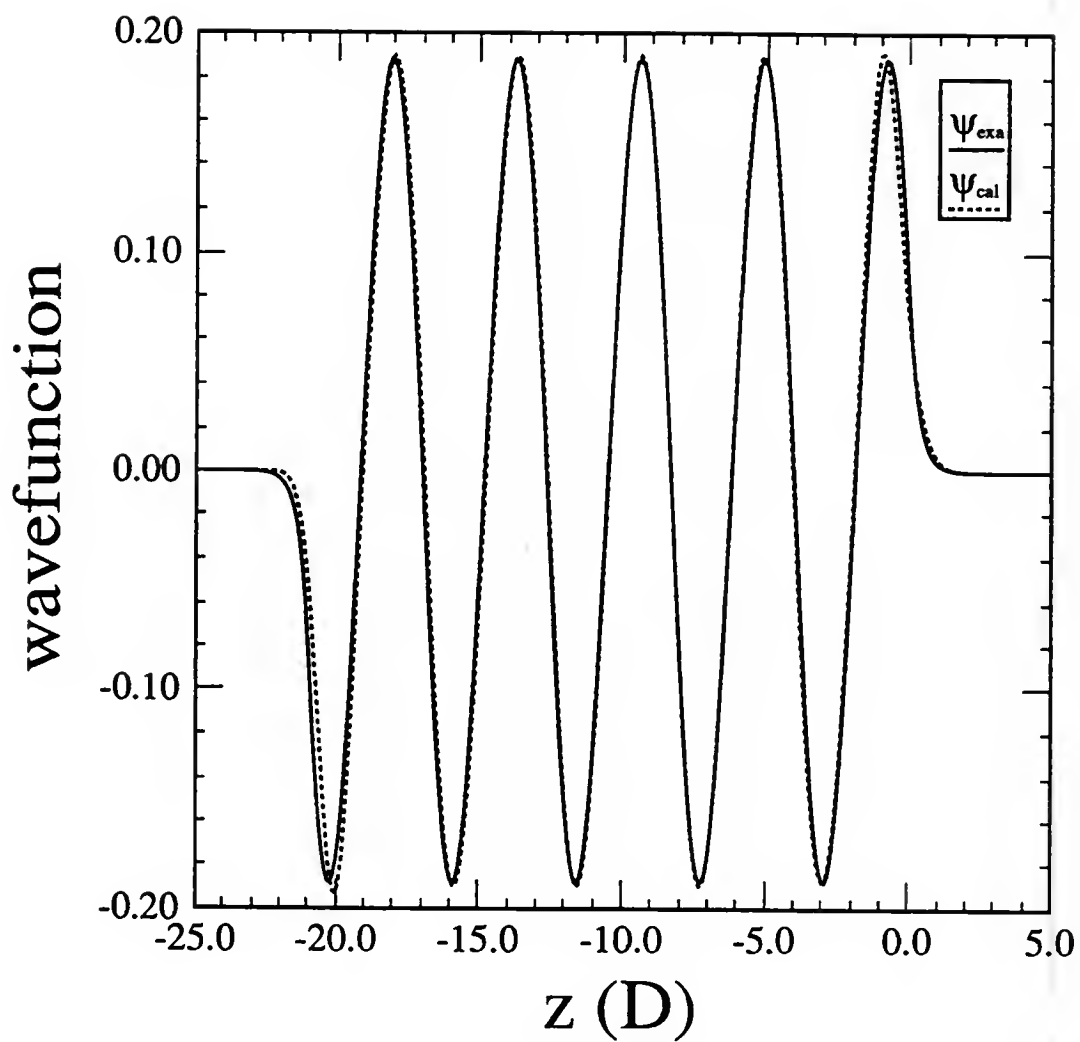
Figure 6.6 Exact and approximate wavefunctions associated with the exact eigenvalue −0.6906 au for an one-dimensional square well.
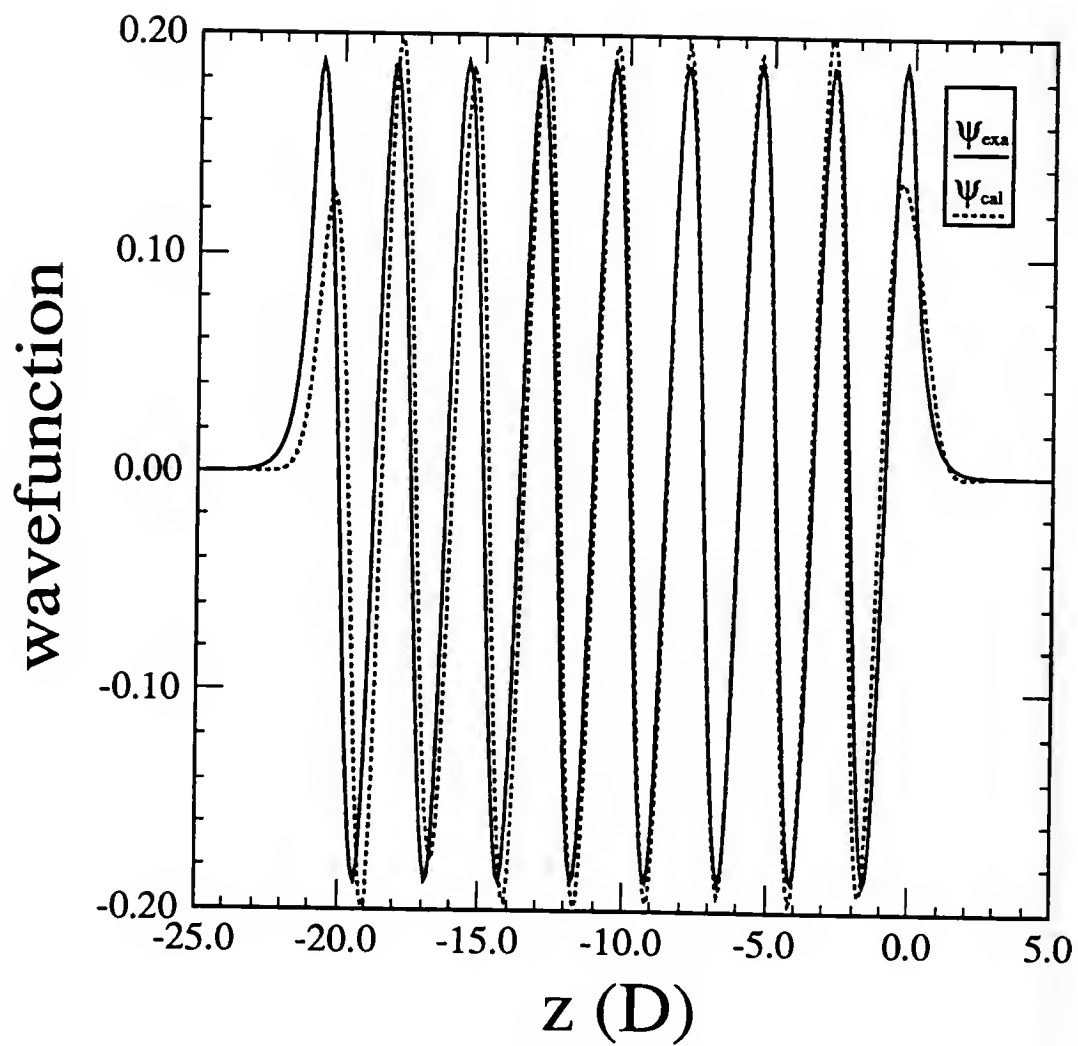
Figure 6.7 Exact and approximate wavefunctions associated with the exact eigenvalue –0.3990 au for an one-dimensional square well.
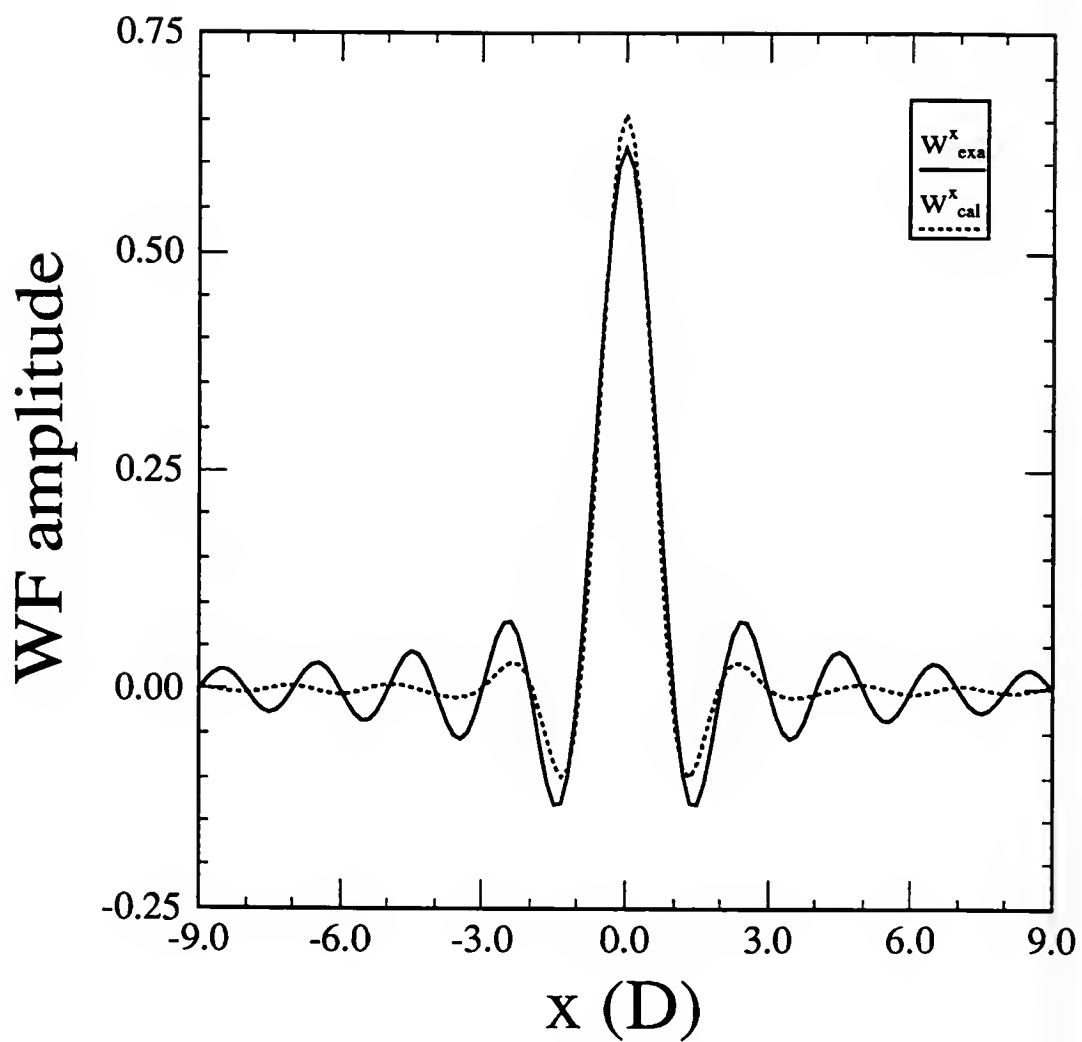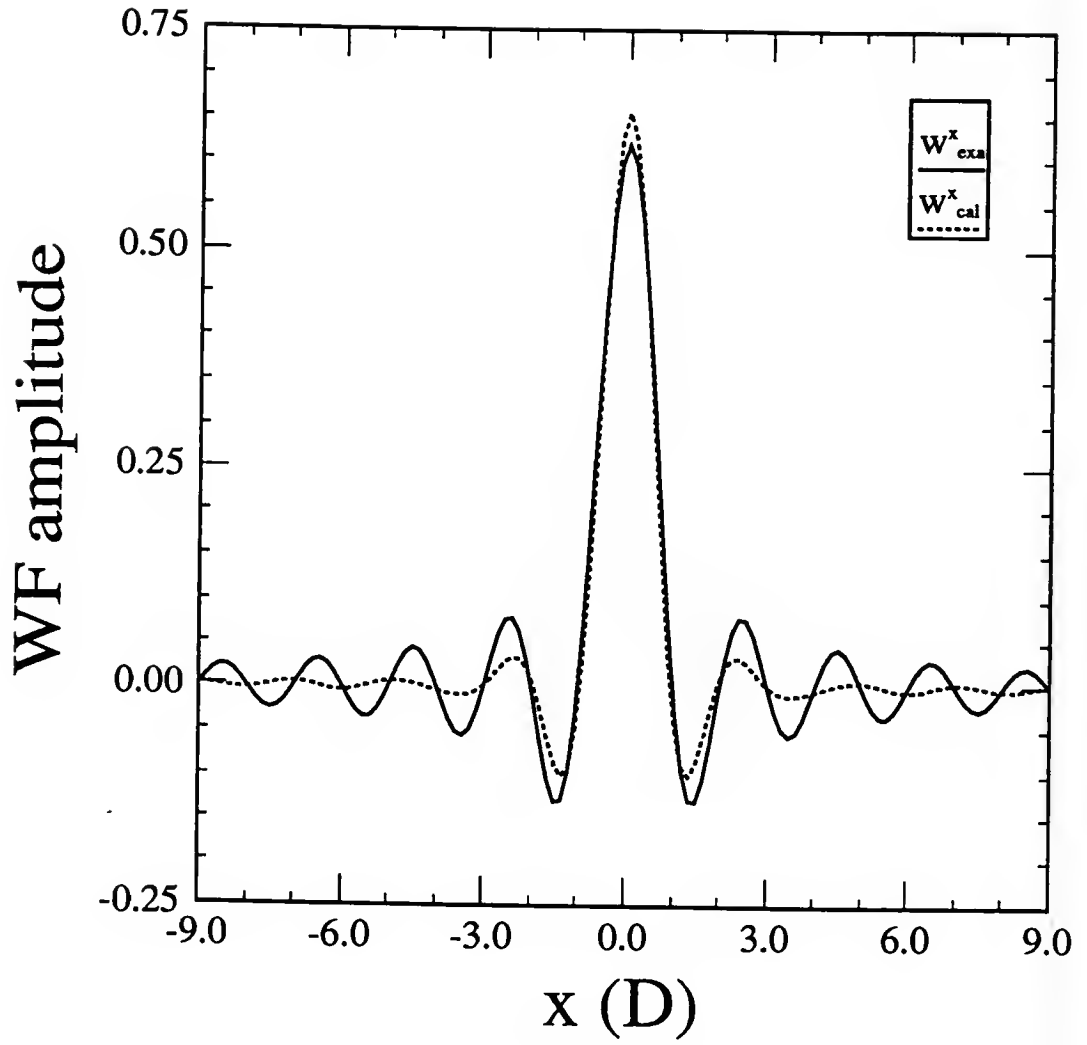
Figure 6.8 Exact and approximate Wannier functions for a slab in the directions parallel to the surface. The latter is a linear combination of Gaussians with an exponent β=0.53.

Figure 6.9 Exact and approximate Wannier functions for a slab in the directions parallel to the surface. The latter is a linear combination of Gaussians with an exponent $\beta=0.52$.
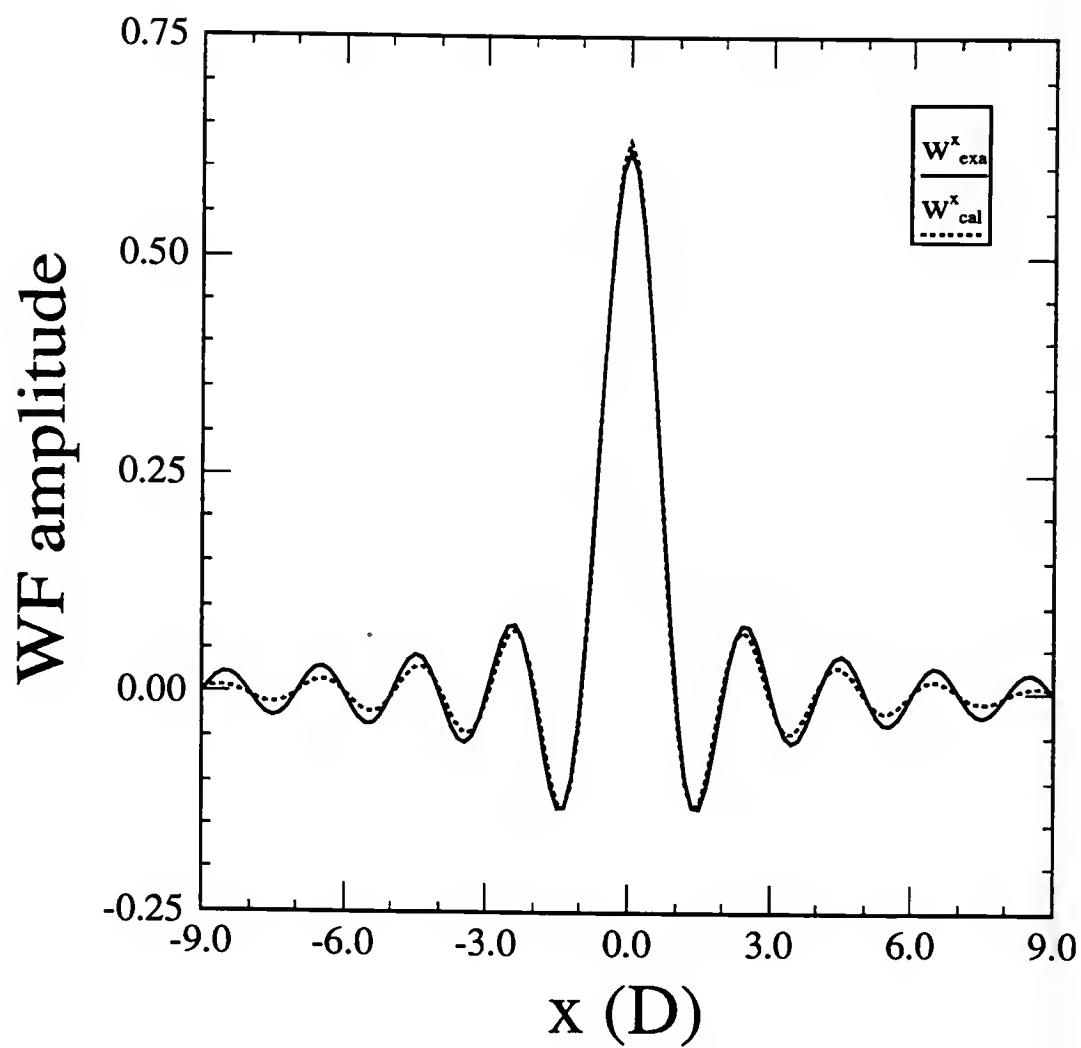
Figure 6.10 Exact and approximate Wannier functions for a slab in the directions parallel to the surface. The latter is a linear combination of Gaussians with an exponent $\beta=0.30$.

6.3 Atomic Basis Functions

Since in low energy atom-surface collisions only the valence electrons of atoms are actively involved in charge exchange, it is a good approximation to ignore the inner-shell electrons and use a pseudopotential for the atomic core. In this section we construct the atomic basis functions for 3s and 3p orbitals of Sodium and a pseudopotential for its atomic core.

We choose Slater-type orbitals (STO) $\phi_a\left(\vec{r}; \zeta, \vec{R}_A\right)$ as basis functions, where a=3s, 3p$_x$, 3p$_y$, and 3p$_z$, ζ is the exponent of the orbitals, and $\vec{R}_A$ is the position of the atomic core. For the convenience of calculation, we use STO-KG functions $\phi_a\left(\vec{r}; \zeta, \vec{R}_A\right)$ which are linear combinations of K Gaussians and satisfy

$$\phi_a\left(\vec{r}; \zeta, \vec{R}_A\right) = \zeta^{\frac{3}{2}}\phi_a\left(\vec{r}; 1, \vec{R}_A\right) \tag{6.53}$$

and are in the form of

$$\phi_{3s}\left(\vec{r}; 1, \vec{R}_A\right) = \sum_{k=1}^{K} d_{3s,k} \cdot g_{1s}\left(\vec{r}; \alpha_k, \vec{R}_A\right) \tag{6.54}$$

$$\phi_{3pj}\left(\vec{r}; 1, \vec{R}_A\right) = \sum_{k=1}^{K} d_{3p,k} \cdot g_{2pj}\left(\vec{r}; \alpha_k, \vec{R}_A\right) \tag{6.55}$$

where j=x, y and z, and $g_{1s}\left(\vec{r}; \alpha_k, \vec{R}_A\right)$ and $g_{2pj}\left(\vec{r}; \alpha_k, \vec{R}_A\right)$ are 1s and 2p type Gaussian primitive functions respectively,

$$g_{1s}\left(\vec{r}; \alpha_k, \vec{R}_A\right) = \left(\frac{8\alpha_k^3}{\pi^3}\right)^{\frac{1}{4}} exp\left(-\alpha_k|\vec{r} - \vec{R}_A|^2\right) \tag{6.56}$$

$$g_{2p}\left(\vec{r}; \alpha_k, \vec{R}_A\right) = \left(\frac{128\alpha_k^5}{\pi^3}\right)^{\frac{1}{4}} r_j exp\left(-\alpha_k|\vec{r} - \vec{R}_a|^2\right) \tag{6.57}$$

We use K=3 and ζ=1.27. The data for α_k, $d_{3s,k}$ and $d_{3p,k}$ [Hehre et al., 70] are listed in Table 6.3.

Table 6.3 Coefficients and exponents for Gaussians in STO-3G functions.

k	α_k	$d_{3s,k}$	$d_{3p,k}$
1	5.27266(-2)	9.00398(-1)	4.62001(-1)
2	1.34715(-1)	2.25595(-1)	5.95167(-1)
3	4.82854(-1)	-2.19620(-1)	1.05876(-2)

6.4 Overlap Matrix Elements

Our localized basis set consists of generalized Wannier functions localized at the sites of the slab and atomic functions centered at the atomic core of the colliding ion as described in the previous sections, that is

$$\{\phi_\mu\} = \{\{\phi_{\vec{n}}\}, \{\phi_a\}\}$$

(6.58)

Since both $\{\phi_{\vec{n}}\}$ and $\{\phi_a\}$ are orthonormal sets, the diagonal elements of the overlap matrix $\mathbf{S}$ are 1 and all the off-diagonal elements are null except $S_{a\vec{n}}\left(\vec{R}_A\right) = \langle\phi_a|\phi_{\vec{n}}\rangle = S_{\vec{n}a}\left(\vec{R}_A\right)$ which are functions of the atomic core position $\vec{R}_A$. Using Eqs. (6.23), (6.53) and (6.54)

$$S_{a\vec{n}}\left(\vec{R}_A\right) = \sum_{k=1}^{K} \sum_{\vec{m}} d_{a,k} B_{\vec{n}\vec{m}} G_{a\vec{m}}\left(\alpha_k, \beta_{m_z}, \vec{R}_A\right)$$

(6.59)

where

$$G_{a\vec{m}}\left(\alpha_k, \beta_{m_z}, \vec{R}_A\right) = \langle g_a\left(\alpha_k, \vec{R}_A\right) | g_{\vec{m}}(\beta_{m_z})\rangle \qquad (6.60)$$

is the overlap matrix of Gaussians and is also a functions of $\vec{R}_A$.

6.5 Hamiltonian and Its Matrix Elements

In this section we construct the one electron Hamiltonian for the system of a Na atom and a jellium slab and calculate its matrix elements in the basis described in the previous sections. The one-electron Hamiltonian of the system is

$$\hat{H} = -\frac{1}{2}\nabla^2 + V_A\left(\vec{r}, \vec{R}_A\right) + V_M(\vec{r}) \qquad (6.61)$$

where $V_A\left(\vec{r}, \vec{R}_A\right)$ is the atomic potential and $V_M(\vec{r})$ is the potential of the slab which we choose to as the one given by Eq. (6.31). However, due to the use of the localized basis functions and the partition method, the effective Hamiltonian in the primary region should be reconstructed, which includes the construction of the pseudopotential for the atomic core and adding a correction term to get correct electronic couplings.

6.5.1 Pseudopotential for the atomic core

In the present study, since we are not intending a full *ab initio* calculation, a pseudopotential for the atomic core is used for $V_A\left(\vec{r}, \vec{R}_A\right)$ to eliminate the inner-shell electrons from the calculation [Kahn et al., 76]. The pseudopotential usually has a form of

$$V_A\left(\vec{r}, \vec{R}_A\right) = \sum_{l=0} V^l\left(\vec{r}, \vec{R}_A\right)\hat{\Omega}_l \qquad (6.62)$$

where

$$\hat{\Omega}_l = \sum_{m=-l}^{l} |lm\rangle\langle lm| \qquad (6.63)$$

is the projection operator on $|lm\rangle$ and the functions V^l can be chosen in one of many possible forms [Szasz, 85] and usually contain some parameters whose values are chosen to give agreement with either the results of *ab initio* calculation or with that of experiments. In this study we choose the form suggested by Schwartz and Switalski [Schwartz and Switalski, 72],

$$V^l\left(\vec{r}, \vec{R}_A\right) = -\frac{Z - N_e}{|\vec{r} - \vec{R}_A|} + A_l \frac{exp\left(-\kappa_l|\vec{r} - \vec{R}_A|^2\right)}{|\vec{r} - \vec{R}_A|} \qquad (6.64)$$

where Z is the atomic number, N_e the number of electrons of the core, and A_l and κ_l are the pseudopotential parameters. The first term is the Coulomb potential of a charge of $Z-N_e$ and the second term is a correction due to the electrons in the inner shells.

Using the pseudopotential the eigenequation for an isolated Na atom is

$$\left[-\frac{1}{2}\nabla^2 + V_A\left(\vec{r}, \vec{R}_A\right)\right]\phi_a\left(\vec{r}, \vec{R}_A\right) = \epsilon_a\phi_a\left(\vec{r}, \vec{R}_A\right) \qquad (6.65)$$

We determine the parameter A_l and κ_l by fitting the eigenvalues ϵ_a with the experimental values $\epsilon_{3s}=-0.18884$ au and $\epsilon_{3p}=-0.11156$ au [Callaway, 69]. Another constrain imposed when choosing the parameters is that the pseudopotentials should become Coulombic at the distance where the core dies off, for example, at $3r_l$, where $3r_l$ is the radius of orbital l. However, the variation of parameter A_l is not too critical [Schwartz and Switalski, 72] and can be chosen in a cer-

tain range. The parameters for our pseudopotential are listed in Table 6.4. The pseudopotentials for 3s and 3p orbitals are plotted in Fig. 6.11.

Table 6.4. Pseudopotential parameters for 3s and 3p orbitals of Na atom.

	A_l	κ_l
3s	1.0	2.415
3p	3.0	0.515

6.5.2 A Correction Term to the Hamiltonian

The partition procedure described in Ch. 5 can be used to describe the evolution of the electronic states and the collisional charge transfer at short distances because of the local nature of the problem. But it complicates the description of the interaction between the surface and the atom when the atom is far away from the surface and the electrons relax, due to the use of the localized basis functions and the partition of the surface. Ignoring this relaxation would introduce an error. Although the error is small and does not effect the dynamics of electronic states to a great extent at small distance, the error accumulated at large distances could cause problems. This error induced by the partition could be significant in the case of collisional neutralization of ions.

To represent the relaxation of the electrons in the localized basis functions we add to the full Hamiltonian a correction term

$$\hat{V}_{loc} = \sum_{\vec{m} \in p} (\epsilon_F - \epsilon_{\vec{m}}) |\chi_{\vec{m}}\rangle \langle \chi_{\vec{m}}| \tag{6.66}$$
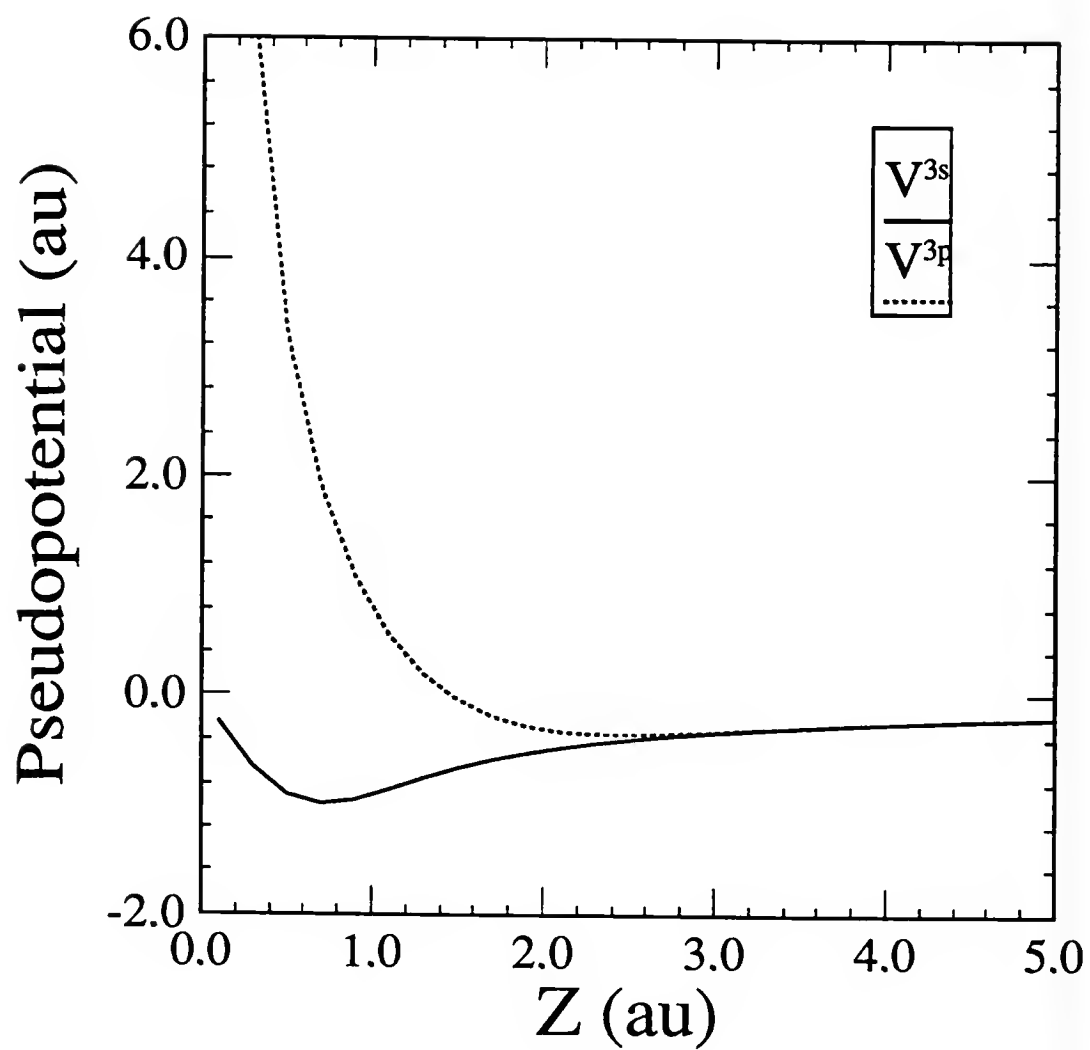
Figure 6.11 Pseudopotentials for 3s and 3p orbitals of the Na atom.

where the summation is over the primary region p and $\epsilon_{\vec{m}} = \langle \chi_{\vec{m}} | \hat{H}_M | \chi_{\vec{m}} \rangle$ with $\hat{H}_M = -\frac{1}{2} \nabla^2 + V_M$ the Hamiltonian of the slab. This term is constructed such that the asymptotic values of the electronic Hamiltonian are correct. With this correction term, the effective Hamiltonian in the primary region is

$$\hat{H}' = \hat{H} + \hat{V}_{loc} \tag{6.67}$$

which will be used in the TDHF calculation in place of $\hat{H}$.

6.5.3 Hamiltonian Matrix Elements

In the primary region the matrix elements of the Hamiltonian, Eq. (6.67), are

$$H'_{\mu\nu} = H_{\mu\nu} + \sum_{\vec{m}\in p} (\epsilon_F - \epsilon_{\vec{m}}) S_{\mu\vec{m}} S_{\vec{m}\nu} \tag{6.68}$$

or explicitly,

$$H'_{aa'} = H_{aa'} + \sum_{\vec{m}\in p} (\epsilon_F - \epsilon_{\vec{m}}) S_{a\vec{m}} S_{\vec{m}a'} \tag{6.69}$$

$$H'_{a\vec{n}} = H_{a\vec{n}} + (\epsilon_F - \epsilon_{\vec{n}}) S_{a\vec{n}} \tag{6.70}$$

$$H'_{\vec{n}\vec{n}} = H_{\vec{n}\vec{n}} + \epsilon_F - \epsilon_{\vec{n}} \tag{6.71}$$

$$H'_{\vec{n}\vec{n}'} = H_{\vec{n}\vec{n}'} \qquad \vec{n} \neq \vec{n}' \tag{6.72}$$

The matrix elements of **H** are calculated as follows

$$\begin{aligned} H_{aa'} &= \langle a | -\frac{1}{2} \nabla^2 + V_A + V_M | a' \rangle \\ &= \epsilon_a S_{aa'} + \langle a | V_M | a' \rangle \end{aligned} \tag{6.73}$$

$$H_{a\vec{n}} = \langle a| - \frac{1}{2}\nabla^2 + V_A|\vec{n}\rangle + \langle a|V_M|\vec{n}\rangle$$

$$= \epsilon_a S_{a\vec{n}} + \langle a|V_M|\vec{n}\rangle \tag{6.74}$$

$$H_{\vec{n}\vec{n}'} = \langle \vec{n}| - \frac{1}{2}\nabla^2 + V_M|\vec{n}'\rangle + \langle \vec{n}|V_A|\vec{n}'\rangle$$

$$= H_{M,\vec{n}\vec{n}'} + \langle \vec{n}|V_A|\vec{n}'\rangle \tag{6.75}$$

where $H_{M,\vec{n}\vec{n}'} = \langle \vec{n}|H_M|\vec{n}'\rangle$ does not depend on $\vec{R}_A$. The matrix elements $\langle a|V_M|a\rangle$, $\langle a|V_M|\vec{n}\rangle$ and $\langle \vec{n}|V_A|\vec{n}\rangle$ depend on $\vec{R}_A$ and are calculated by using the basis functions as linear combinations of Gaussians. Neglecting all the three-center integrals, we further have

$$\langle \vec{n}|V_A|\vec{n}'\rangle = \delta_{\vec{n}\vec{n}'}\langle \vec{n}|V_A|\vec{n}\rangle \tag{6.76}$$

When it approaches the surface, the ion causes charge rearrangement and forms an image potential in the solid, which is important at low collisional energies. When the image potential is considered the corrected Hamiltonian is

$$\hat{H}' = \hat{H} + \hat{V}_{rearr} \tag{6.77}$$

where

$$\hat{V}_{rearr} = \hat{V}_{loc} + \hat{V}_{im} \tag{6.78}$$

$$\hat{V}_{im} = -\frac{1}{4Z_A}\left(I - \sum_a |a\rangle\langle a|\right) \tag{6.79}$$

CHAPTER 7
INTEGRATION OF LINEARIZED TDHF EQUATIONS

The linearization procedure introduced in Ch. 4 has been implemented in a computation code and has been used in the integration of TDHF equations for both atomic systems [Runge et al., 90] and atom-surface systems [Feng et al., 91]. In its applications, we repeatedly tested and improved this procedure and the computing programs. In this chapter we discuss some of the computational aspects of our application of this procedure.

In Sect. 7.1 we introduce an approximation for the driving term and present the algorithm for integration of the linearized TDHF equations. In Sect. 7.2 the flowchart of the computation program for the integration is presented. In Sect. 7.3 we discuss the stability and convergence of the solutions of the equations and the choice of several computational parameters.

7.1 The Algorithm for Numerical Integration of TDHF Equations

The linearization procedure splits the TDHF equation into two linearized time-dependent differential equations in a small time interval $t_0 \leq t \leq t_1$, one for a time-dependent density matrix reference, $\mathbf{P}^0(t)$, and another for the change of the density matrix due to the motion of the nucleus, $\mathbf{Q}(t)$.

Omitting the electron-electron interaction, the coefficient matrix $\mathbf{W}$ of the equation is time-independent and the equation for $\mathbf{P}^0(t)$, Eq. (4.37), has the formal solution of the form of Eq. (4.47). The equation for $\mathbf{Q}(t)$, Eq. (4.38), has a formal solution of Eq. (4.50) with a kernel $\Gamma_{k\lambda\rho l}$ which is a time integral of the driving matrix $\bar{\mathbf{D}}'(t)$. Since the time interval is chosen to be small, we can approximate the driving term by a function linear in time, that is,

$$\bar{\mathbf{D}}'(t) = \mathbf{C}{\cdot}(t - t_0) \tag{7.1}$$

where the coefficient matrix $\mathbf{C}$ is given by

$$\mathbf{C} = \frac{\bar{\mathbf{D}}'(t_1)}{t_1 - t_0} \tag{7.2}$$

The term $\bar{\mathbf{D}}'(t_0)$ does not appear in the above equations, since the matrix $\bar{\mathbf{D}}'(t)$ is proportional to the changes in the time interval, $\Delta \mathbf{S}^{-1}$ and $\Delta \tilde{\mathbf{H}}$, and $\bar{\mathbf{D}}'(t_0)$ is actually zero, as can be seen from Eq. (5.16). Substituting Eq. (7.1) into Eq. (4.51), we have

$$\begin{aligned}
\Gamma_{k\lambda\rho l}(t, t_0) = {}& i\frac{t - t_0}{w_k - w_l^*}exp[-i(w_k - w_l^*)(t - t_0)] \\
& + \frac{1}{\left(w_k - w_l^*\right)^2}\{exp[-i(w_k - w_l^*)(t - t_0)] - 1\}
\end{aligned} \tag{7.3}$$

7.2 Computation Program

All the computation programs have been tested and run on SUN3/50 workstation, SUN4/490 and FPS 500EA1/1 computers. The flowchart of the main program of integration for linearized TDHF equations, TDLINEAR.F is given in Fig. 7.1.
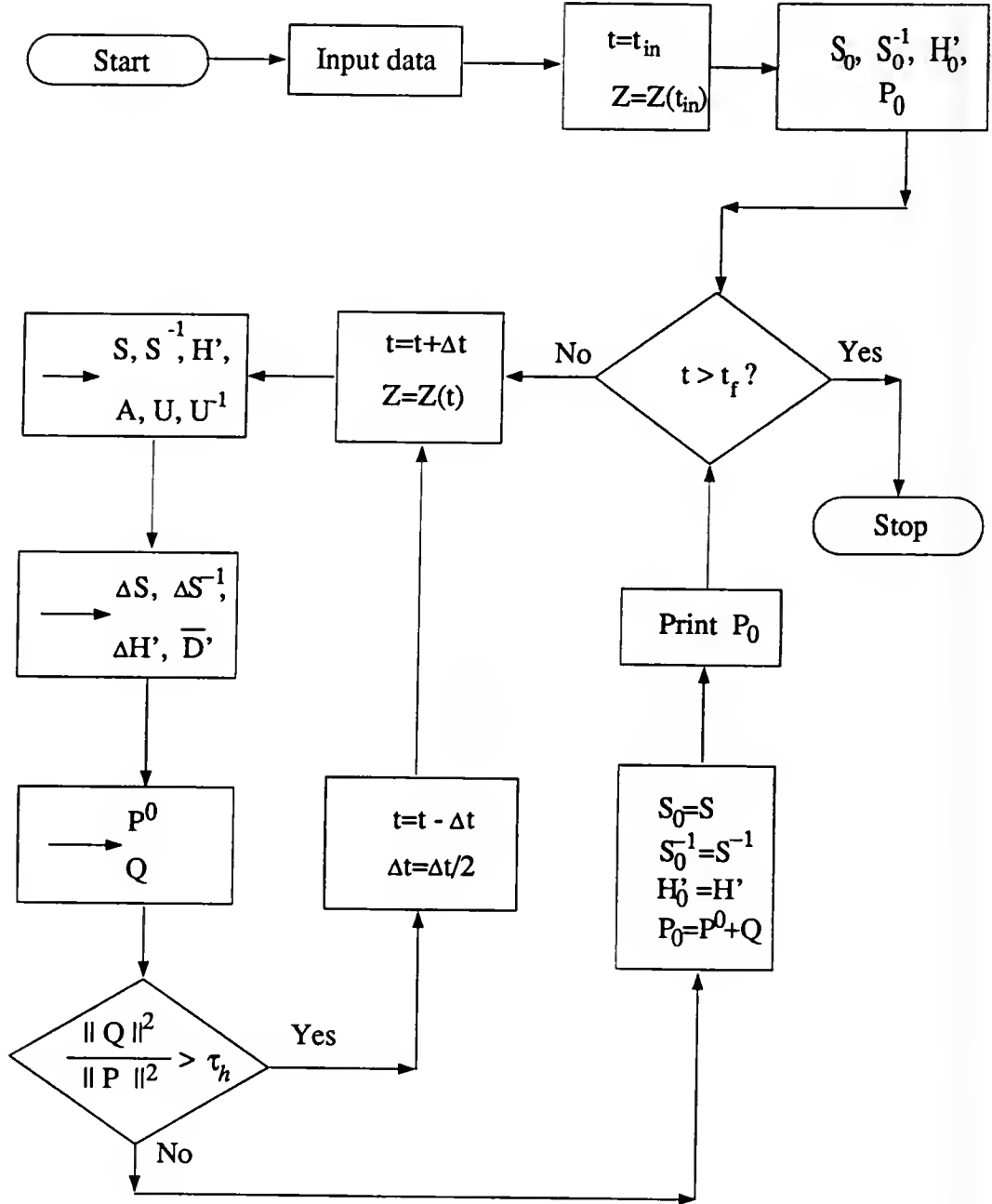
Fig. 7.1 Flowchart of program TDLINEAR.F for integration of the linearized TDHF equations.

7.3 Stability and Convergence of the Numerical Integration

The solutions of TDHF equations are obtained by integration of the linearized equations in steps. Since possible errors, induced by the linearization and the approximation that the driving term is proportional to time, depend on the integration time interval, integration has to be performed in many small steps. This could create a problem in that the computational errors may be accumulated in the course of the integration and cause the solution unstable. The programs we used give stable results against small changes of physical and computational parameters, such as atom-surface interaction parameters, collision energy, time, and initial and final distances. We have introduced several computation parameters to test and improve the stability and convergence of the computation.

7.3.1 Tolerances

To achieve the minimum error and better efficiency, the integration is conducted with a variable time interval $\Delta t = t_1 - t_0$, where t_0 is the starting time and t_1 is the ending time of the interval. After the integration over one step, the quotient $||Q_{pp}(t_1)||^2 / ||P_{pp}^0(t_1)||^2$ is checked against a designated higher tolerance τ_h. If it is found greater than τ_h, the program returns to the original starting point t_0 to repeat the calculation with a step size reduced to $\Delta t/2$. Such procedure is repeated after each integration until the quotient is less than τ_h, then the program proceeds to perform integration in the next step with the reduced step size. To accelerate the calculation in the region where the solutions change little, we introduce also

a lower tolerance τ_l, such that if $||\mathbf{Q}_{pp}(t_1)||^2/||\mathbf{P}^0_{pp}(t_1)||^2 < \tau_l$, the step size in the next step will be doubled. Both τ_h and τ_l have been carefully checked to assure the convergence of the solutions.

We use $\tau_h=10^{-6}$ and $\tau_l=10^{-7}$ in our calculations. Checking calculations with smaller tolerances $\tau_h=10^{-7}$ and $\tau_l=10^{-8}$ have also been conducted for selected energies. While the computing time for the smaller tolerances is increased significantly, the solutions for the TDHF equations change little in the entire collision. For example, The calculations with $\tau_h=10^{-7}$ and $\tau_l=10^{-8}$ required 5,830, 3,741 and 2,156 steps for the collisional energies of 1.0, 10.0 and 100.0 au, respectively; the calculations with $\tau_h=10^{-7}$ and $\tau_l=10^{-8}$ required 11,151, 7,282 and 4,156 steps, respectively, while the electronic populations changes less than 0.005 au for all times.

7.3.2 Initial and Final Distances

Although the atom and the surface are regarded as uncoupled when the distance between them is greater than the interaction range, the initial and the final distances used in the calculation must exceed the distances chosen by physical considerations.

We have checked the convergence of the results while changing the initial position Z_{in} and final position Z_f for selected collisional energies, and found that the results became stable when $Z_{in} >12$au and $Z_f >16$ au. For Z_{in} and Z_f in the range of 16–30 au, the electronic populations vary less than 0.005 au for

collisional energies of 1.0, 10.0 and 100.0 au. We use Z_{in}=20 au and Z_f=20 au in our calculations.

CHAPTER 8
APPLICATIONS

The time-dependent molecular method developed in Chapter 2 has been applied to ion-atomic systems to study collisional charge transfer and has provided useful insight [Runge et al., 90]. In this Chapter we further extend our TDMO method to ion-surface systems [Feng et al., 91], with the help of the linearization procedure developed in Chapter 4. Ion-surface systems are much more complicated than atomic systems, and the direct application of the TDMO method to these systems will lead to an infinite number of time–dependent differential equations. An attempt has been made to use a TDMO method in atom-surface scatterings by modeling the surface with a cluster [Olson and Garrison, 85]. The partition method for extended systems and the localized basis functions we have developed provide a convenient way to treat extended systems and requires us to solve only a few effective TDHF equations.

The application presented in this chapter is a combination of the methods developed in previous chapters. Our purpose is to test the TDMO method and partition procedure on an extended system and to develop a complete and practical method for investigation of dynamics in atom-surface collisions. In order to simplify the problem, it is necessary to use some approximations in the treatment

of the model, trajectory and electron–electron interaction, which will be elaborated in the text.

In Sect. 8.1, we describe the model system of Na–W(110) and calculate the electronic couplings and atom-surface interaction potentials. Sect. 8.2 is devoted to the trajectory of the colliding nucleus. A simple potential is used in the application, which allows an analytic form for the trajectory. Dynamic aspects of the system, such as initial conditions and incident parameters, are also discussed. In Sect. 8.3 we describe the charge transfer process in the collision. In Sect. 8.4 we present the results for the charge transfer. The evolutions of the electronic populations of atomic states and of the surface site are obtained by performing the linear integration of the TDHF equations. The charge transfer as a function of collision energy is calculated. To further explore the cause underlying its energy dependence, the electronic populations are examined as functions of the inverse of the initial velocity of the colliding ion.

8.1 Na–W(110) Model System

8.1.1 Hamiltonian and Basis Functions

The system we consider consists of a jellium slab described in Ch. 6 and a Na atom. The slab is located between $-D \leqslant z \leqslant 0$, where D is the thickness of the slab. The location of the Na atom is $\vec{R}_A(t)$, which is a function of time. Using the partition method developed in Ch. 5, we divide the system into a primary region and a secondary region, with the primary region consisting of the

Na atom and only one site on the surface, which is the one at the "impact point" at $\vec{R}_{\vec{0}} = (0, 0, 0)$, and the secondary region being the remainder of the surface.

The effective one electron Hamiltonian in the primary region is given by Eq. (6.67). The potential of the slab V_M is assumed to be a step potential given by Eq. (6.31) with a potential well depth $V_0 = 0.846$ au. A pseudopotential for the atomic core is used for the atomic potential V_A, as described in Ch. 6, to eliminate the inner–shell electrons. To simplify the calculation, the electron-electron interaction is ignored.

The set of localized basis functions includes the generalized Wannier functions for the slab constructed in Ch. 6 and atomic functions for 3s, $3p_x$, $3p_y$ and $3p_z$ orbitals of Na, which are the STO-3G functions described in Ch. 6.

8.1.2 Electronic Couplings

We neglect the image potential and the differential overlap between the atomic basis functions and the basis functions in the secondary region, so that

$$S_{a\vec{m}} = \left(\Delta S^{-1}\right)_{a\vec{m}} = H_{a\vec{m}} = \Delta H_{a\vec{m}} = 0 \qquad \vec{m} \in s \qquad (8.1)$$

where s stands for the secondary region. The matrix elements of Hamiltonian, Eq. (6.67), are calculated in Ch. 6. The off-diagonal Hamiltonian matrix elements between the atomic orbitals and between the atomic orbitals and surface site $\vec{R}_{\vec{0}}$ are related to the electronic couplings, which determine charge rearrangement during the collision. In Fig. 8.1 the matrix elements $H'_{3s,3p_z}$, $H'_{3s,\vec{0}}$ and $H'_{3p_z,\vec{0}}$ are plotted as functions of the distance between the atomic core and the surface,

with both the atomic core and the slab site of the primary region on the z–axis. The couplings between $3p_x$ or $3p_y$ and $\vec{0}$ are zero by symmetry and are not plotted. At large distances from the surface, the atom behaves just like an isolated one and the off–diagonal elements between the atomic orbitals of different symmetry are zero. As the atom gets close to the surface the influence of the surface begins to be felt and the amplitudes of these elements begin to increase. The figure shows that the range of the electronic couplings is about 8 au. The couplings are large as the distance decreases below 4 au; consequently, a strong orbital mixing and charge transition may occur.

8.2 Atom-Surface Interaction Potentials and Trajectory

8.2.1 Atom-Surface Interaction Potentials

We assume that the atom-surface interaction potential contains contributions from two parts: the interaction between the surface and the bare core of the atom, and the average electronic energy. Depending on the charge states, the interaction potential has different forms. For the ion plus surface, the potential is

$$V_{\Sigma A+}\left(\vec{R}_A\right) = V_{cc}\left(\vec{R}_A\right) + H'\left(\vec{0},\vec{0}\right) \qquad (8.2)$$

where $V_{cc}\left(\vec{R}_A\right)$ is the interaction potential between the ion core and the surface and is chosen to be a Born-Mayer type potential [Hulpke and Mann, 83]

$$V_{cc}\left(\vec{R}_A\right) = V_1 \sum_{\vec{m} \in p} exp\left(-\alpha|\vec{R}_A - \vec{R}_{\vec{m}}|\right) \qquad (8.3)$$

with the Born-Mayer parameters V_1=188.6 au and α=1.92 au, where the summation is over the primary region. The term $H'\left(\vec{0},\vec{0}\right) = \langle \chi_{\vec{0}}|H'|\chi_{\vec{0}}\rangle$ is the diagonal
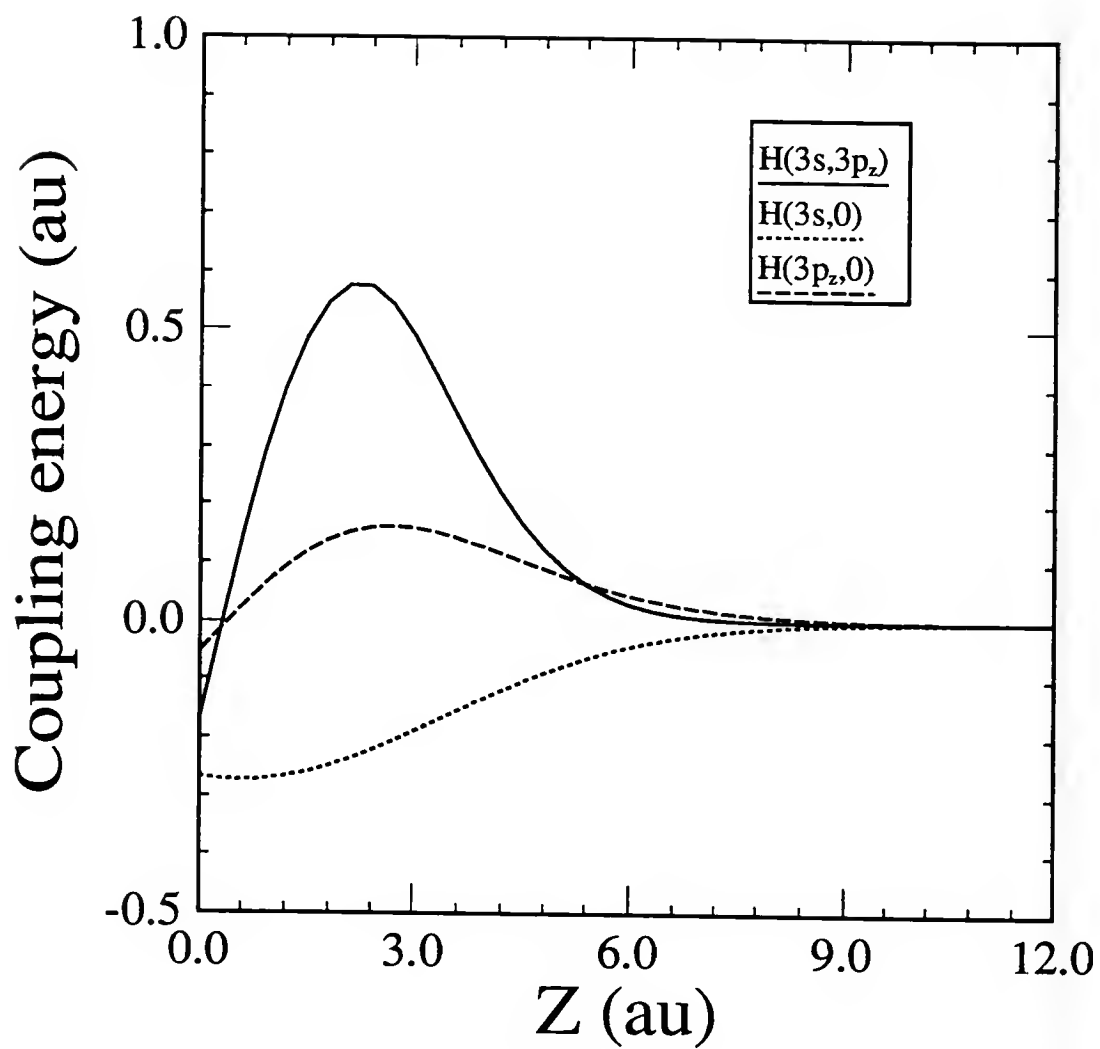
Figure 8.1 Coupling energies between the atomic orbitals and the surface site $\vec{0}$. The site $\vec{0}$ and the atomic core are on the z–axis, and $\vec{0}$ is on the first layer at $\vec{R}_{\vec{0}}$.

matrix element of the effective Hamiltonian corresponding to the surface site in the primary region. When an electron is transferred to one of the atomic orbitals, the atom-surface interaction potential is given by

$$V_{\Sigma^+ A(a)}\left(\vec{R}_A\right) = V_{cc}\left(\vec{R}_A\right) + H'(a, a) \tag{8.4}$$

where a is 3s, $3p_x$, $3p_y$ or $3p_z$, and $H'(a, a) = \langle \chi_a | H' | \chi_a \rangle$

Fig 8.2 plots the interaction potentials of $V_{\Sigma A^+}\left(\vec{R}_A\right)$, $V_{\Sigma^+ A(3s)}\left(\vec{R}_A\right)$, $V_{\Sigma^+ A(3p_z)}\left(\vec{R}_A\right)$ and $V_{\Sigma^+ A(3p_x)}\left(\vec{R}_A\right)$ as functions of the distance between the Na atomic core and the W(110) surface. Potential $V_{\Sigma^+ A(3p_y)}\left(\vec{R}\right)$ is not shown in the figure since it is equal to $V_{\Sigma^+ A(3p_x)}\left(\vec{R}\right)$. As one can see from the figure, the contribution to the total potential from the electronic energy, which contains the interaction between electrons and the surface positive background and the atomic core, is negative, but its amplitude varies with the states. In case of $3p_x$ and $3p_y$ orbitals, the electronic energies are very small and $V_{\Sigma^+ A(3p_x)}\left(\vec{R}_A\right)$ and $V_{\Sigma^+ A(3p_y)}\left(\vec{R}_A\right)$ are close to the core-core potential $V_{cc}\left(\vec{R}_A\right)$. For other cases, the potential change due to the interaction between electrons and the slab potential or the atomic potential are strong at short distance. The ion-surface potential $V_{\Sigma A^+}\left(\vec{R}_A\right)$, which is below the atom–surface potential at large distances, crosses $V_{\Sigma^+ A(3s)}\left(\vec{R}_A\right)$ and $V_{\Sigma^+ A(3p_z)}\left(\vec{R}_A\right)$ at about $z=5.5$ au and stays higher as the distance decreases.

8.2.2 Trajectory

The trajectory of the projectile in the collision problem has a significant effect on the dynamics of the electronic states. In Ch. 1 we have discussed
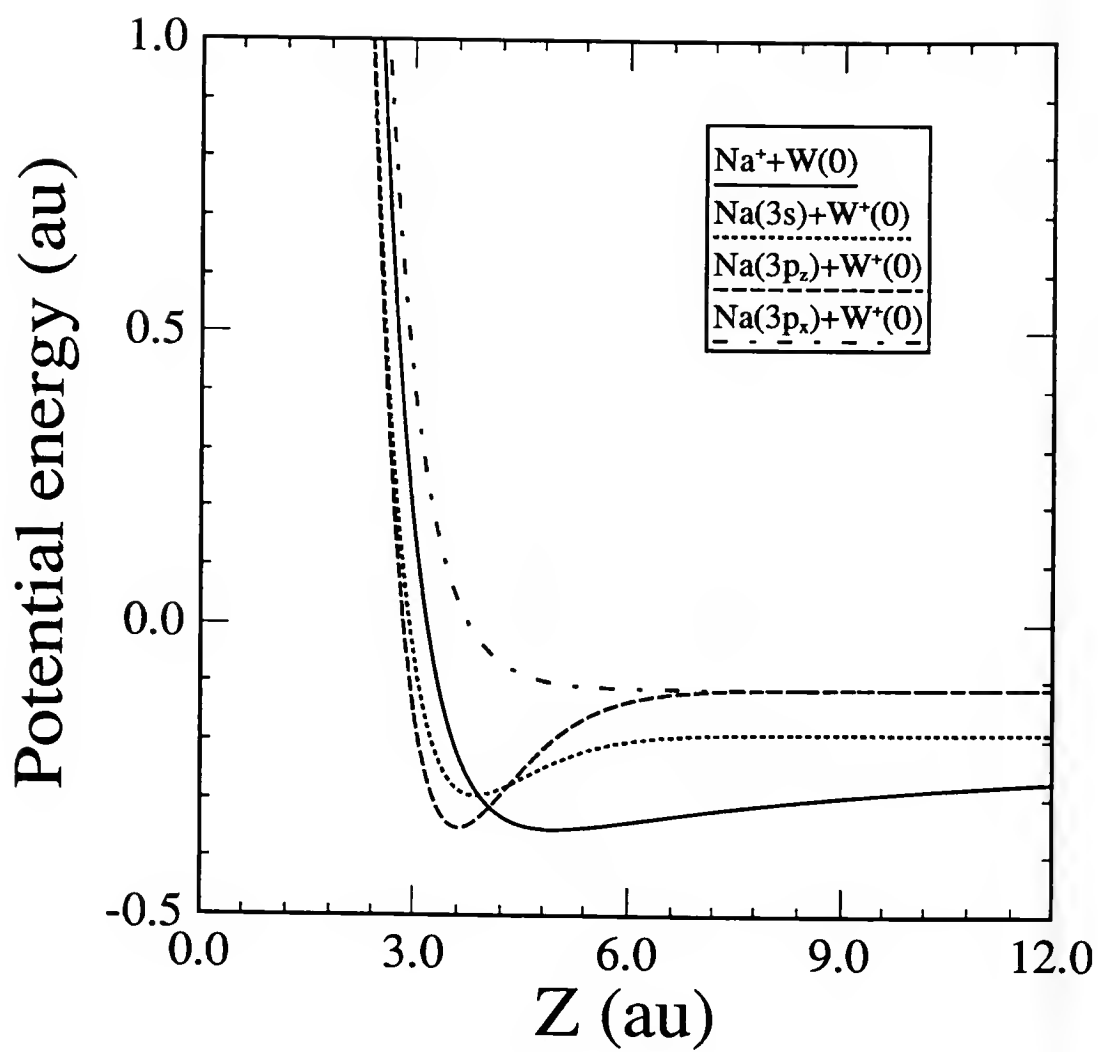
Figure 8.2 Ion-surface potential for $V_{\Sigma A+}\left(\vec{R}_A\right)$ and atom-surface potentials for $V_{\Sigma+A(3s)}\left(\vec{R}_A\right)$, $V_{\Sigma+A(3p_z)}\left(\vec{R}_A\right)$ and $V_{\Sigma+A(3p_x)}\left(\vec{R}_A\right)$.

at length this subjects as well as the merits and the applications of a variety of approaches. For the range of collision energy of the Na atom we are interested in, the trajectory of the nucleus can be treated as a classical one which couples with the electronic degrees of freedom of motion. For example, from the atom-surface potentials $V_{\Sigma A^+}\left(\vec{R}_A\right)$ and $V_{\Sigma^+ A(a)}\left(\vec{R}_A\right)$ described above, one can construct average potential energy curves corresponding to various configurations to obtain a nuclear trajectory which depends on the charge states of the atom. The effect of the coupling between the electronic motion and the nuclear motion can also be taken into account by introducing an effective potential relating to the coupling [Runge et al., 90].

Although a thorough study of the trajectory and its effects on the charge transfer is a valuable and interesting topic, we neglect the coupling between the nuclear motion and the electronic degrees of freedom of motion to concentrate on the TDHF method. Instead we use a simple trajectory $\vec{R}_A(t)$ for the colliding atom core which is determined by an atom-surface core-core interaction potential $V_{cc}\left(\vec{R}_A\right)$. This is justified for the hyperthermal collision energies of present interest. For the same reason we neglect the image potential in the metal.

In this case the trajectory has a prescribed form and does not depend on the electronic state of the atom. Let t=0 when Z_A is a minimum, then the trajectory is

$$
\begin{cases}
X_A(t) = X_A(t_{in}) + v_x(t - t_{in}) \\
Y_A(t) = Y_A(t_{in}) + v_y(t - t_{in}) \\
Z_A(t) = \frac{1}{\alpha} ln\left[\left(\frac{m_a v_z^2}{2V_1}\right)^{-1} cosh\left(\frac{\alpha v_z t}{2}\right) \right]
\end{cases}
\tag{8.5}
$$

where m_a is the mass of the atom, t_{in} is the initial time, and v_x, v_y and v_z are the x, y, and z components of the initial velocity of the nucleus, respectively. The closest distance from the surface the atom can get to is decided by v_z and is given by $Z_A^{min} = \frac{1}{\alpha} ln \left(\frac{2V_1}{m_a v_z^2} \right)$. In Fig. 8.3 we show trajectories of the Na atom with the initial kinetic energies of 1, 10 and 100 au and a normal incident angle.

The initial distance and the final distance between the atom and the surface are chosen such that further increases in either will not affect charge transfer. It has been found that it is enough to use 20 au for both initial and final distances for all energies. We consider only the incidence normal to the surface in this study.

8.3 Charge Transfer

In the course of the collisions, the Na ions approach, collide with the surface and then recede along their classical trajectory. In the meantime, electrons interact and evolve quantum mechanically. By the time the collisions are over, the charges have been considerably rearranged, and some of them transferred to the ions. For those neutralized ions, a variety of possible electronic states may be populated, which leads to the atomic orbital orientation and alignment. For the normal incidence by the ion there is no orbital polarization along x- or y- axes, since the only non-zero couplings in this case are those between the surface state and the 3s and $3p_z$ orbitals.

The two basic mechanisms for charge transfer in atom-surface collisions are the near-resonance process and the Auger process. In the model we are studying, since the energies of the atomic states participating in the charge transfer are in the
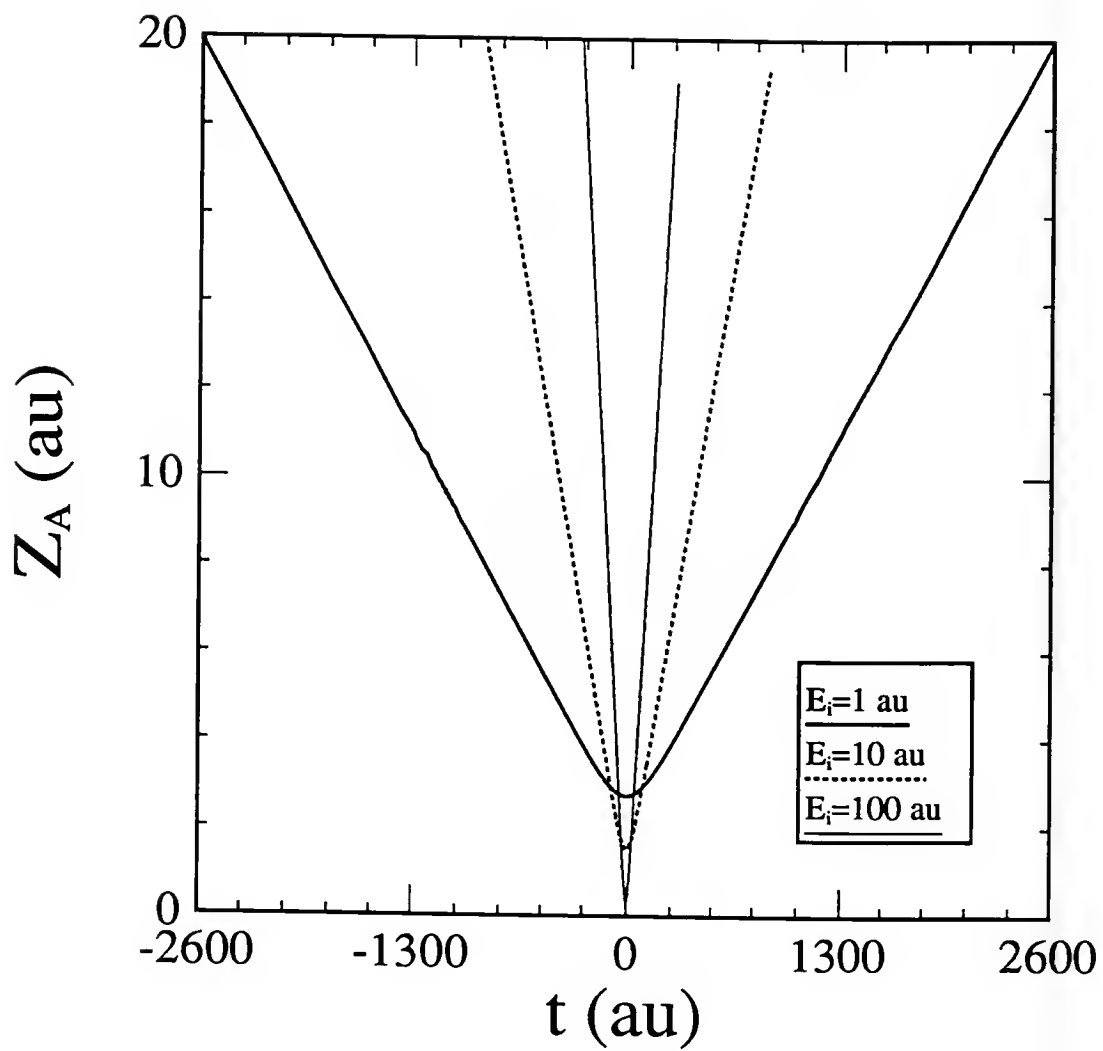
Figure 8.3 Trajectories for the Na atom with the initial kinetic energies of 1, 10 and 100 au and a normal incident angle. Time t is set to zero when the atom is at the closest distance from the surface.

range of the electronic band of the surface at all distances, the charge transfer in the system is expected to be dominated by the near–resonance process. Thus, we assume that the Auger process is negligible and only the near-resonance charge transfer process takes place in the collision. The fact that all the potential energies are close at small distances, as shown in Fig. 8.2, justifies our assumption that the near–resonance process is the dominant charge transfer mechanism.

The density matrix elements for an isolated surface at temperature $T=0K$ are

$$\bar{P}^{\gamma}_{\vec{n}\vec{m}} = \sum_{|\vec{k}| \leq k_F} U^{\dagger}_{\vec{n}\vec{k}} U_{\vec{k}\vec{m}} \tag{8.6}$$

where the matrix $\mathbf{U}$ is defined in Ch. 6 and k_F is the wave vector corresponding to the Fermi energy which is evalued in Appendix C. Since the surfaces of the jellium slab considered here are parallel to the x-y plan, Eqs. (6.45) and (6.46) can be used to simplify the calculation.

At the initial time, the surface and the atom are not coupled due to a very large initial distance between them. We assume both the surface and the ion are in their ground states initially; this leads to $P_{aa'}(t_{in}) = 0$ and $P_{a\vec{0}}(t_{in}) = 0$ and the only non-zero density matrix element in the primary region is $P^{0}_{\vec{0}\vec{0}}(t_{in}) = \bar{P}_{\vec{0}\vec{0}}$.

Applying the partition method developed in Ch. 5 and the linearization procedure developed in Ch. 4, we come up with the effective TDHF equation (5.15) in the primary region with a linear coefficient matrix $\mathbf{W_{pp}}$. Using Eq. (8.1)

$$\mathbf{W_{pp}} = \left(\mathbf{S_0^{-1} H_0}\right)_{\mathbf{pp}} = \left(\mathbf{S_0^{-1}}\right)_{\mathbf{pp}}(\mathbf{H_0})_{\mathbf{pp}} + \left(\mathbf{S_0^{-1}}\right)_{\mathbf{ps}}(\mathbf{H_0})_{\mathbf{sp}}$$
$$= \left(\mathbf{S_0^{-1}}\right)_{\mathbf{pp}}(\mathbf{H_0})_{\mathbf{pp}} \tag{8.7}$$

In the effective TDHF equation the matrices $\mathbf{S}$, $\Delta\mathbf{S}$, $\mathbf{H}$ and $\Delta\mathbf{H}$ are time dependent through the known trajectory $\vec{R}_A(t)$ given by Eq. (8.5). The equation contains a driving term $\bar{\mathbf{D}}'$ given by Eq. (5.16), in which all the matrix multiplications are performed in the primary region except for $\mathbf{P}^0_{ps}(t_{in})\tilde{\mathbf{H}}^{\dagger}_{0sp}$ and $\tilde{\mathbf{H}}^{\dagger}_{0ps}\mathbf{P}^0_{sp}(t_{in})$, which are time-independent and have to be calculated only once.

The Effective TDHF equation is integrated by use of the linearization procedure introduced in Ch. 4. An numerical approximation we used in this application is to replace the driving matrix $\bar{\mathbf{D}}'$ by a function linear of time t in the time interval $t_0 \leq t \leq t_1$, in which the linearized TDHF equation is integrated. The error caused by this approximation has been reduced by decreasing the step size until a stable result has been reached.

8.4 Results

We have applied the time-dependent molecular orbital method to the above Na–W(110) model with the initial kinetic energy of the atom in the range of 1 au to 170 au. The collisional charge transfer is characterized by the electronic population and orbital polarization parameters defined in Ch. 3. For the normal incidence, the atomic orbitals are polarized only along the z-axis.

8.4.1 Evolution of Electronic Populations

The evolution of the electronic density matrix is obtained by integrating the TDHF equation step by step. The electronic populations of the atomic orbitals and surface site are calculated according to the definitions given in Ch. 3. Since

the electron spin polarization is ignored, the electronic population of an orbital is simply twice that for one spin on that orbitals.

In Fig. 8.4(a) and Fig. 8.4(b) we show evolutions of the electronic populations of 3s and $3p_z$ orbitals, $n(3s)$ and $n(3p_z)$, respectively, for a collision energy of 1 au. The electronic population of the surface site $\vec{0}$, $n(0)$, is shown in Fig. 8.4(c). In these figures, the time is chosen such that t is negative when the atom is moving toward the surface and is positive when it is moving away from the surface, and at $t=0$ the atom is at the closest distance from the surface. The trajectory is plotted in Fig. 8.4(d) as a reference on the distance between the atomic core and the surface. Initially, the atom is ionized. At large distances, the interaction between the surface and the atom is so weak that they behave almost like isolated ones without charge exchange between them. At around $z=5au$, $n(3s)$ and $n(3p_z)$ begin to rise, indicating that the atom enters the interaction region. As the atom gets closer, the interactions are strong and the electronic populations of the atomic orbitals quickly grow to significant values. Since all the three orbital energies are close at small distances and even cross each other at some points, electrons hop among the three orbitals rapidly, resulting in fast oscillations in electronic populations. As the atom moves away from the surface, the charge exchange is reduced and the electronic populations gradually approach steady values. It is noticed from the figures that the evolution pattern is not symmetric on the way in and on the way out, especially for 3s orbital, reflecting its dependence of the charge redistribution. It can be seen from the figures that

the oscillation frequencies of the populations change with the distance. A careful check has shown that the frequencies are proportional to the energy differences at that distance but independent of the populations of the states.

Similar patterns are seen for the collisions at energies of 10 au and 100 au. Fig. 8.5(d) shows the trajectory of the atom at initial energy of 10 au, Figs. 8.5(a), 8.5(b) and 8.5(c) present the results for $n(3s)$, $n(3p_z)$ and $n(0)$ at this energy, respectively. Figs. 8.6(a), 8.6(b), 8.6(c) and 8.6(d) plot $n(3s)$, $n(3p_z)$, $n(0)$ and the trajectory, respectively for the collision of initial energy at 100au.

8.4.2 Electronic populations after collisions

The electronic populations approach steady final values as the atom moves far away from the surface. The final charge distribution depends on the collision energy. We are interested in wether there is a pattern for the variation of the electronic populations after the collision and wether such a pattern, if it exists, can be understood physically and provide information about the interaction and dynamics of the ion-surface collision.

We calculate the electronic populations after the collision for a collision energy range between 1 au and 170 au. The electronic population of the 3s orbital after the collision, $n(3s)$, is shown in Fig. 8.7 as a function of the collision energy. We found that Na ions are neutralized at all energy range, and that the population is relatively lower at the higher energies, indicating that the neutralization probability is smaller. An energy threshold for charge transfer of 0.02–0.04 au has been reported for the Na-W system [Hurkmans et al., 76], below which the charge
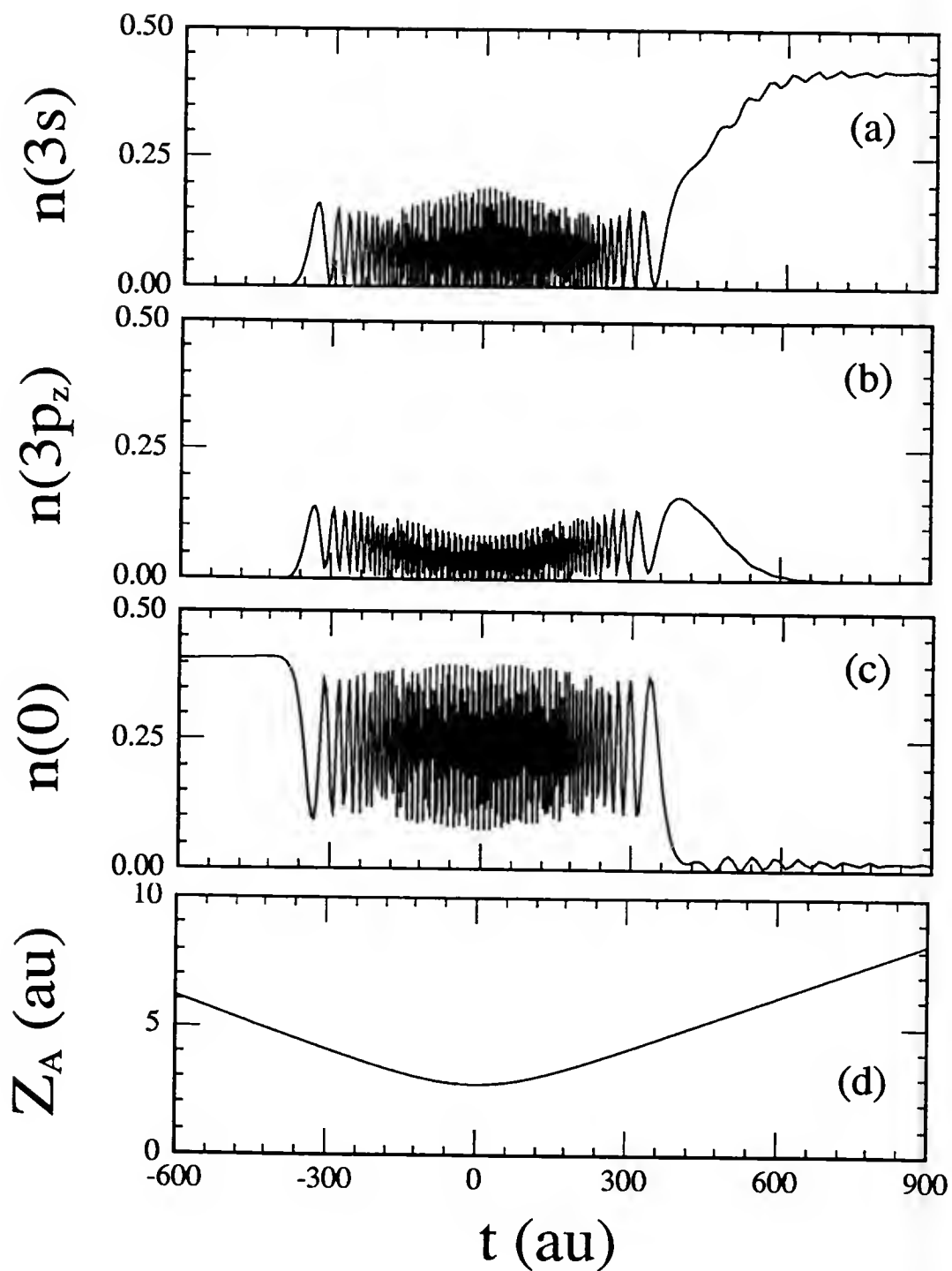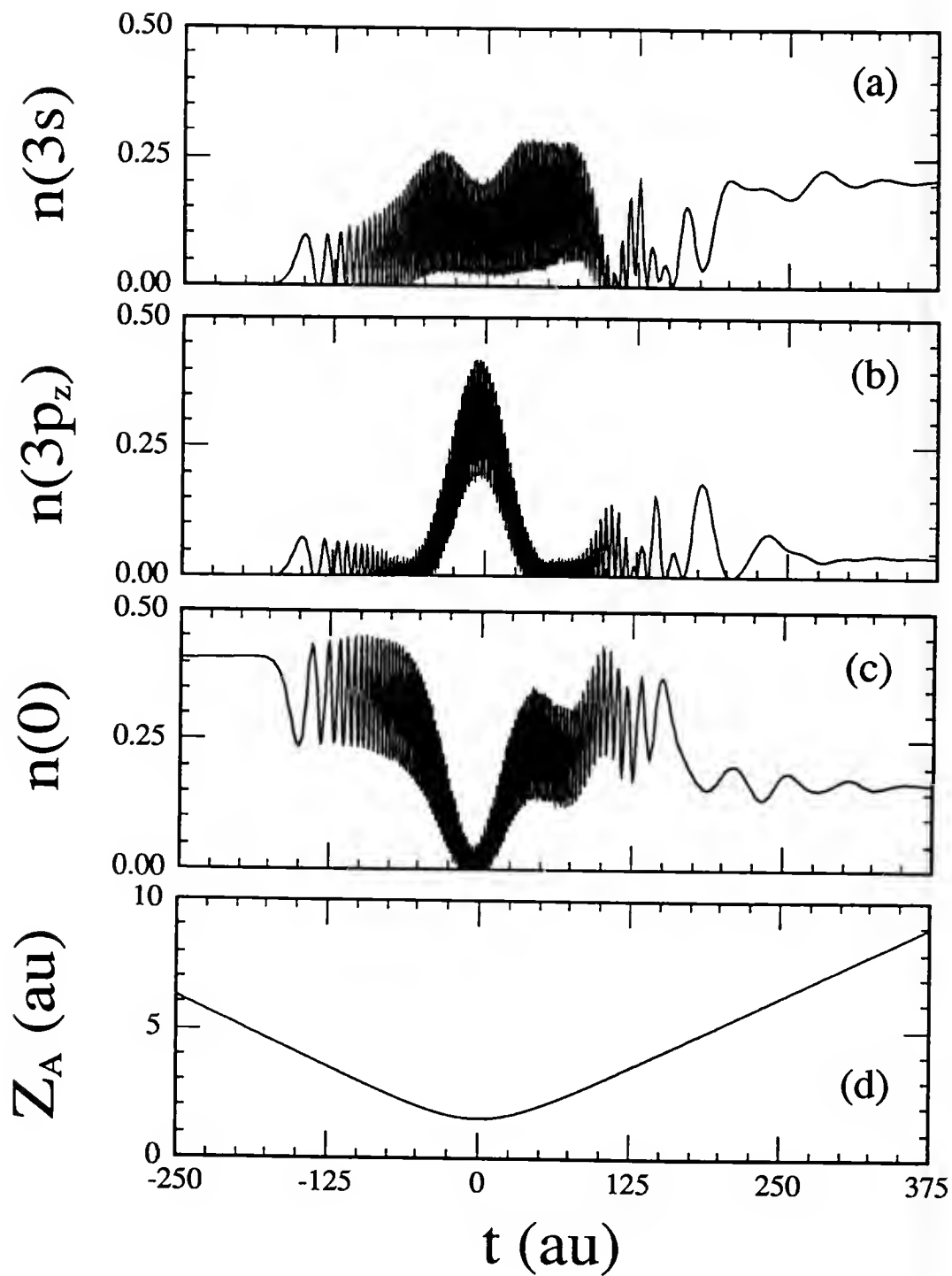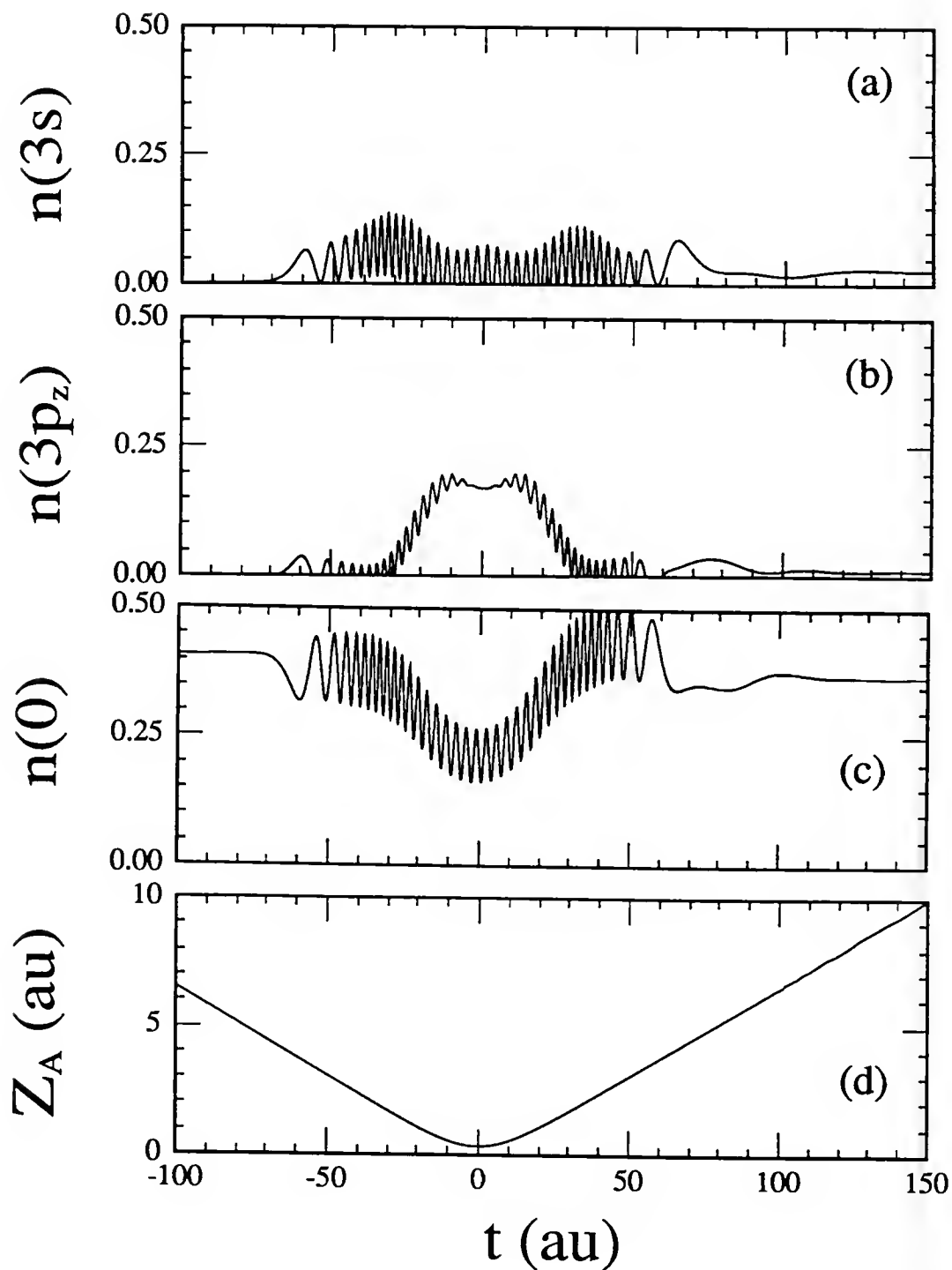
Figure 8.4 The electronic populations and trajectory of Na atom with a collision energy of 1 au. (a) The electronic population of 3s orbital, (b) the electronic population of $3p_z$ orbital, (c) the electronic population of surface site $\vec{0}$, (d) trajectory.

Figure 8.5 The electronic populations and trajectory of Na atom with a collision energy of 10 au. (a) The electronic population of 3s orbital, (b) the electronic population of $3p_z$ orbital, (c) the electronic population of surface site $\vec{0}$, (d) trajectory.

Figure 8.6. The electronic populations and trajectory of Na atom with a collision energy of 100 au. (a) The electronic population of 3s orbital, (b) the electronic population of $3p_z$ orbital, (c) the electronic population of surface site $\vec{0}$, (d) trajectory.

transfer is cut off. We found no threshold in this study, the reason being that our energy range is above the expected threshold. The electronic population oscillates between zero and its maxima with a frequency that decreases with the energy. There is an abnormal region around an energy of 4 au, where the oscillations are slower than that in the adjacent regions.

In Fig. 8.8, the electronic population of the $3p_z$ orbital after the collision, $n(3p_z)$, is shown as a function of the collision energy. At small energies, $n(3p_z)$ is zero; it begins to increase slowly at E=1.9 au; it grows faster with an oscillatory amplitude after E=2.5 au. A noticed difference is that the amplitudes of the oscillation of $n(3p_z)$ are small although the frequency is about the same as that for $n(3s)$. Unlike $n(3s)$ whose maxima steadily decreases with the energy, the amplitude of $n(3p_z)$ varies slowly with the energy, with its peak at 4.5 au, 16 au and 80 au. The electronic population of the atom n_A, which is the sum of $n(3s)$ and $n(3p_z)$ in our case, is shown in Fig. 8.9.

In Figs. 8.10 and 8.11, the electronic populations of 3s and $3p_z$ orbitals are plotted as functions of the inverse of the initial velocity, respectively. As one can see from the figures, the oscillations of the electronic populations have almost constant frequencies in relatively wide ranges of the inverse of the collisional velocity. For the inverse of the velocity in the range between 10 au and 40 au, which corresponds to energy between 4 au and 170 au, the period of the electronic populations is about 1 au of the inverse velocity. For the inverse velocity in the range between 70 au and 150 au, which corresponds to energy between 1 au and 3

au, the period of the electronic populations is about 4.7 au of the inverse velocity. Finally, in Fig. 8.12 the electronic populations of atomic orbitals is plotted as a function of the inverse of the initial velocity.
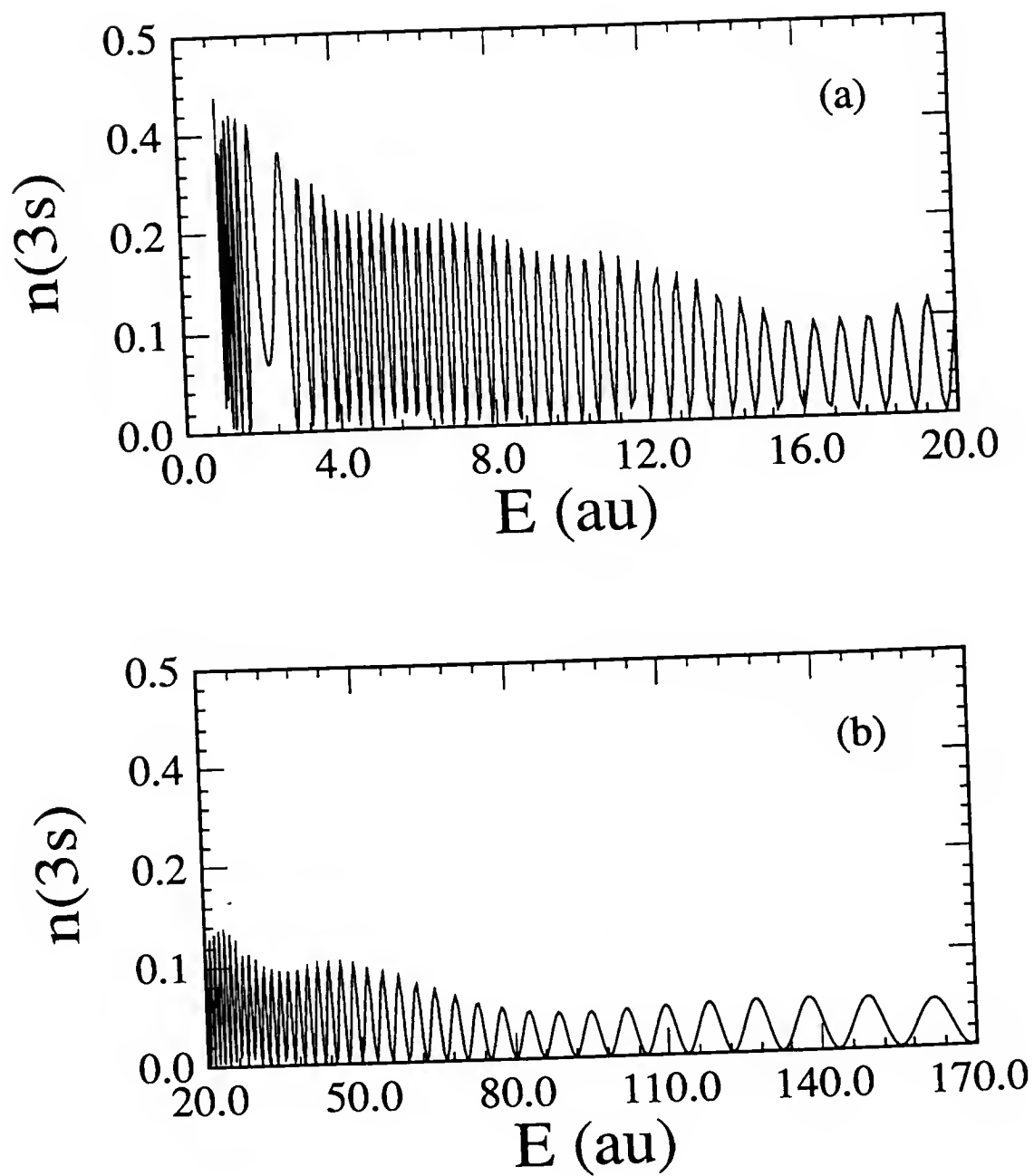
Figure 8.7 The electronic population of 3s orbital of Na atom vs. the collisional energy E. (a) E=1–20 au; (b) E=20–170 au.

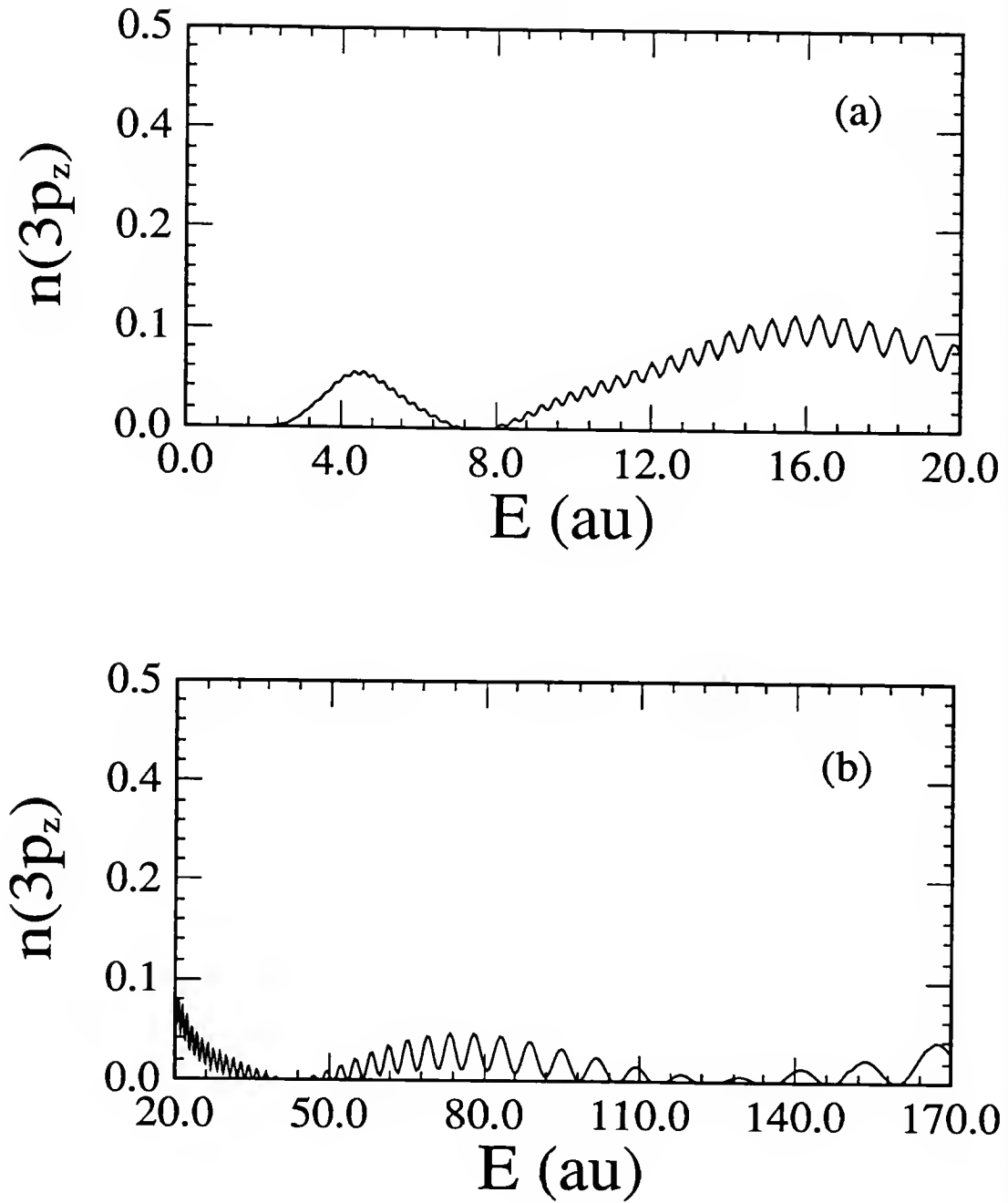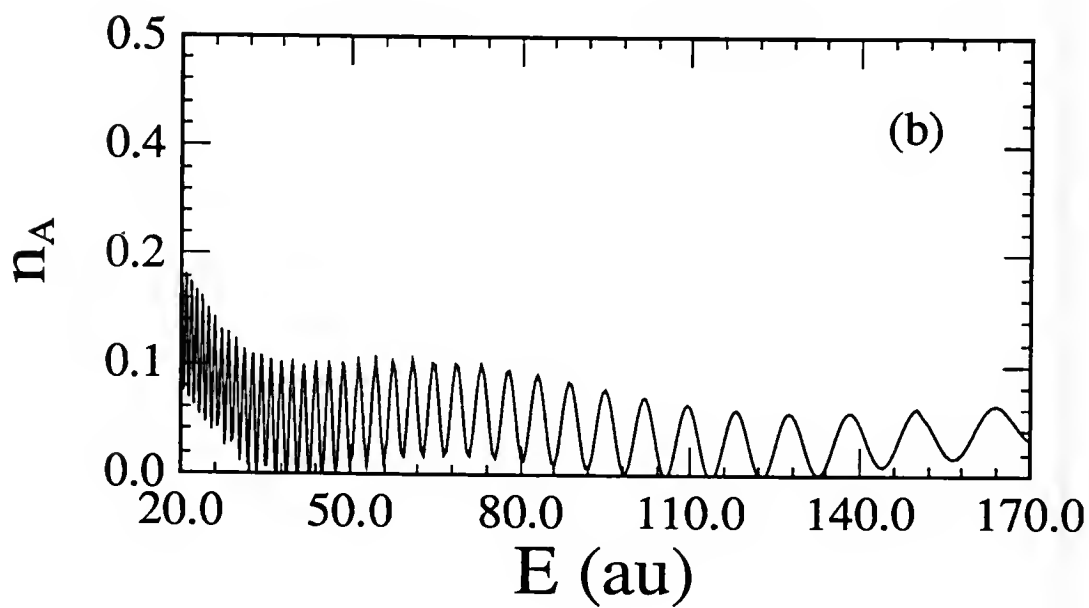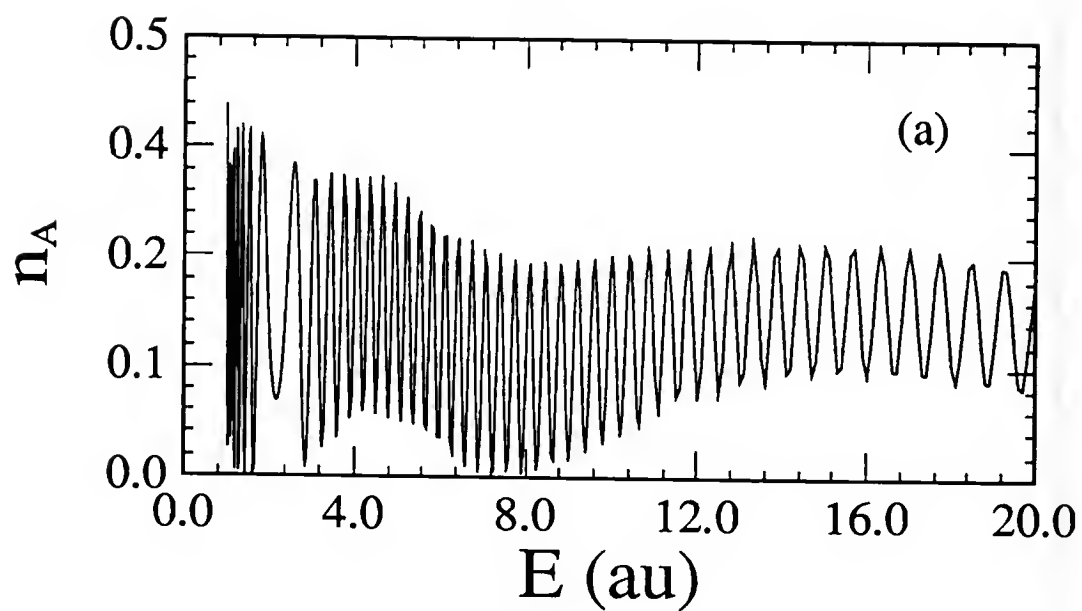Figure 8.8 The electronic population of 3p$_z$ orbital of Na atom vs. the collisional energy E. (a) E=1–20 au; (b) E=20–170 au.

Figure 8.9 The electronic population of Na atom vs. the collisional energy E. (a) E=1–20 au; (b) E=20–170 au.
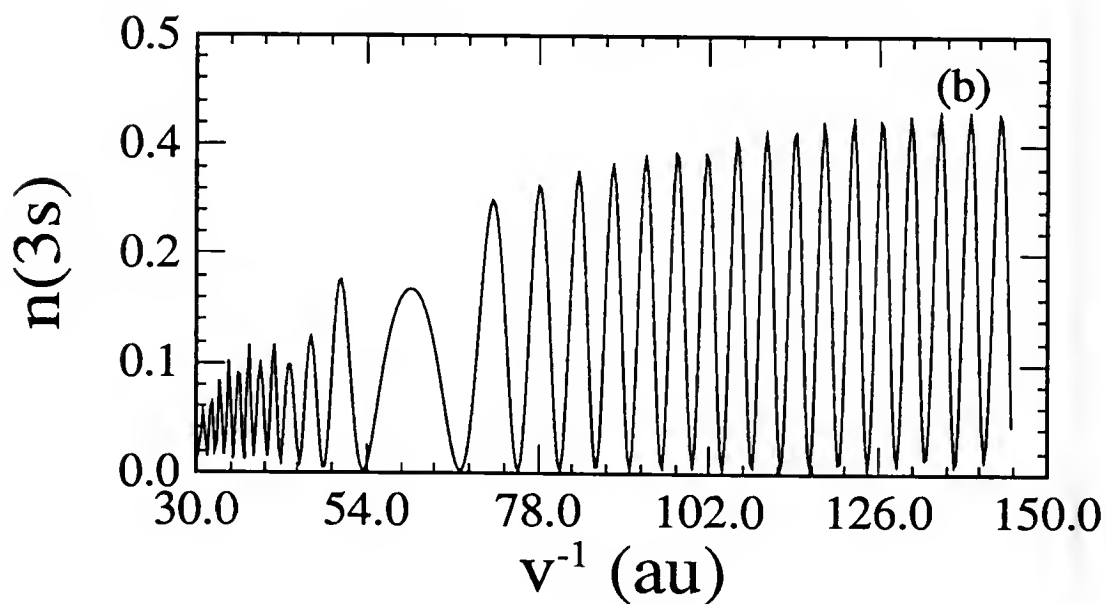
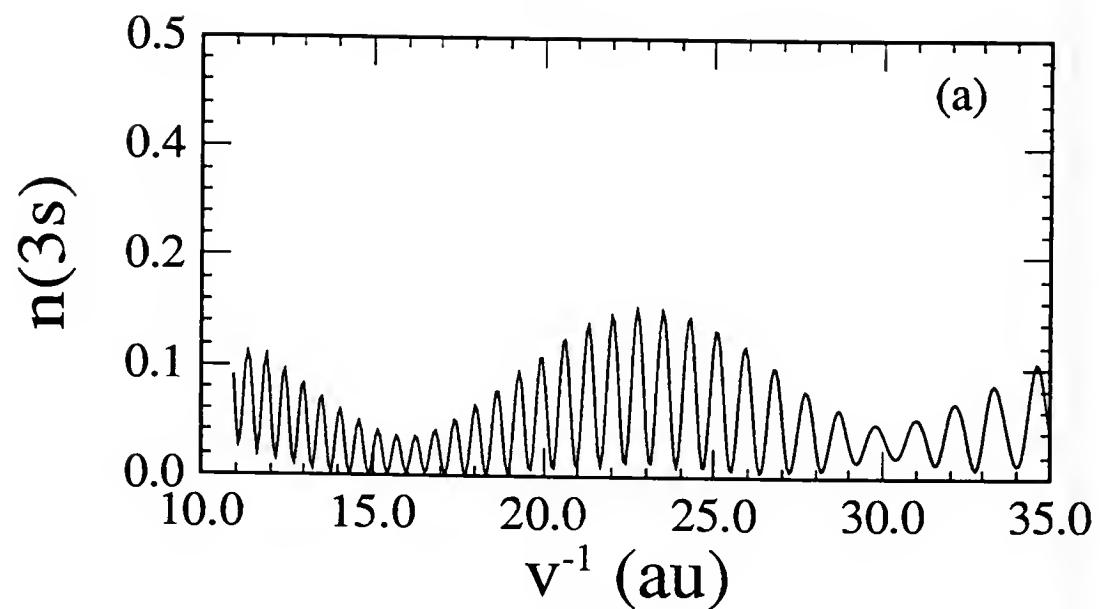Figure 8.10 The electronic population of 3s orbital of Na atom vs. the inverse of the collisional velocity v^{-1}. (a) v^{-1}=10—35 au; (b) v^{-1}=35—150 au.

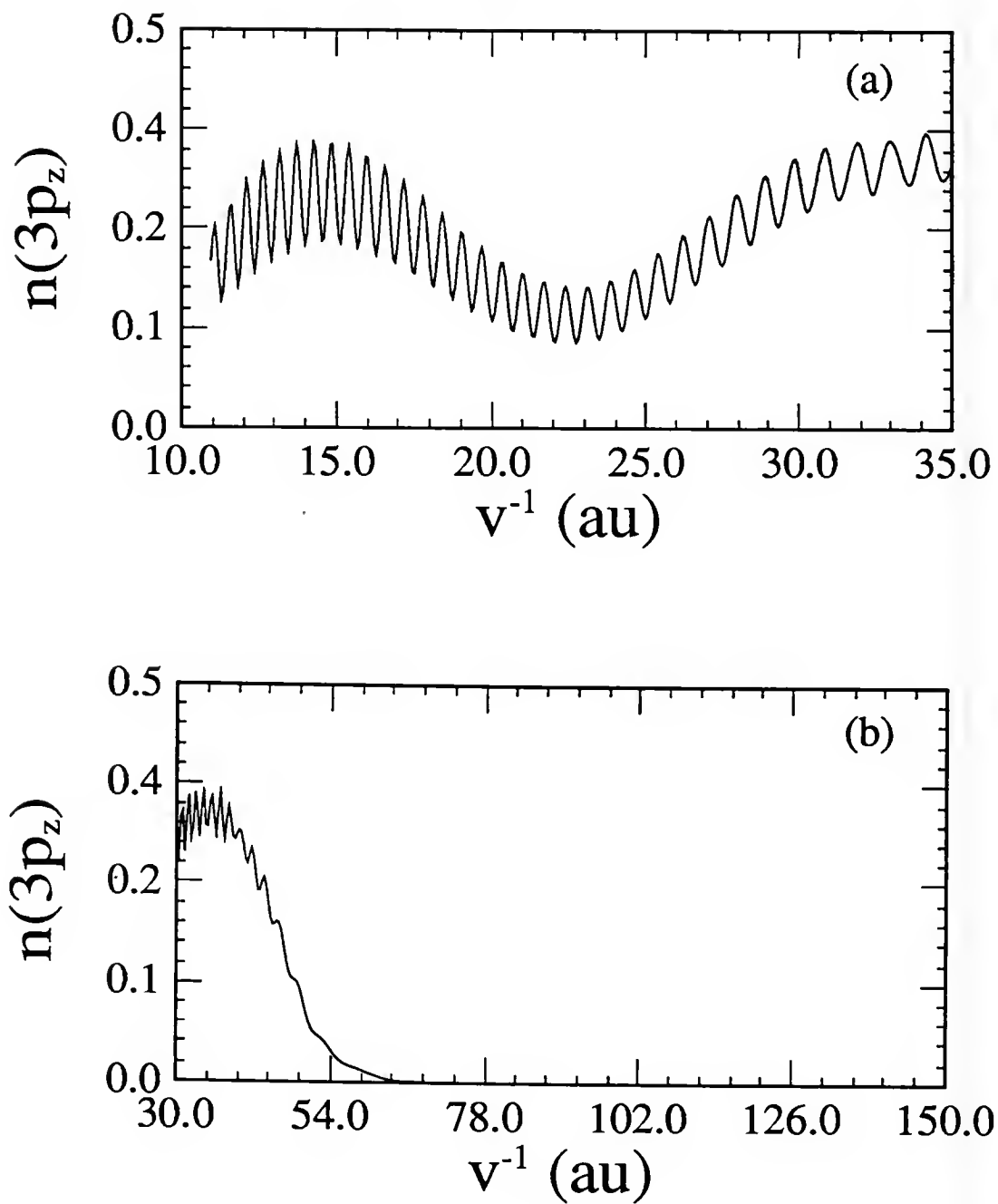Figure 8.11 The electronic population of $3p_z$ orbital of Na atom vs. the inverse of the collisional velocity v^{-1}. (a) $v^{-1}=10$—35 au; (b) $v^{-1}=35$—150 au.
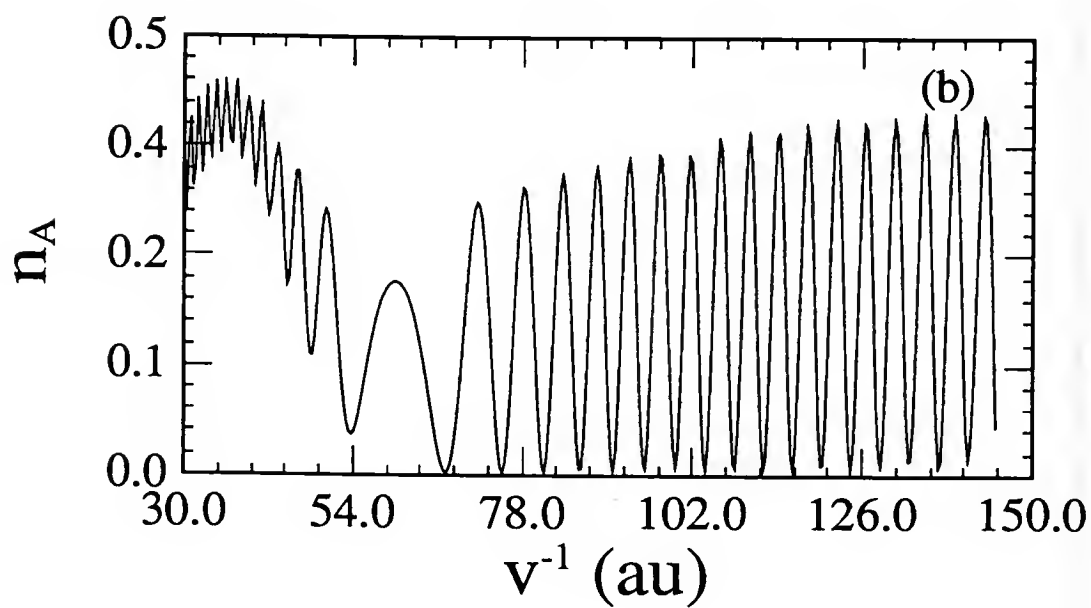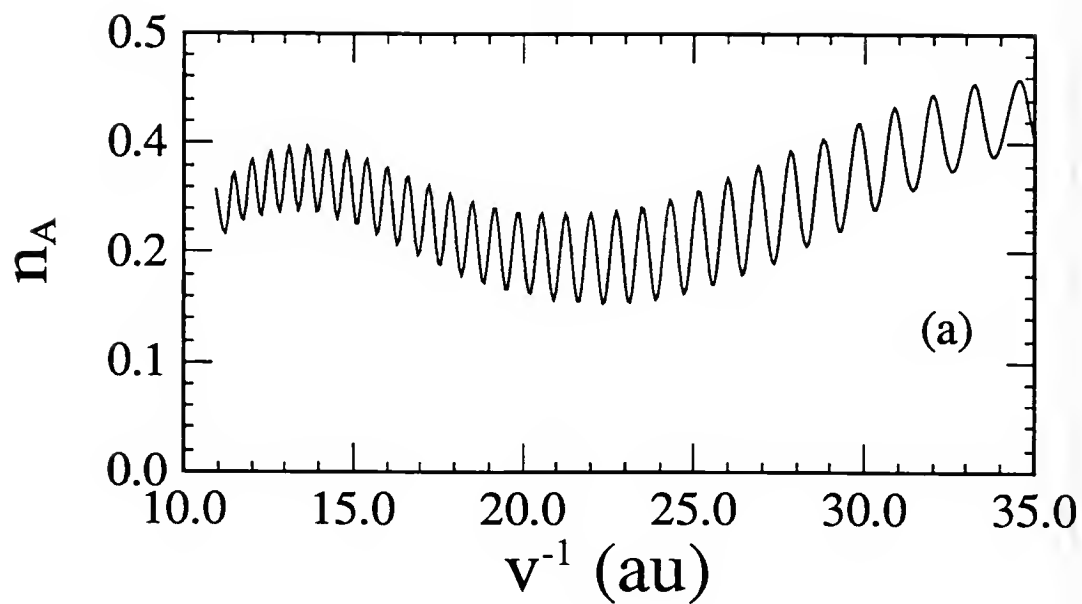
Figure 8.12 The electronic population of Na atom vs. inverse of the collisional velocity v^{-1}. (a) v^{-1}=10—35 au; (b) v^{-1}=35—150 au.

CHAPTER 9
DISCUSSION AND CONCLUSIONS

This work presents a theoretical approach to atom-surface collisions at low energies. In Ch. 2 through Ch. 6, we have developed a time-dependent molecular orbital (TDMO) method to study charge transfer in ion-surface collisions. The electronic density matrix has been used to described the evolution of electronic states and distribution of charges on the atomic orbitals during and after collisions. We have also used the density matrix to define the orbital polarization parameters which characterize anisotropic distribution of electrons over orbitals in our extended systems. To make the TDMO useful for applications, we also developed other theoretical tools, including the local time linearization method for integration of TDHF equations, the partition method based on the localized basis functions for treatment of electronic states in extended systems, and the expansions in generalized Wannier functions in extended systems which lack translational symmetry. In Ch. 8, we have applied thie method to a model system. In this chapter we discuss these theoretical methods and their applications to the study of the dynamics of electronic processes in atom-surface collisions. Analysis and conclusions are related to the physical features of the problems and the comparison with other theoretical methods. We also discuss the application

of this approach to charge transfer in the collision of Na with W(110). At the end of this chapter, suggestions for further work are furnished.

To study electronic processes in atom-surface collisions, a pertinent theory should be able to describe both electronic states and electronic interactions. Some of the current approaches in the field, while trying to describe the evolution of electronic states, are unable to simultaneously treat the electronic interactions in a consistent way, and have to rely on particular models or use parameterized electronic potentials [for example, Blandin et al., 76]. Although some of these approaches come up with results comparable with experiments, their value in providing a deep insight into the complicated electronic processes seems limited. The molecular orbital method, which is capable of this task, has been used to study some time-independent atom-surface phenomena, e.g., chemisorption, and has achieved certain success [Grimley and Posani, 74]. For time-dependent phenomena, although the idea of the TDMOs has been used in some approaches [Tully, 77; McDowell, 85], there has not been much advancement made in obtaining these orbitals, a formal theory within this framework has not been established and applied to collisional phenomena in extended systems.

In this work, we have developed a TDMO method for atom-surface collisions. The TDMOs are constructed with atomic functions and localized basis functions of surfaces. To eliminate the artificial couplings at large distances, introduced by the expansion of the molecular orbitals with atomic orbitals centered on moving nuclei, the atomic functions are chosen to be in the form of travelling atomic

orbitals (TAO). The atom-surface and electronic couplings, which depends on the electronic configurations as well as on time through the trajectory of the atom, $\vec{R}_A(t)$, are obtained from the TDMOs. Starting with the system Hamiltonian, we have derived the TDHF equation for the electronic density matrix which describes the evolution of the TDMOs. There are several advantages in formulating things in this way. First, by using the density matrix we can correctly describe the evolution of the occupied orbitals all the time without having to identify the occupied orbitals, which change with time in dynamic systems. Secondly, the density matrix is convenient in describing the charge distribution and the orbital polarization of subsystems. Thirdly, the self-consistency between the effective field and the density matrix is achieved automatically in the TDHF equations and the self-consistent iteration procedure used in its time-independent counterpart is thus avoided. It should be noted that the basic TDMO formalism developed in Ch. 2 is completely general and will not rely on particular basis functions.

One of the interesting phenomena in collisions is the orbital polarization of the colliding atoms, which occurs when the electrons populate the possible orbitals with a different probability and the electronic cloud has a distorted form or a particular spacial orientation. Study of the orbital polarization provides a deeper and clearer understanding of the electronic processes accompanying the collisions. The TDMO approach can lead to a characterization of electron distribution on individual states during the entire collision, which is an advantage over other approaches which calculate the total charge on the scattered atoms only

after collisions. We have defined the orbital polarization parameters in extended systems by tensor operators and expressed them in terms of the density matrix. We also defined the polarization parameters for subsystems, which will be useful for comparison with experimental data of atomic orbital polarization. As the distance between the atom and the surface approaches infinity, our definitions of the atomic orbital parameters for the colliding atom becomes that for an isolated atom.

Here we interrupt the discussion of physics of the collision problem and our method and turn our attention to the mathematical aspects of solving the TDHF equations. These differential-integral equations, for which the exact solutions are hard to obtain, are often solved by linearization procedures, which linearize the equations by assuming that the changes of their solutions are slow in a small time interval. However, since the density matrix is expected to be a fast oscillatory function in our case, we can not use the conventional procedure that uses a constant zeroth order solution. We notice that the time dependence of the density matrix results from two causes: the change of the effective field due to the nuclear motion, and the change due to electronic transition between states. While the former changes slowly for low energy collisions, the electrons jump between states with a frequency proportional to the inverse of the energy difference of the states, that could be high in case of the near-resonance charge transfer process. The linearization procedure we proposed treats the change of the density matrix in a short time as a sum of a time-dependent reference density matrix $P^0(t)$, which satisfies a linearized TDHF equation for the density matrix

when the nuclear position is fixed in space, and a matrix $Q(t)$, which is the first order change of the density matrix and satisfies another linearized TDHF equation which is coupled with that for $P^0(t)$. We have obtained for a general case the formal solutions for $P^0(t)$ and $Q(t)$ from an exponential transformation, and the analytical solutions for a special case where the electron-electron interaction is ignored. Computational programs have been developed to solve the TDHF equations in atom-surface collisions using this linearization procedure. The key to implementing this procedure is that $Q(t)$ should be small compared with $P^0(t)$. We employ variable step sizes and check this criterion after every integration. The stability and convergence of the solutions have also been checked.

One of the major problems when applying the TDMO approach to extended systems is the treatment of the great number of electronic states. Collisional charge transfer in atom-surfaces interactions is a process which involves a few electrons and strong couplings in a short period of time. We have developed a partition method to split the system into a primary region and a secondary region and constructed in the small primary region the effective TDHF equations which are coupled with the secondary region through a time-dependent driving term. In the secondary region, the electrons are effected by the colliding atom indirectly through their coupling with the electrons in the primary region, and the states of the electrons are approximately unchanged during the collision. Apparently, the primary region should be chosen to have a size of the order of the interaction range; we will come back to it in the discussion of the results. This partition

method can also be applied to other systems which contains strong and local interactions.

Our partition method requires a set of localized basis functions. We have further extended the idea of using the generalized Wannier functions (GWFs) for extended systems, which are orthonormal and localized around the sites in the systems. We have derived a formalism to obtain these functions by a variational principle, which shows that GWFs can be constructed from the system Hamiltonian without having the knowledge of the eigenfunctions. These GWFs are written in the form of linear combinations of Gaussians for practical reasons and can be used in studies of local phenomena in extended systems which lack translation symmetry. We also argue that, because the GWFs quickly recover the form of the Wannier functions of a bulk when they are away from the defects, only a small number of functions need to be determined for quasi-periodic systems which lose translational symmetry only in certain directions or contains defects in local areas. The GWFs have been constructed for a jellium surface, for which the three dimensional calculation is reduced to a one dimensional calculation. The eigenvalues and eigenfunctions calculated using GWFs as basis functions are in good agreement with the exact ones. To complete our basis set, we constructed the atomic basis functions for the valence orbitals through a pseudopotential for the atomic core. In doing so, the inner electrons are eliminated since they do not play an important role in charge transfer.

We have applied the TDMO method to the collisional charge transfer in

Na–W(110). The surface is modeled by a jellium with its band parameters fitted to those of the W(110) conduction band. In the present applications of this method, some simplifications are used, including ignoring the electron-electron interaction, using a prescribed trajectory, and using a simple model for the surface. Discussion of the results includes the electronic couplings and atom-surface interactions, evolution of the electron populations and the energy dependence of the electron populations.

We have calculated the electronic couplings and the interaction potentials of the system. The couplings between the atomic orbitals show an interaction range of 8 au. At the short distances, the couplings between the surface and atomic orbitals are about the same order as that calculated from the WKB approach in parabolic coordinates [Grozdanov and Janve, 78] and that from muffin-tin potentials [Muscat and Newns, 79]; there are no other results to compare with for the coupling between the 3s and $3p_z$ orbitals. The strong couplings at short distances indicate that the orbitals are heavily mixed and a strong electron exchange is possible. At larger distances, the decay of the couplings is faster than the results calculated by other methods, which could be attributed to the fact that only a small number of Gaussians are used in our calculations when writing the basis functions as linear combinations of Gaussians. The results for interaction potentials corresponding to various configurations are shown in Fig. 8.2. However, there is to our knowledge no experimental data for Na–W to compare with. All the potentials except for $Na(3p_x)$–$W^+(0)$ and $Na(3p_y)$–$W^+(0)$

have minima at certain distances from the surface. The positions of the minima for Na(3s)–W$^+$(0) and Na(3p$_z$)–W$^+$(0) are at 4.0 au, while that for Na$^+$–W(0) is 4.6 au. The important information obtained from the calculation is that potentials corresponding to different configurations are within 0.1 au at short distances, which makes the near-resonance charge transfer process the dominant one.

The evolution of the electronic populations for atomic orbitals and surface orbital have been calculated, which offers a useful insight into the dynamic behavior of charge transfer. Unfortunately, spectroscopy techniques have not yet been developed to provide corresponding data for comparison. Common to all the energies, the charges begin to slowly transfer to the atomic orbitals when the atom approaches to 8 au from the surface, and then rapidly increase at about 5 au where the potential curves cross. All the electron populations contain fast oscillations within the distance range of 5 au, which is characteristic of the near-resonance charge transfer. Recalling that the density matrix is the sum of a time-dependent background $P^0(t)$ and a small change $Q(t)$, the rapid oscillations are decided by the evolution of $P^0(t)$ and slow changes of the amplitudes are attributed to the accumulation of the change of the density matrix $Q(t)$. The pattern of the evolution of the populations varies with the orbital and energy. Noticing that these curves on the outward path have different shapes than those on the inward path, it means that the evolution of the electron populations depends on the amount of charge on the orbitals. The frequency of the oscillations varies with the distance and is higher in the short distance range. Our check indicates that, for a collisional

energy, the frequency is roughly inversely proportional to the energy differences between the potential energies of atomic state and the surface state. This seems to support the explanation that the transition rate between two orbitals depends on the energy difference. However, the frequency also varies with the collisional energy, and is higher at lower energies, probably because the coupling between the electronic motion and the nuclear motion should be taken into account at lower energies. The total charge in the primary region before and after the collision but has been found to change less than 15% for E=1–120 au, which is an indication that the charge transfer occurs indeed mainly in the primary region. A more accurate calculation should however consider a larger primary region, especially for high energies.

We have studied the energy dependence of the electron populations and found oscillations in the whole energy range between 1 au and 170 au, with a frequency that decreases steadily with increasing the collision energy. Such an oscillatory structure has been encountered in some experiments on ion-metal surface collisions [Erickson and Smith, 75; Taglauer and Heiland, 76; Tolk et al., 76]. This is believed to arise from the quantum phase interference between the states whose energies are close in the near-resonance charge transfer process, and will be explained here by a simple model [Tolk, et al., 76]. Consider an atom-surface system with two potential curves corresponding to the ion-surface and atom-surface configurations, which are split by a small difference $\Delta E(R)$, where R is the distance of the atom to the surface. When the atom enters the interaction

region, the coupling between the two states becomes comparable with $\Delta E(R)$ and the charge transfer occurs. As the electrons on these two states evolve along their potential curves, a differential phase $\Delta\phi$ is developed between the two states, until the atom leaves the interaction range. After the collision the populations of the atomic configuration and ion configuration are expressed as

$$n_a = \alpha_a + \beta cos^2(\Delta\phi/2) \tag{9.1}$$

$$n_i = \alpha_i + \beta cos^2(\Delta\phi/2) \tag{9.2}$$

where α_a, α_i and β are slowly varying functions of the incident ion energy. The phase is given by (using $\hbar=1$)

$$\Delta\phi = \int \Delta E(t)dt = \int \frac{\Delta E(R)}{v(R)} dR \tag{9.3}$$

where $v(R)$ is the normal component of the nuclear velocity. Since the velocity is nearly constant in a wide range, the above equation is approximated by

$$\Delta\phi \approx \frac{2}{v_i} \int_{R_0}^{R_m} \Delta E(R)dR \tag{9.4}$$

where v_i is the initial velocity component perpendicular to the surface, and R_m and R_0 are the interaction range and turning point, respectively. This Model predicts an oscillation frequency proportional to the inverse of the incident velocity, v_i^{-1}. We have studied the dependence of populations on v_i^{-1} and found that the oscillation frequency is roughly constant in the region v_i^{-1}=70–144 au and in the region v_i^{-1}=10–40 au. The fact that the frequency changes slowly with v_i indicates that

$v(R)$ is not constant. To further check this theoretical explanation, the calculation should be done for the collisions with different incident angles to examine the angular dependence of the peak positions. In ionization spectroscopy experiments [Overbosch et al., 80] the oscillation of the ion yield is not seen. A possible reason is that the experiment did not measure enough points. It is also possible that, since the oscillations of the populations are very fast in the low energy range, the final yield of the ions in the experiment is actually an average of the product yields with different initial velocities.

The charge transfer exhibits a difference between the 3s and $3p_z$ orbitals. For 3s, the charge transfer occurs in the whole energy range between 1 au and 170 au and its intensity oscillates between 0 and peaks. In contrast, the oscillations for $3p_z$ are smaller in the low energy range, and the amplitude of the peaks is slowly varying with three maxima at E=4.5 au, 16 au and 80 au. The threshold for Na–W reported in experiment [Hurkmans et al., 76] is 0.02–0.04 au. Our calculation shows that the $3p_z$ orbital has a very high threshold at 2.5 au. However, the evolution calculation for collision energy of 1 au shows that charges are actually transferred to $3p_z$ orbitals when the atom is in the interaction range. They jump between $3p_z$ and other orbitals and then, on the outward path, transfer to the surface and 3s orbitals. The calculation should be extended to lower the energy range to see wether a threshold for 3s orbitals exists. It will also be interesting to do calculation for different incident angles to study the time-dependence and the thresholds of the electronic populations for $3p_x$ and $3p_y$ orbitals.

This work has constructed the basic framework of the TDMO method and introduced some accessory tools for applying it to atom-surface collisions. In the development of this method, we have not tempted to use empirical data to fit the our results with experimental ones. We believe that keeping the theory in its most general form is probably the biggest intrinsic advantage of the TDMO method over the approaches which can not treat the effective potentials and the charge transfer self-consistently and have to rely on the empirical results. In our applications, we have made some approximations and simplifications which can either be removed or be made more accurate.

However, insofar our model is simple and the results are preliminary, some extension and applications of this method are suggested here.

(a) Size of the primary region. In principle, the size of the primary region should be of the order of the interaction range, but the experiences of other works using similar partition methods have shown that a smaller primary region could give satisfactory results [McDowell, 82; de Malo et al., 87]. Investigation of the convergency of results with the primary region size can determine the optimum size of the primary region.

(b) Orbital polarization. We have formulated the method to study the orbital polarization. However, the orbital polarization shows in a limited way in the application presented in this work when the collision is limited to the normal incidence. Application to incidence with a finite angle will provide more information about the electronic interactions in the collisions, and will be a new test of the theory.

(c) Trajectory. Again, due to the limit of time, the application of the method has been confined to use a simple prescribed trajectory. Although the trajectory study is relatively independent of the TDMO method itself, it should be given a great deal of attention for its importance to the problem. Our studies should be extended to include the coupling between the electronic motion and the nuclear motion. Such a study could use the effective force containing the couplings, along the lines we have applied to atomic collisions [Runge et al, 91], or within the eikonal method [Micha, 83].

(d) Electron-electron interaction. Ignoring the electron-electron interaction in our application is not necessary, but it simplifies the calculations. Including this interaction will make the TDHF equations more demanding of computing time. Another aspect of electron-electron interactions is the appearance of image potentials in the metal. These can be neglected at the higher energies we consider, but would be more important in threshold studies.

(e) Basis functions. The TDMO method has been cast in such a way that it uses localized basis functions but does not depend on the particular form of them. This allows the freedom of applying this method to more practical models and using other localized basis functions. An example is the localized basis functions developed by Smith and his co-workers in studies of surface electronic structure [Smith and Gay, 75; Smith et al., 80].

APPENDIX A
CALCULATION OF COEFFICIENT MATRIX $\mathbf{B^x}$

The one dimensional Wannier function for a free electron gas is [Callaway, 76]

$$w_{n_x}^x(x) = \frac{1}{\sqrt{d}} \cdot \frac{\sin\left[\frac{\pi}{d}(x - n_x d)\right]}{\frac{\pi}{d}(x - n_x d)} \tag{A.1}$$

where d is the lattice constant. We consider a function $w_{n_x}^{x,m_x}(x)$ which is a linear combination of $2L_x+1$ Gaussians

$$w_{n_x}^{x,m_x}(x) = \sum_{m_x=n_x-L_x}^{m_x=n_x+L_x} B_{n_x m_x}^x(\beta_{m_x}) g_{m_x}^x(\beta_{m_x}, x) \tag{A.2}$$

where

$$g_{n_x}^x(\beta_{m_x}, x) = b_{m_x} exp\left[-\beta_{m_x}(x - n_x d)^2\right] \tag{A.3}$$

is a one dimensional 1s primitive Gaussian with a constant $b_{m_x} = \left(\frac{2\beta_{m_x}}{\pi}\right)^{1/4}$.

We use the least square method [Shavitt, 63] to determine the coefficient matrix $B_{n_x m_x}^x(\beta_{m_x})$ which minimizes the difference between $w_{n_x}^x(x)$ and $w_{n_x}^{x,m_x}(x)$. The deviation between $w_{n_x}^x(x)$ and $w_{n_x}^{x,m_x}(x)$ is

$$D = \int_{-\infty}^{\infty} \left[w_{n_x}^x(x) - \sum_{m_x=n_x-L_x}^{m_x=n_x+L_x} B_{n_x m_x}^x g_{m_x}^x(\beta_{m_x}, x)\right]^2 dx \tag{A.4}$$

The choice of the linear coefficients $B_{n_x m_x}^x(\beta_{m_x})$ which leads to the minimum D, according to the least square method, requires the vanishing of the partial

derivatives, $\partial D / \partial B^x_{n_x m_x} = 0$, which gives

$$\int_{-\infty}^{\infty} g^x_{m_x}(\beta_{m_z}, x) \left[w^x_{n_x}(x) - \sum_{m'_x = n_x - L_x}^{m'_x = n_x + L_x} B^x_{n_x m'_x} g^x_{m'_x}(\beta_{m_z}, x) \right] dx = 0 \qquad \text{(A.5)}$$

Defining the overlap matrix of the Gaussians

$$G^x_{n_x m_x}(\beta_{m_z}) = \langle g^x_{n_x}(\beta_{m_z}) | g^x_{m_x}(\beta_{m_z}) \rangle \qquad \text{(A.6)}$$

and a matrix

$$C^x_{n_x m_x}(\beta_{m_z}) = \langle w^x_{n_x} | g^x_{m_x}(\beta_{m_z}) \rangle \qquad \text{(A.7)}$$

Eq. (A.5) is then written as a matrix equation

$$\mathbf{C^x = B^x G^x} \qquad \text{(A.8)}$$

from which we obtain the coefficient matrix

$$\mathbf{B^x = C^x (G^x)^{-1}} \qquad \text{(A.9)}$$

Because of the translation symmetry in the x direction

$$B^x_{n_x m_x}(\beta_{m_z}) = B^x_{n'_x m_x}(\beta_{m_z}) \qquad \text{(A.10)}$$

and only one row of $\mathbf{B^x}$ must be found.

APPENDIX B
CALCULATION OF TOTAL BAND ENERGY Ω

For a jellium slab with a step potential

$$V(\vec{r}) = \begin{Bmatrix} 0 & z \geq 0 \\ -V_0 & -D \leq z < 0 \\ 0 & z < -D \end{Bmatrix} \qquad \text{(B.1)}$$

the total energy of a band, using the generalized Wannier functions $w_{\vec{n}}(\vec{r})$ which

are written as of linear combinations of Gaussians $g_{\vec{m}}(\beta_{m_z}, \vec{r})$, is

$$\Omega = \sum_{\vec{n}} \langle w_{\vec{n}} | \hat{H} | w_{\vec{n}} \rangle$$

$$= \sum_{\vec{n}} \sum_{\vec{m}} \sum_{\vec{m}'} B_{\vec{m}\vec{n}}^{\dagger} B_{\vec{n}\vec{m}'} \langle g_{\vec{m}}(\beta_{m_z}) | \hat{H} | g_{\vec{m}'}(\beta_{m_z}) \rangle \qquad \text{(B.2)}$$

where

$$B_{\vec{n}\vec{m}} = B_{n_z m_z}^z \cdot B_{n_x m_x}^x (\beta_{m_z}) \cdot B_{n_y m_y}^y (\beta_{m_z}) \qquad \text{(B.3)}$$

is an element of the coefficient matrix $\mathbf{B}$, and $\hat{H}$ is the Hamiltonian,

$$\hat{H} = -\frac{1}{2}\nabla^2 + V(\vec{r}) \qquad \text{(B.4)}$$

The matrix element for the kinetic energy is [Shavitt, 63]

$$\langle g_{\vec{n}} | -\frac{1}{2}\nabla^2 | g_{\vec{m}} \rangle = \beta_{\vec{n}\vec{m}}(3 - 2\beta_{\vec{n}\vec{m}}R_{\vec{n}\vec{m}}^2)G_{\vec{n}\vec{m}} \qquad \text{(B.5)}$$

where $\beta_{\vec{n}\vec{m}} = \frac{\beta_{n_z}\beta_{m_z}}{\beta_{n_z}+\beta_{m_z}}$, $R_{\vec{n}\vec{m}} = \left| \vec{R}_{\vec{n}} - \vec{R}_{\vec{m}} \right|$ and

$$G_{\vec{n}\vec{m}} = \langle g_{\vec{n}} | g_{\vec{m}} \rangle = \left(\frac{4\beta_{\vec{n}\vec{m}}}{\beta_{n_z} + \beta_{m_z}} \right)^{3/4} exp\left(-\beta_{\vec{n}\vec{m}}R_{\vec{n}\vec{m}}^2\right) \qquad \text{(B.6)}$$

140

is the overlap matrix of the Gaussian functions.

Noticing the potential $V(\vec{r})$ is constant in x and y directions, the matrix elements for the potential are

$$\langle g_{\vec{n}}|V|g_{\vec{m}}\rangle = \langle g^x_{n_x}(\beta_{m_x})|g^x_{m_x}(\beta_{m_x})\rangle \cdot \langle g^y_{n_y}(\beta_{m_x})|g^y_{m_y}(\beta_{m_x})\rangle$$

$$\cdot \langle g_{n_x}|V|g_{m_x}\rangle \tag{B.7}$$

$$= G^x_{n_x m_x}(\beta_{m_x}) \cdot G^y_{n_y m_y}(\beta_{m_x}) \cdot \langle g_{n_x}|V|g_{m_x}\rangle$$

Calculation shows that

$$\langle g_{n_x}|V|g_{m_x}\rangle = -\frac{V_0}{2}[erf(l_2) - erf(l_1)] \tag{B.8}$$

where $erf(l)$ is the error function [Gauatschi, 72] and

$$l_1 = \sqrt{\beta_{n_x} + \beta_{m_x}}\left[\frac{\beta_{n_x}n_z + \beta_{m_x}m_z}{\beta_{n_x} + \beta_{m_x}}d\right] \tag{B.9}$$

$$l_2 = \sqrt{\beta_{n_x} + \beta_{m_x}}\left[D + \frac{\beta_{n_x}n_z + \beta_{m_x}m_z}{\beta_{n_x} + \beta_{m_x}}d\right] \tag{B.10}$$

Substituting Eqs. (B.5) and (B. 8) into Eq. (B.4) the matrix element of the Hamiltonian becomes

$$\langle g_{\vec{n}}| - \frac{1}{2}\nabla^2|g_{\vec{m}}\rangle = G_{\vec{n}\vec{m}}\{\beta_{\vec{n}\vec{m}}(3 - 2\beta_{\vec{n}\vec{m}}R^2_{\vec{n}\vec{m}})$$
$$- \frac{V_0}{2}[erf(l_2) - erf(l_1)]\} \tag{B.11}$$

Using $\mathbf{B}^x$ and $\mathbf{B}^y$ obtained in Appendix A and substituting $\mathbf{B}^z = (\mathbf{G}^z)^{-\frac{1}{2}}$ and Eq. (B.11) into Eq. (B.1), the total band energy Ω can be calculated.

APPENDIX C
CALCULATION OF ELECTRONIC PROPERTIES OF THE FINITE SLAB

We consider a finite jellium slab which models the W(110) surface and has $N_s = N_x N_y N_z$ sites which form a cubic mesh, where N_x is the number of sites in the x-direction, N_y is the number of sites in the y-direction and N_z is the number of sites in the z-direction. We choose N_x=21, N_y=21 and N_z=22. It should be pointed out that the sites are chosen from mathematical considerations and are not the lattice points in W(110) and that the distance between sites, d, is not equal to Tungsten's lattice constant a. In Sect. 6.2 we calculated generalized Wannier functions for the slab, assuming it satisfies the cyclic boundary conditions in x- and y-directions. In this appendix we describe how the Fermi energy of the slab was calculated.

Tungsten has an FCC structure with a lattice constant a=5.97 au; in each unit cell there are two atoms with six valence electrons each, which gives a density of valence electrons ρ=0.0564 au. We choose d=2.61 au so that average number of electrons per mesh cell, or ρd=1.

The energy of a level is

$$E_{\vec{k}} = E_{k_x} + E_{k_y} + E_{k_z} \qquad (C.1)$$

with $E_{k_x} = \frac{k_x^2}{2}$, $E_{k_y} = \frac{k_y^2}{2}$, where

$$k_x = \frac{2\pi j_x}{(N_x - 1)d} \qquad j_x = 0, 1, \cdots \qquad \text{(C.2)}$$

$$k_y = \frac{2\pi j_y}{(N_y - 1)d} \qquad j_y = 0, 1, \cdots \qquad \text{(C.3)}$$

and E_{k_z} is the exact eigenvalue for $k_z(j_z)$, j_z=1, 2, . . ., for a one-dimensional square well, which is listed in Table 6.2.

Starting with the lowest level, we fill each level with two electrons. When all the $N=(N_x-1)(N_y-1)(N_z-1)$ electrons are located in levels, the energy of the highest occupied level is the calculated Fermi energy. Using the bottom of the band ϵ_b=−0.846 au, we found that the calculated Fermi energy is ϵ_F=−0.192 au, which is in agreement with the experimental value of W(110), −0.191 au.

BIBLIOGRAPHY

A. A. Abrahamson, Phys. Rev. **178**, 76(1969).

F. J. Alinghaus, J. G. Gay and J. R. Smith, Phys. Rev. **B21**, 2055(1980).

N. Andersen, in *"Fundamental Processes of Atomic Dynamics"*, edited by J. S. Briggs, H. Kleinpoppen and H. Luts (Plenum, New York, 1987).

N. Andersen, J. W. Gallagher and I. V. Hertel, in *"Electronic and Atomic Collisions"*, edited by D. C. Lorents, W. E. Meyerhof and J. R. Peterson (North-Holland, New York, 1986).

N. Andersen and S. E. Nielsen, Z. Phys. **D5**, 309(1987).

N. Andersen, J. W. Gallagher and I. V. Hertel, Phys. Rep. **165**, 1(1988).

P. W. Anderson, Phys. Rev. **124**, 41(1961).

S. L. Anderson, G. D. Kubik and R. N. Zare, Chem. Phys. Lett. **105**, 22(1984).

D. R. Bates and R, McCarroll, Proc. Roy. Soc. **A245**, 175(1958).

A. Blandin, A. Nourtier and D. W. Hone, J. Phys. **37**, 369(1976).

K. Blum, *"Density Matrix Theory and Applications"* (Plenum, New York, 1981).

R. Brako and D. M. Newns, Surf. Sci. **108**, 253(1981).

R. Brako and D. M. Newns, Rep. Prog. Phys. **52**, 655(1989).

J. Callaway, Phys. Rev. **187**, 192(1969).

J. Callaway, *"Quantum Theory Of Solid State"* (Academic, 1976).

E. E. B. Campbell and I. B. Hertel, in *"Fundamental Processes of Atomic Dynamics"*, edited by J. S. Briggs, H. Kleinpoppen and H. Luts (Plenum, New York 1987).

L. Cohen and C. Frishberg, J. Chem. Phys. **65**, 4234(1976).

K. T. R. Davies, K. R. S. Devi, S. E. Koonin and M. R. Strayer, in *"Treaties of Heavy-Ion Science"*, edited by by S. Allan Bromley (Plenum, New York, 1982).

L. R. S. Devi and J. D. Garcia, J. Phys. **B16**, 2837(1983).

K. P. de Malo, M. C. dos Santos, M. Matos and B. Kirtman, Phys. Rev. **B35**, 7847(1987).

P. A. Dirac, Proc. Cambridge Philos. Soc. **26**, 376(1930).

D. E. Eastman and W. D. Grobman, Phys. Rev. Lett. **29**, 1378(1972).

R. L. Erickson and D. P. Smith, Phys, Rev. Lett. **34**, 297(1975).

U. Fano and J. H. Macek, Rev. Mod. Phys. **45**, 553(1973).

P. K. Feibelman, Phys. Rev. lett. **54**, 2627(1985).

E. Q. Feng, K. Runge and D. A. Micha, Interna. J. Quantum Chem. to appear(1991).

W. Gautschi, in *"Handbook of Mathematical Functions"*, edited by M. Abramowitz and I. A. Stegun (Dover, New York, 1972).

J. G. Gay and J. R. Smith, Phys. Rev. **B9**, 4151(1974).

J. G. Gay and J. R. Smith, Phys. Rev. **B11**, 4906(1975).

B. Gazdy and D. A. Micha, Phys. Rev. **A33**, 4446(1986).

B. Gazdy and D. A. Micha, Phys. Rev. **A36**, 546(1987).

R. Gomer, Solid State Phys. **30**, 355(1975).

T. B. Grimley, V. C. J. Bahsu and K. L. Sebastian, Surf. Sci. **124**, 305(1983).

T. B. Grimley and C. Posani, J. Phys. **C7**, 2831(1974).

T. P. Grozdanov and R. K. Janve, Phys. Lett. **65A**, 396(1978).

H. D. Hagstrum, J. Vac. Sci. Technol. **12**, 7(1975).

H. D. Hagstrum, in *"Inelastic Ion-Surface Collisions"*, edited by N. H. Tolk, J. C. Tully, W. Heiland and C. W. White (Academic, New York, 1977).

H. D. Hagstrum, in *"Electron and Ion Spectroscopies of Solids"*, edited by L. Fiermans, J, Vennik and W. Dekeyser (Plenum, New York, 1978).

H. D. Hagstrum and G. E. Becker, Phys. Rev. **B8**, 1580(1973).

M. O. Hale, I. V. Hertel, and S. R. Leone, Phys. Rev. Lett. **53**, 2296(1984).

A. J. Heeger, in *"Solid State Physics"*, edited by F. Seitz, D. Turnbull and H. Ehrenreich, (Academic, New York, 1969), **23**.

W. J. Hehre, R. Ditchfield, R. F. Stewart and J. A. Pople, J. Chem. Phys. **32**, 2769(1970).

I. V. Hertel, H. Schmidt, A. Bahring, and E. Meyer, Rep. Prog. Phys. **48**, 375(1985).

R. Hippler, in *"Fundamental Processes in Atomic Collision Physics"*, edited by H. Klienpoppen, J. s. Briggs, and H. O. Lutz, (Plenum, New York, 1985).

R. Hippler, W. Harbich, M. Faust, H. O. Lutz and L. J. Dube, J. Phys. **B19**, 1507(1986).

P. Hohenberg and W. Kohn, Phys. Rev. **136**, B864(1964).

S. H. Holloway and J. W. Gadzuk, J. Chem. Phys. **82**, 5203(1985).

E. Hood, F. Bozso and H. Metiu, Surf. Sci. **161**, 491(1985).

E. Hulpke, Surf. Sci. **52**, 615(1975).

E. Hulpke and K. Mann, Surf. Sci. **133**, 171(1983).

A. Hurkmans, E. G. Overbosch, K. Kodera and J. Los, Nucl. Instru. Meth. **132**, 453(1976).

L. R. Kahn, R. Baybutt and D. G. Truhlar, J. Chem. Phys. **65**, 3826(1976).

H. Kasai and A. Oliji, Surf. Sci. **183**, 147(1987).

S. R. Kasi, M. Kilburn, H. Kang, J. W. Rabaais, L. Tavernini and P. Hochmann, J. Chem. Phys. **88**, 59(1988).

S. R. Kasi, H, Kang, C. S. Sass and J. W. Rabalais, Surf. Sci. Rep. **10**, 1(1989).

B. Kirtman and C. de Melo, J. Chem. Phys. **75**, 4592(1981).

W. Kohn and J. Onffroy, Phys. Rev. **B8**, 2485(1973).

W. Kohn and L. Sham, Phys. Rev. **140**, A113(1965).

J. Kondo, in *"Solid State Physics"*, edited by F. Seitz, D. Turmbull and H. Ehrenreich, (Academic, New York, 1969), **23**.

K. C. Kulander, L. R. S. Devi and S. E. Koonin, Phys. Rev. **A25**, 2968(1982).

N. D. Lang, Phys. Rev. **B27**, 2019(1983).

N. D. Lang and K. Norskov, Physica Scripta **T6**, 15 (1983).

N. D. Lang and A. R. Williams, Phys. Rev. Lett. **37**, 212(1976).

H.-W. Lee and T. George, Surf Sci. **159**, 214(1985).

P. O. Lowdin, in *"Quantum Chemistry"*, edited by P. O. Lowdin (Academic, New York, 1970), **5**.

H. K. McDowell, J. Chem. Phys. **77**, 3263(1982).

H. K. McDowell, J. Chem. Phys. **83**, 772(1985).

R. McWeeny, Rev. Mod. Phys. **32**, 335(1960).

V. K. Mendevev, A. G. Naumovets and A. G. Fedorus, Soviet Phys. **12**, 301(1970).

D. A. Micha J. Chem. Phys. **78**, 7135(1983).

D. A. Micha and B. Gazdy, Phys. Rev. A36, 539(1987).

J. P. Muscat and D. M. Newns, Phys. Rev. **B19**, 1270(1979).

J. W. Negele, Rev. Mod. Phys. **54**, 913(1982).

D. M. Newns, Phye. Rev. **178**, 1123(1969).

D. M. Newns, Surf. Sci. **154**, 658(1985).

D. M. Newns, K. Makoshi, R. Brako and J. N. M. van Wunnik, Physica Scripta **T6**, 5 (1983).

S. E. Nielsen and N. Andersen, Z. Phys. **D5**, 322(1987).

J. K. Norskov and B. I. Lundqvist, Surf. Sci. **80**, 179(1979).

J. A. Olson and B. H. Garrison, J. Chem. Phys. **83**, 1392(1985).

E. G. Overbosch, R. Rasser, A. D. Tanner and J. Los, Surf. Sci. **92**, 310(1980).

G. S. Panev, N. Andersen, T. Andersen and P. Dalby, Z. Phys. **D5**, 331(1987).

J. A. Pople and D. L. Beveridge, "*Approximate Molecular Orbital Thoery*" (McGraw-Hill, New York, 1970).

A. Richard and H. Eschenbacher, Nucl. Instru. Meth. Phys. Res. **B2**, 444(1984).

P. Ring and P. Schuch, "*The Nuclear Many-Body Problem*" (Springer, New York, 1980).

K. Runge, D. A. Micha and E. Q. Feng, Interna. J. Quantum. Chem. Symp. Proc. (1990), to appear.

T. W. Rusch and R. L. Erickson, in "*Inelastic Ion-Surface Collisions*", edited by N. H. Tolk, J. C. Tully, W. Heiland and C. W. White (Academic, New York, 1977).

M. E. Schwartz and J. D. Switalski, J. Chem Phys. **57**, 4125(1972).

K. L. Sebastian, Phys. Lett. **98A**, 39(1983).

K. L. Sebastian, Phys. Rev. **B31**, 6976(1985).

I. Shavitt, in "*Method In Computational Physics*", edited by B. Alder, S. Fernbach and M. Rotenberg (Academic, New York, 1963).

S. Shindo and R. Kawai, Surf. Sci. **165**, 477(1986).

J. C. Slater and G. F. Koster, Phys. Rev. **95**, 1167(1954).

D. P. Smith, Surf. Sci. **25**, 171(1971).

J. R. Smith and J G. Gay, Phys. Rev. **B12**, 4238(1975).

J. R. Smith, J G. Gay and F. J. Arlinghaus, Phys. Rev. **B21**, 2201(1980).

K. W. Sulston, A. T. Amos and S. G. Davison, Phys. Rev. **B37**, 9121(1988).

A. Szabo and N. Ostlund, "*Modern Qunatum Chemistry: Introduction to Advanced Electronic Structure Theory*" (Macmillan, New York, 1982).

L. Szasz, "*Pesudopoetential Theory of Atomis and Molecules*" (John Wiley & Sons, New York, 1975).

E. Taglauer and W. Heiland, Appl. Phys. **9**, 261(1976).

N. H. Tolk, J. C. Tully, J, Krause, C. W. White and S. N. Neff, Phys. Rev. Lett. **36**, 747(1976).

H. C. Tully, in *"Modern Theoretical Chemistry, Dynamics of Molecular Collisions"*, edited by W. H. Miller (Plenum, New York, 1976).

H. C. Tully, Phys. Rev. **B16**, 4324(1977).

G. Wannier, Phys. Rev. **52**, 191(1937).

A. R. Williams, P. J. Feibeman and N. D. Lang, Phys, Rev. **B26**, 2560(1982).

S. C. Ying, J. Phys. (Paris) **38**, C4-184(1977).

A. Yoshimori, K. Makoshi and H. Kawai, in *"Dynamical Porcessed and Ordering on Solid Surfaces"*, edited by A. Yoshimori and M. Tsukada, Spring Series in Solid-State Sciences 59 (Spring-Verlag, Berlin 1984).
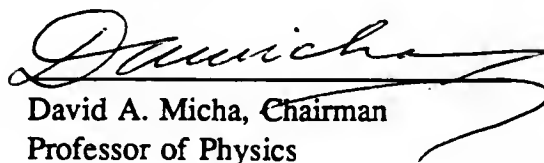
R. N. Zare, *"Angular Momentum"* (Wiley, New York, 1988).

BIOGRAPHICAL SKETCH

Eric Quinn Feng was born on April 13, 1951, in Shanghai, China. All of his early education took place in Beijing, China. In the Spring of 1977 he completed his undergraduate education in physics, and received a diploma from Peking University. In the Fall of 1978, he went to Graduate School at the University of Chinese Science and Technology to begin his graduate education. In the Fall of 1981, he graduated from that Graduate School with a Master of Science degree in physics.

In the Spring of 1982, he came to the USA, and enrolled in the Department of Physics at the University of Florida for further studies. After completion of the qualifying examination for the admission to the Ph.D. program, he joined the Quantum Theory Project in the Fall of 1984 and began research for his doctoral thesis.

I certify that I have read this study and that in my opinion it conforms to acceptable standards of scholarly presentation and is fully adequate, in scope and quality, as a dissertation for the degree of Doctor of Philosophy.
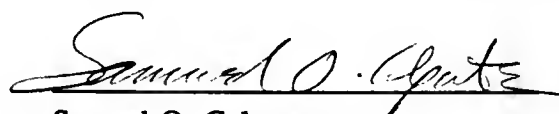
David A. Micha, Chairman
Professor of Physics

I certify that I have read this study and that in my opinion it conforms to acceptable standards of scholarly presentation and is fully adequate, in scope and quality, as a dissertation for the degree of Doctor of Philosophy.
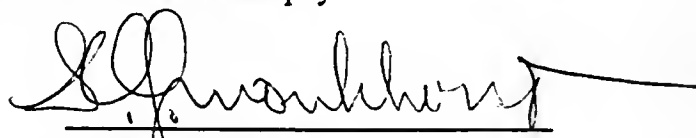
Rodney J. Bartlett
Graduate Research Professor
of Chemistry

I certify that I have read this study and that in my opinion it conforms to acceptable standards of scholarly presentation and is fully adequate, in scope and quality, as a dissertation for the degree of Doctor of Philosophy.
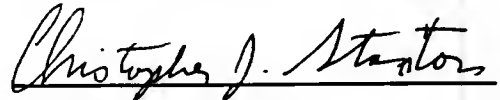
Samuel O. Colgate
Associate Professor of Chemistry

I certify that I have read this study and that in my opinion it conforms to acceptable standards of scholarly presentation and is fully adequate, in scope and quality, as a dissertation for the degree of Doctor of Philosophy.

Hendrik J. Monkhorst
Professor of Physics

I certify that I have read this study and that in my opinion it conforms to acceptable standards of scholarly presentation and is fully adequate, in scope and quality, as a dissertation for the degree of Doctor of Philosophy.

Christopher Jay Stanton
Assistant Professor of Physics

This dissertation was submitted to the Graduate Faculty of the Department of Physics in the College of Liberal Arts & Sciences and to the Graduate School and was accepted as partial fulfillment of the requirements for the degree of Doctor of Philosophy.

May 1991

Dean, Graduate School